EVALUATION OF GRIDDED PRECIPITATION PRODUCTS FOR STREAMFLOW MODELLING IN GIN WATERSHED, SRI LANKA

Passang Dorji Doya

(208349T)

Degree of Master of Science

Department of Civil Engineering

University of Moratuwa
Sri Lanka

February 2022

EVALUATION OF GRIDDED PRECIPITATION PRODUCTS FOR STREAMFLOW MODELLING IN GIN WATERSHED, SRI LANKA

Passang Dorji Doya

(208349T)

Supervised by

Dr P. K. C. De Silva

Thesis submitted in partial fulfillment of the requirements for the degree
Master of Science in Civil Engineering

UNESCO Madanjeet Singh Centre for
South Asia Water Management (UMCSAWM)
Department of Civil Engineering

University of Moratuwa
Sri Lanka

February 2022

DECLARATION OF THE CANDIDATE AND SUPERVISOR

"I declare that this is my own work and this thesis does not incorporate without acknowledgement any material previously submitted for a Degree or Diploma in any other University or institute of higher learning and to the best of my knowledge and belief it does not contain any material previously published or written by another person except where the acknowledgement is made in the text".

Also, I hereby grant to University of Moratuwa the non-exclusive right to reproduce and distribute my thesis/dissertation, in whole or in part in print, electronic or other medium. I retain the right to use this content in whole or part in future works (such as articles or books).

UOM Verified Signature

26/01/2022

Passang Dorji Doya

Date

The above candidate has carried out research for the Masters/MPhil/PhD thesis/ Dissertation under my supervision

UOM Verified Signature

27/01/2022

Dr P. K. C. De Silva

Date

ABSTRACT

Evaluation of Gridded Precipitation Products for Streamflow Modelling in Gin Watershed, Sri Lanka

An accurate representation of spatial precipitation is significant for hydrological studies. Spatial precipitation is also the basic input for distributed hydrological models and the accuracy of spatial precipitation affects the performance of hydrological models. In many parts of the world, ground-based observation networks are inadequate to capture spatial precipitation because gauge stations cannot be set up anywhere as financial and geographical factors play a vital role in the establishment. To overcome those challenges two existing gridded precipitation data (TRMM and APHRODITE) are used to simulate discharge in the Gin watershed of Sri Lanka. The coefficient of determination improves to 0.78 and 0.65 respectively for TRMM and APHRODITE data after bias correction. While comparing two gridded precipitation data to observed data, the TRMM data shows superior to APHRODITE with the same value of daily and a monthly average rainfall of 11.15 mm and 339.29 mm respectively. The standard deviation shows 21.16 for daily and 167.72 for a monthly scale with the difference of 31.00 % and -0.06 % to observed the data set.

The HEC-HMS model is used for generating streamflow from the two gridded and observed data against gauge data. From the other four-parameter (SCS Unit Hydrograph, Simple Canopy, SCS Method, Simple Surface, and Recession) soil moisture accounting parameter calculation was challenging as it has to be carefully determined. The three most sensitive parameters are soil percolation, tension zone storage, and impervious area while the groundwater storage two (GW2) is the least sensitive parameter. Model performance criteria such as RMSE, NSE, and PBIAS are carried out for calibration and validation. The observed data performed good in the simulation of streamflow compared to two gridded precipitation data with an NSE value of 0.70, RMSE Std Dev value of 0.50, and PBIAS of -8.40 % for calibration and NSE value of 0.66, RMSE Std Dev value of 0.66, and PBIAS of -2.34 % for validation. The result shows that the TRMM data is more suitable to be used for hydrological modelling for and water resources management in ungauged areas in Sri Lanka.

Keywords: APHRODITE, BIAS, CDF, HEC-HMS, SMA, TRMM

DEDICATION

I dedicate my dissertation work to my parents and plenty of friends. A special feeling of gratitude to my loving parents, Mr. Jaw Chung Doya and Mrs. Nim Jem Doya for their consistent support, inspiration, and encouragement. Even my gratitude goes to my sister, Pem Choden Doya for providing her endless assistance throughout my life.

I also commit this dissertation to my handful of South Asian friends, Mr. Utsab Phuyal (Nepal), Mr. Virendra Kumar (India), Ms. Farhana Azmi (Bangladesh), and Mr. Rajesh Gurung (Bhutan) for their limitless support in research and other activities for being without bound for any assistance during my stay at the University of Moratuwa.

ACKNOWLEDGEMENT

Firstly, I am immensely grateful to my supervisor, Dr. Kasun De Silva for his useful advice, continuous assistance, and staying power at some point in my master's study. Furthermore, I would like to beholden to Prof. R.L.H. Lalith Rajapakse, Dr. Janaka Bamunawala, Dr. Luminda Gunawardhana, Dr. Nimal Wijayaratna, and Mr. Harsha Ratnasooriya for guiding and indicating the way forward to accomplish milestones for my research. Their wide range of knowledge, experience, and ideas has advocated for me all the time of my educational research and even in some extreme situations. I would kindly thank Mr. Wajira Kumarasinghe for being supportive and being an inspiration, motivational, and guidance in ample ways during my study at the University of Moratuwa. Moreover, I would like to be wholeheartedly grateful to the Bhutan Jamchong Thuendrel Foundation (South Asian Foundation Office), and SAF Madanjeet Singh Centre for South Asia for providing full scholarships to upgrade my master studies in Water Resources Engineering and Management. In the end, I would like to express my gratitude to my mother and father, my sister, and my close friend. Without their consistent support and understanding, it may be impossible to reach this extent and complete my study.

TABLE OF CONTENT

LIST OF FIGURES

LIST OF TABLES

LIST OF ABBREVIATIONS

AMSRE	Advanced Microwave Scanning Radiometer
AMSU	Advanced Microwave Detector Unit
Avg	Average
Diff	Differences
FDC	Flow Duration Curve
GIS	Geographic Information System
GV	Ground verification
GW1	Groundwater layer 1
GW2	Groundwater layer 2
IO	Indian Ocean
JMA	Japan Meteorological Agency
MAE	Average-error magnitude
MHS	Microwave Humidity Detector
MRI	Meteorological Research Institute
NASA	National Aeronautics and area management
PBIAS	Percent bias
PMW	Passive microwave
PR	Combined precipitation radar
PRMS	Precipitation-Runoff Modelling System
PRMS	Precipitation-Runoff Modelling System
PVE	Streamflow volume errors,
RF	Rainfall
SbPP	Satellite-based precipitation products
SF	Streamflow
Sim	Simulated
SMA	Soil Moisture Accounting
SRE	Satellite-based rainfall estimate
SSMIS	Special microwave imaging sensors
SSMIS	Special microwave imaging sensors
USACE	United States Army Corps of Engineers
WB	Water balance
WMO	World Meteorological Organization

CHAPTER 1

1 INTRODUCTION

1.1 General

Precipitation is a key driving factor of the hydrological cycle and the main input for hydrometeorological models and research related to climate (Sorooshian et al., 2011). Therefore, accurate and valid precipitation information with adequate time and spatial resolution are significant for various ranges of a product like climate modelling and flood prediction (Miao et al., 2015). Unfortunately, precipitation is one of the most challenging atmospheric variables to quantify because it varies greatly on small scales in area and time. Customarily, meter observation is a method of obtaining precipitation information on site. However, traditional rain gauges and weather radar networks are rare and inadequate to record spatial and temporal changes in precipitation systems (Michelson, 2004; Yong et al., 2010).

Hydrological modelling in statistically sparse gauge stations around the world has always been a challenge. This example is more complicated when it comes to large, transboundary river basins. Many professionals in the field of hydrology believe that the majority of water catchments in the world are either unmeasured or incorrectly measured (Kundzewicz et al., 2008). Therefore, with the emergence of the predictions in the ungauged basins (PUB) program, with the help of the Global Hydrological Association, there are projects to strengthen those issues (Hrachowitz et al., 2013; Sivapalan, 2003). Although this initiative has achieved excellent results (Janardhana Raju et al., 2010; Sivapalan, 2003; Wagener et al., 2005), it is necessary to reach high-quality agreements in the areas of the invention of methods and statistical sources that can help in cases of poor calibration, carry out hydrological prediction and research.

Researchers tend to use long-range satellite base precipitation products (SbPP), especially in developing regions, due to the limited rain gauge network. These SbPPs are appealing because they are freely available and provide time-consistent, temporally, and spatially confine detailed data, which is attractive for hydrological applications. Therefore, SbPP can solve many of the shortcomings encountered when measuring precipitation by ground precipitation meters. However, the accuracy of SbPP should be tested before use (Irvem & Ozbuldu, 2019a; Jiang et al., 2019).

The Asian Precipitation High-Resolution Observation Data Integration Towards Evaluation (APHRODITE Water Resources) project for water resource assessment has been carried out since 2006 by the Institute for Human Nature (RIHN) and the Meteorological Research Institute (MRI / JMA) of the Japan Meteorological Agency to develop daily precipitation datasets on high-resolution grids across Asia (Yatagai et al., 2012) which is a super-resolution product of the rain gauge. These are used to validate decision-making in climate model simulations and statistically reduce the output of a natural climate simulation so that local precipitation forecasts are consistent with future climate changes due to the man-made greenhouse effect.

The APHRODITE products are used for this type of function because they contain a large amount of rainfall information and use interpolation methods that consider the influence of the terrain. Therefore, they provide a convenient database for converting biased model precipitation form to reasonable form, especially in hilly areas. Therefore, APHRODITE can provide training data and information to reduce size in a super integrated method (Krishnamurti et al., 2016). Satellite products are also used in supersets. Satellite predictions generally have good temporal and spatial sampling rates and fewer missing readings than rain gauges. However, model results and satellite data need to be verified with rainfall gauge data (Chen et al., 2008). Most importantly, the benefit of satellite products over rain gauges is timely delivery. Very few countries have good networks that collect data on time and follow the best operations and grids in near real-time. But it is difficult to try across borders, sometimes it is essential.

The APHRODITE (Integrated Assessment of Asian Precipitation High-Resolution Observational Data) project has evolved the most superior for daily precipitation dataset with a high-resolution grid (0.25 ° latitude/longitude grid) for the Asian place. The APHRODITE water sources task has been implemented through the Institute of

Human and Nature (RIHN) and the Meteorological Institute of the Japan Meteorological enterprise (MRI / JMA) since 2006 (Yatagai et al., 2012).

APHRODITE's daily grid precipitation is the best long-term daily product (after 1951) on a continental scale that includes a dense community of each day precipitation records in Asia (inclusive of the Himalayas, South and Southeast Asia, and the mountains in the canter East). This data is compiled from various valid websites among 5,000 and 12,000 which is 2.3 to 4.5 times the records supplied through the global telecommunications device community, which is utilized in most of the precipitation merchandise of daily network (Yatagai et al., 2014).

The TRMM satellite was launched in November 1997 and commenced production in 1998. TRMM`s product consists of satellite and GV (ground verification). Considering 1998, the product has been changed regularly to improve the unified procedure of numerous algorithms and approaches (Suryantoro et al., 2010). The Tropical Rainfall Measuring Mission (TRMM) is a collaboration of two country-wide space companies, NASA (National Aeronautics and Area Management) and NASDA Japan (Japan`s countrywide Aerospace Development Organization), and has now been converted into JAXA (Japan Aerospace Exploration Agency). TRMM is used to degree rainfall in tropical regions and has diverse low-tilt and orbit sensors. The inclination (inclined orbit) is the attitude among the reference subject and the slope of the sphere measurement (Suryantoro et al., 2010).

The TRMM inside the polar (non-synchronous) orbit is inclined 35° from the equator, and the orbital top at the beginning of the launch became 350 kilometres, which was changed to 403 kilometres from August 24, 2001, until now. In orbit, TRMM orbits the earth for approximately 90 minutes/1 circles, 16 times a day. There are numerous styles of TRMM product data. In this study, TRMM 3B42V7 version was selected for daily scale (Levina et al., 2016).

In this study, the aim is to systematically quantify the performance of two gridded precipitation data (TRMM and APHRODITE) in the Gin River Basin of Sri Lanka for comparing streamflow.

1.2 Problem Identification

In many developing regions of the world, terrestrial networks for observing total precipitation are often unevenly distributed in space. Furthermore, due to the lack of statistical data, recorded fines can also cause problems (Hughes, 2006). These issues will affect the overall performance of the model in water flow simulation. With the help of the World Meteorological Organization (WMO), an extensive network of rain gauges is ready, with gauges measuring 100-250 square kilometers in mountainous areas and 600-900 square kilometers in lowlands (WMO, 1995).

Accurate measurement of precipitation on the spatial spread and time scale is essential. This is not very useful for weather forecasters and climate scientists, but for hydrologists, farmers, emergency, and industrial managers (Ebert et al., 2007).

However, it is not adequate to characterize the spatial pattern of precipitation in densely inhibited with the presence of rain gauge station data. Similarly, rain gauge distribution indicates they are generally established in places with adequate infrastructure. And such an existence of a rain gauge does not give sufficient rainfall distribution (Hong et al., 2007).

Recently, trend analysis for precipitation become one of the key interests in the research field (Nisansala et al., 2020). The local changes are observed when the scale of global or regional returns back to the national or sub-national level (Caloiero, 2015). In addition, precipitation analysis provides decision-makers with important information about water resources management, development, policy planning, and disaster risk reduction activities (Barua et al., 2013).

The same scenario also reports that the rainfall trend in Sri Lanka has changed significantly in the past few decades (Alahacoon & Edirisinghe, 2021). Due to the landscape scenario of Sri Lanka, the Indian Ocean (IO) monsoon condition influence systematic rainfall migrations in various geographical areas of the country throughout the year (Clift & Plumb, 2008).

Many authors have studied to know trend analysis based on data collected from a fewer number of rain gauges in Sri Lanka (Costa, 2008; Naveendrakumar et al., 2018; Nisansala et al., 2020). Therefore, no spatial variability was recorded in these studies. The drawback of such studies is that they are not suitable for portraying trends at the regional or climatic sector level because the obtained values are narrow to small areas.

In the earlier studies, the foremost way to overcome the above limitations is to rely on satellite precipitation estimates and calibrate gauge data to accurately reflect the spatial variability of precipitation events (Banerjee et al., 2020; Gebrechorkos et al., 2019; Kamau Muthoni et al., 2019; Katsanos et al., 2016). The study is carried out to overcome limited or scarce data to determine the suitability of two gridded precipitation data in line with observed data.

1.3 Objectives/Specific objectives

1.3.1 Overall Objective of the study

To assess the performance of two gridded precipitation data (APHRODITE and TRMM) for modelling streamflow in a selected watershed to check the potential of outflow simulation.

1.3.1 Specific Objectives

- To compare two gridded precipitations data (TRMM 3B42 V7 and APHRODITE) with gauge data.
- To check the accuracy and suitability of the two gridded precipitation data as inputs for streamflow simulations.
- To calibrate and validate HEC- HMS model.
- To examine the suitability of two gridded precipitation data in scarcity or lack of streamflow data.

CHAPTER 2

2 LITERATURE REVIEW

2.1 Introduction

Precipitation datasets are generally acquired from dispersed and different gauge stations. In most regions, the required datasets are struggling to be obtained in areas where there are no or limited adequate precipitation datasets (Irvem & Ozbuldu, 2019b). In addition, the precipitation datasets acquired from the gauge stations contain errors of spatial representation (Porcù et al., 2014; L. Singh & Saravanan, 2020). Despite its importance, there are currently not enough weather stations, especially in mountainous areas, which are sparsely and unevenly distributed, making it challenging to acquire adequate data on rainfall. Most of the rain gauges are locations (i.e., cities and airports); therefore, these rain gauges may not adequately portray the area in which they are located. However, satellite-based precipitation products provide adequate and constant observational datasets (Panegrossi et al., 2016) to determine the distribution of precipitation in regions used globally.

Around the world, many studies comparing TRMM and ground observations have been conducted (Huffman et al., 2007; Islam & Uyeda, 2007; Karaseva et al., 2012; Nair & Srinivasan, 2009; Nastos et al., 2016; Xue et al., 2013). The Barros (2000); Huffman (2007); Islam & Uyeda (2007); Karaseva (2012); Nair & Srinivasan (2009); Nastos (2016); Xue (2013) used TRMM and rain gauge to be observed and study the monsoon rainfall in Nepal's mountainous area in 1999. It is said that TRMM has higher consistency in low-altitude stations compared with high-altitude stations (Tan & Duan, 2017).

Precipitation datasets in the watershed area come from recorded measurements. In addition, other ground-based observations, such as weather radar and tree gauges, are used to record rainfall, which is generally considered the most reliable source of rainfall information (Tapiador et al., 2012). Precipitation data acquired from surface observations can be convenient; however, their expenses and the inadequate density of surface stations have some limitations, mostly in mountainous areas of the world with inconvenient transportation (Nishat & Rahman, 2009).

The motives of APHRODITE are to develop adequate, high-resolution, rain gauge-based products. These are to verify the high-resolution climate model simulation (Yatagai et al., 2012) and the relatively constant statistical reduction of climate simulation results, and to perform local precipitation prediction based on future climate changes caused by man-made greenhouse effects.

The author used a daily precipitation dataset with a resolution of 0.25° in the Asian monsoon region (APHRO_MA_V1901) produced by the APHRODITE project (Yatagai et al., 2012). The data period is from 2007 to 2015 and the coverage exceeds 08° to 558°N and 608° to 1558°E. The maximum input data was from 1998 and gradually decreased until 2004 (Yatagai et al., 2009). After calculating the total monthly rainfall, APHRODITE was used.

The linear regression method is one of the suitable methods used for predicting hydrological signature indexes, including baseflow indexes (Bloomfield et al., 2009; Albert I. J. M. van Dijk et al., 2013; Gallart et al., 2007; Longobardi & Villani, 2008). This method uses the physical characteristics of the river basin (i.e., the descriptor) and the (Baseflow index) BFI obtained from the measured basin to generate a linear regression. It is used to predict BFI in unmeasured river basins (Beck et al., 2013; Bloomfield et al., 2009). Some studies have shown that some catchments have a significant impact on BFI.

Other studies also simulated BFI using climate-related indicators such as average annual precipitation and average annual potential evaporation (Albert I. J. M. van Dijk et al., 2013; A. I.J.M. Van Dijk, 2010). A similar study summarizes the regression using the average annual rainfall, slope, and grassland percentage of and predicts BFI (Bloomfield et al., 2009; Brandes et al., 2005; Gebert et al., 2007; Haberlandt et al., 2001; Mazvimavi et al., 2005; A. I.J.M. Van Dijk, 2010). In addition to BFI, linear regression is also a helpful approach for predicting other hydrological features (Su et al., 2016; Zhang et al., 2014). The limitation of the linear regression approach is the inability to predict BFI using constant parameters and handle interactions at different spatial scales (Qian et al., 2010). This causes large errors in large drainage areas. The region may be from the climate regime.

Precipitation fluctuates with area and time. Therefore, it is significant to be aware of their outbreak patterns to be able to successfully predict local climate behavior (Santos et al., 2019). Categories such as agriculture, flood protection, and human supply projects require an understanding of rainfall planning, management, and operation (Jale et al., 2019; Soares et al., 2016). A probabilistic model with a cumulative distribution function (CDF) allows you to simulate hydrological data based on frequency. Some CDFs have been used for many years to check the behavior and variability of precipitation. Gonçalves, Blanco, Santos, and Oliveira (2018) estimated the probability of annual precipitation in the Gumbel distribution by normal and exponential distribution for the year of El Nino and La Niña in the state of Para. Based on 413 measurement points, the author found from a satellite that the normal distribution is the best match for precipitation data.

The gridded precipitation information (APHRODITE and TRMM) provides unique results when replicating records found on a large scale. However, some distortions need to be corrected at the same time as the initial reading level analysis.

2.2 Hydrologic Model

Many other computers that can be used to simulate the rainfall-runoff process include soil and water assessment tools (Ramanarayanan, 2009.), Hydrological Engineering Centre's Hydrological Modelling System; HEC-HMS, Variable Permeability Model (Liang et al., 1994), HBV light model (Seibert, 2005), and J2000 model (Peter Krause, 2002) is widely used by hydrological modelers all over the world (Adib et al., 2020), (Azmat et al., 2016), & (Bao et al., 2005.). However, due to the inability to obtain long-term data, including meteorological and runoff data, the hydrological time series model inherited the uncertainty of runoff estimates (Ratnayake & Pitawala, 2014).

As per Sorooshian et al. (2008), a model is a simple depiction of the actual system. The supreme model provides near-real outcomes with the fewest parameters and the least complication of the model. Models are primarily used to predict the behavior of the system and to understand wide ranges of hydrological processes. The model contains numerous parameters that define the properties of the model. A flow model can be termed as a set of equations that help estimate the flow based on the various parameters used to describe the characteristics of the basin. The two significant inputs needed for all models are precipitation data and catchment areas. In addition, river basin characteristics such as soil characteristics, vegetation coverage, catchment topography, soil moisture content, and aquifer characteristics are taken into account. Hydrological models are now regarded as an essential tool for the management of water resources and the environment.

2.2.1 Types of Models

Rainfall-runoff models are categorized according to the model's data and parameters and the range to which the physical principles are applied in the model. It is categorized as a local and distributed model basically on the model parameters as a function of area and time as well as deterministic and stochastic models based on another basis.

Deterministic models provide a similar outcome for a set of input values, while probabilistic models can produce different output values for a set of inputs. As per Moradkhani and Sorooshian (2008), the synthetic model treats the whole basin as a lone unit and does not take spatial variability into account, so it produces output independent of the process. A spatial modelling process in which a distributed model can make spatially distributed predictions by dividing the whole basin into smaller units (usually an irregular network of squares or triangles). This allows to spatially change the parameters, outputs, and inputs.

Another categorization is the static model and the dynamic model based on temporal aspects. The static version excludes time at the same time as the dynamic version. Soroosian et al. (2008) categorized the models into event-based and continuous models. The former produces the best result at precise intervals and the latter produces a continuous result. The significant categorization is the empirical model, the conceptual model, and the physics-based model.

2.2.2 Lumped Water Balance Model

The lumped model is simple but worked well in various studies (Cameron et al., 1999; Uhlenbrook et al., 2009; X. Yang & Michel, 2000). Other studies comparing the lumped model with the distributed model found that both provided similar accuracy (Boyle et al., 2001; K. Ajami et al., 2004; Lobligeois et al., 2014; Reed et al., 2004; Refsgaard & Knudsen, 1996; Sayama et al., 2011; Shah et al., 1996; Smith et al., 2012) and could calibrate the lumped model more efficiently (Bormann et al., n.d.). Vansteenkiste et al. (2014) found that in the Belgian catchment area, the point model performed better than the distributed model in terms of seasonal events and total water balance, with very small partial flow differences compared to the distributed model. In addition, the lumped model provides a valuable integrated view of pool exit responses, such as (Reed et al., 2004) distributed model cross-comparison project in the Oklahoma region. Martínez Santos and Andrew used a lumped dispersion approach to model a natural recharge in the semi-arid aquifers of Spain.

2.2.3 Monthly Water Balance Models

Monthly water balance models are abundantly utilized to determine the availability of water, catchment feature, water resource management, and assess the hydrological impact of climate change. Perhaps the most important and rational reason to use the monthly water balance model for water resource planning and predict the impact of weather changes is the excess of monthly runoff and monthly hydroclimatic statistics. For wetlands, it is adequate to use a model work out with 3-5 parameters to symbolize most hydrological conditions in the watershed area. However, in dry and semi-arid areas, a particularly complex model can rely on 10 to 15 parameters (Xu & Singh, 1998).

According to Xu & Singh (1998), monthly water balance models mainly reconstruct the hydrology of catchment areas, assess the impacts of climate change, and assess seasonal and geographical patterns of water supply and irrigation needs.

The duration d_i of the *ith* sorted observation is its exceedance probability P_i . If *Pi* is estimated using a Weibull plotting position, the duration d_i for any q_i (with $i = 1,...,N$) is

$$d_i = P(Q < q_i) = P_i = \frac{i}{N+1} \quad [2\text{-}1]$$

where N is the length of the streamflow series and q_i is the *ith* sorted streamflow value.

The FDC affords historic facts on the water regime: on the seriousness of the drought and the importance of excessive outflow. Multiple time resolutions for streamflow statistics are available on a monthly, annually, and daily range which is utilized for FDC construction. However, the finer the resolution, the better the data on river hydrological tendency provided with the facts of the FDC (V. U. Smakhtin, 2001). FDCs can be built monthly for the entire monthly recording period (Vogel & Fennessey, 1994); under the premise of all similar months (V. Y. Smakhtin et al., 1997); or based on a particular month

2.2.4 Soil Moisture Accounting (SMA) Algorithm

The basic difference between the SMA version (soil moisture accounting) and the HEC-HMS version is in evapotranspiration and groundwater infiltration. These are not noticeable in event-based modeling, but not in hydrological continuous modeling. Soil moisture has a significant impact on the hydrological response of the catchment. However, due to the complication of the model structure and the demanding parameter estimation in the context, the simulation model often does not follow (Holberg, 2015; Tramblay et al., 2010). At HEC-HMS, the soil moisture algorithm and deficit and constant loss strategies are the best loss techniques that evapotranspiration takes into account (Samady, 2017).

For predicting the amount of streamflow at Gin watershed, evaluating the water resources requires a long simulation, so this observation is used in the SMA parameter. The results of the final model may help planners to assess water resources, floods, and droughts for future infrastructure tasks. Water loss due to infiltration, evaporation, and soil moisture should not be neglected. The HEC-HMS model has been selected for its performance and simplicity and has been effectively tuned and validated in several catchment and river basins around the globe. Additionally, this software is readily available from sources that manage a set of SMA algorithms.

2.2.5 Model Structure

This study uses HEC-HMS 4.7 version application. It has made great strides with the help of US Navy Engineers and was developed to simulate the types of rainfall-runoff in dendritic basin structures (Meenu et al., 2013). The format of the HEC-HMS model includes watershed models, climate versions, meteorological models, operating specifications, and time series of input data (USACE, 2016).

2.2.5.1 Basin model

The basin model manager is an illustration of the actual item. It describes the many elements of the hydrological system, along with sub-catchment areas, reaches, intersections, sources, sinks, reservoirs, and diversion It can integrate into the model by using HEC-GeoHMS or manually with HEC-HMS. Individual elements require some parameters to relate to hydrological devices (Bhuiyan et al., 2017). These elements are interconnected to ease water flow and form a dendritic network.

2.2.5.2 Control specifications manager

The control specification manager is an important component of the project which is mainly utilized to control the simulation time interval.

2.2.5.3 Meteorological component

Meteorological problems are the details of the main calculation, based on which precipitation inputs are distributed temporally and spatially throughout the river basin. The spatiotemporal distribution of precipitation is performed using the inverse distance method and the Thiessen method. There are many methods for calculating evapotranspiration, such as the Thornthwaite and Penman-Monteith methods. Similarly, there is always the possibility of creating large pools containing multiple manipulated specification managers and 10 meteorological components in comparison with each other, especially in some phases of the simulation process.

2.2.5.4 Input data

Hydrological models often require temporal precipitation data collection to estimate the average precipitation in a watershed. Gathering flow information over time is often referred to as an observed flow or a specific flow. This primitive is the baseline for an all-weather dataset like precipitation, observed flow, evapotranspiration, wind velocity, sunshine hours, and humidity.

2.2.6 Soil Moisture Accounting

The Soil Moisture Accounting (SMA) approach in the HEC-HMS model is a single-dimensional, semi-disbursed depiction of the soil method. The hydrological model allows water to flow into a single route with a time step path. This works well for various packages, but it can reduce model precision on a large spatial scale.

One-dimensional models cannot capture complex flow behavior due to numerous landscapes and anisotropic soils. HEC-HMS seeks to solve these problems for semi-distributed modelling and several storage components within the soil profile. A complete description of the mathematical model can be discovered in the technical manual, HEC (2000), and Bennett (1998). Soil moisture accounting takes a precipitation hyetograph as its enters and routes it through the canopy, surface, and soil storages, considering groundwater, base flow, and evapotranspiration procedures earlier than outputting a streamflow hydrograph.

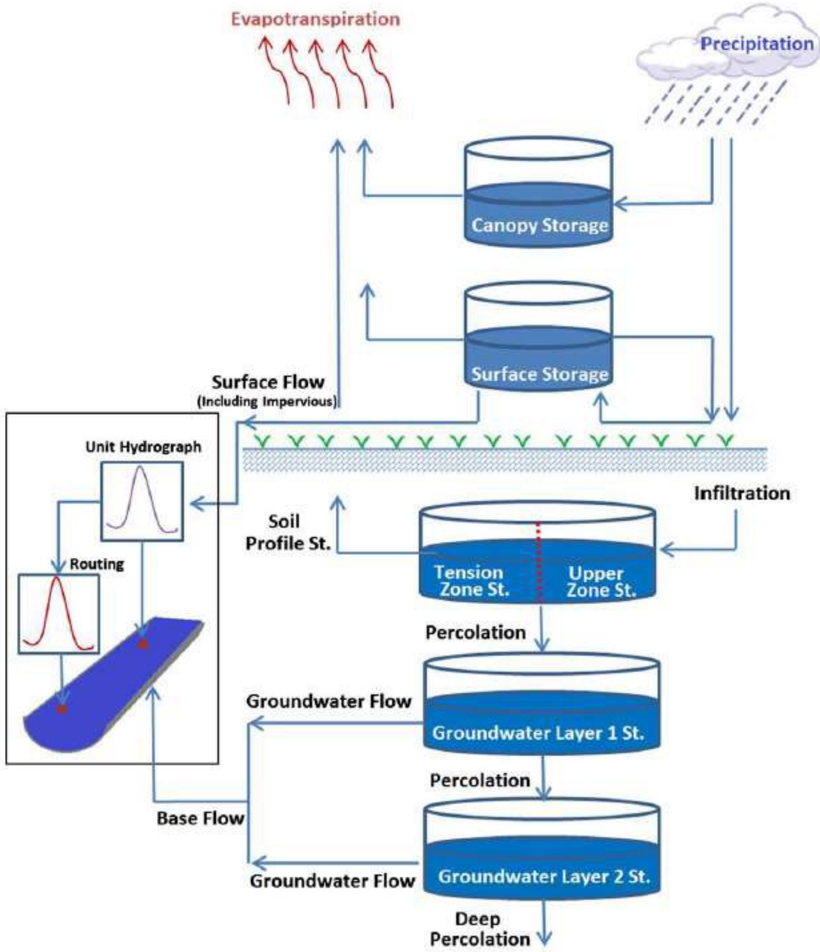

Figure 2-1: Schematic of SMA model (Feldman, 2000b)

When precipitation happens, first the cover storage is filled. The surface storage is next as quickly as each of these storage components are filled, precipitation has a possibility of infiltrating into the ground. If the precipitation intensity is higher than the infiltration capacity of the soil profile, more precipitation becomes a surface runoff in place of infiltrating. When precipitation infiltrates into the soil, it fills the tension region first, and then the higher region. Precipitation can percolate from the upper place into the groundwater layer 1 (GW1) storage, but not from the tension area. Some water in GW1 is directed to base 1 and travels with the flow reservoir. At the same time, it penetrates groundwater layer 2 (GW2). Water can move from GW2 to the second base and move with the flow reservoir. Otherwise, it penetrates the deep aquifer and is considered lost from the system. Water in the baseflow reservoir is converted to running water based on the characteristics of the reservoir, which consists of quantity and flow coefficient.

The SMA model is initially used by the United States Army Corps of Engineers (USACE) within 46,422 km^2 of the Nashville area to examine the overall performance of the HEC-HMS model using the SMA algorithm. Estimate parameter values with as few parameters as possible that can be changed indefinitely in the future of model calibration, and check the methodology to minimize the uncertainty associated with the preliminary settings of the parameters (Fleming & Neary, 2004).

The HEC-HMS model is used to predict floods in the Sturgeon Creek basin in Manitoba, Canada, using the SMA algorithm. When using the occasional continuous modeling of the HEC-HMS model, there was sufficient consensus between the determined and simulated flows. The outcome of this study suggests that the HEC-HMS model may be a suitable device for predicting HFC in Manitoba (Bhuiyan et al., 2017).

2.2.7 Continuous Hydrological Modelling (SMA Algorithm)

In evaluations up to the event-based model, the continuous hydrological model takes into account soil moisture stability in catchments over time and is suitable for simulating daily, monthly, and seasonal runoff (Ponce, 1989).

Fleming and Neary (2004) simulated the streamflow within the Cumberland River basin inside the United States. They established a technique for predicting the twelfth SMA parameter. A geographic information system (GIS) is utilized for predicting seven parameters, and the very last parameters were determined by using streamflow recession assessment if one wants to allow calibration and validation techniques within the watershed. For the time that surface runoff must turn out to be contributing to streamflow, the tension region depth is adjusted, and prominence turns into located on matching the observed and simulated streamflow peaks. The ultimate parameters were adjusted in simulated and observed top flows when interflow and groundwater flow were the number one contributor to the streamflow. The remaining parameters were adjusted in simulated and observed peak flows when interflow and groundwater flow have been the primary contributors to the streamflow. The daily data for four years and the evaporation data on the month scale are used. Parameter estimation is used for streamflow recession evaluation is used for the Gin watershed.

To better the accuracy of the model, calibration and validation are performed entirely based on the gauge outlets in the basin. The emphasis on this model has been changed to match the peak flow within the length of calibration and validation.

2.2.8 Sensitivity Analysis for Watershed

Samady (2017) ran the HEC-HMS model using the SMA algorithm to simulate the course of a stream to investigate the effects of a drought on the lower part of the Colorado River in Texas. As a result of the sensitivity evaluation, maximum infiltration rate, maximum soil storage, base flow (GW2) storage, tension zone storage, and deep penetration rates had a significant impact on the simulation effect compared to other parameters. For factors within model calibration, the easiest way to adjust the parameters for intermediate current storage capacity (GW1) and low percolation rate (GW2) was to reduce the calibration parameters to prevent overriding. GW2 penetration rates are a sensitive conceptual parameter.

2.2.9 Parameter Estimation

Fleming and Neary (2004) predict seven parameters canopy interception storage, maximum infiltration rate, soil zone percolation rate, tension zone storage, maximum soil storage, surface depression storage, and groundwater (GW1) percolation rate of the SMA model. The parameters were taken from land use, land cover, and ground records calculated by GIS. The surface depression storage was based on Fleming and Neary (2004), as displayed in Table 2-1.

Table 2-1: Surface depression storage value (Fleming & Neary, 2004)

Description	Slope (%)	Surface Storage (mm)
Paved Impervious Areas	NA	3.18–6.35
Flat, Furrowed Land	0–5	50.8
Moderate to Gentle Slopes	5–30	6.35–12.70
Steep, Smooth Slopes	>30	1.02

Four of the parameters (groundwater 1, two storage depths, and coefficient) are estimated by analyzing historic streamflow recession measurements. Groundwater 2

(GW2) penetration rate is the only parameter that is not estimated from the above methods but has been adjusted for model calibration.

2.2.10 Parameter Estimation (Land use and Land Cover)

The precipitation intercepted by vegetation is known as canopy interception. The canopy storage capacity varies depending on the structure of the vegetation and weather factors. Canopy storage can be calculated using soil and ground cover and canopy layers intercept values are provided in Table 2-2, as suggested by Bennett et al. (2004).

Table 2-2: Canopy storage values (Bennett & Peters, 2004; Fleming & Neary, 2004)

Vegetation Type	Canopy Interception (mm)
General vegetation	1.27
Grasses and deciduous trees	2.032
Trees and coniferous tree	2.54

2.2.11 Initial Parameter Estimation

Estimated and calibrated parameters obtained from similar studies Fleming and Al. (2004); McEnroe (2010); Gyawali et al. (2013); Holberg (2015) and Samady (2017) suggests that the estimated parameters are usually in the same range, except the impervious surface values are lower than those used in other studies because impervious percentage varies from one place to another. For the Gin watershed, the initial parameter is used according to the literature review.

2.3 Model Calibration

The HEC-HMS model consists of two types of calibration: manual and automated. Each of them can limit the goal features.

2.3.1 Automated calibration

The HEC-HMS model's automatic calibration method uses an iterative approach to reduce target features such as total absolute error, total squared error, peak percentage error, and peak weighted mean square error (HEC, 2000).

2.3.2 Manual Calibration

The standard digits for the HEC-HMS model do not consistently yield cost-effective results due to the different variety of individual parameters. Within the garage depths and depths factor, the limits are 2.54 to 1,500 mm and 0.1 to 10,000 hours (Fleming & Neary, 2004). Fleming et al. (2004) carried out the HEC-HMS model of the Cumberland River basin and observation statistics chosen from 1994 to 1999. Of these years, 1994, 1998, and 1999 were selected for calibration because the six-year information showed a very frequent runoff-to-precipitation ratio. All guidance and automatic calibration techniques have been followed.

2.4 Model Validation

Refsgaard and Knudsen (1996) defined model verification as "a method of exhibiting that a particular area accuracy model can make adequate predictions during the calibration period." Model validation is mainly used to figure out the efficacy of parameterization and calibration methods. It is entirely based on Refsgaard et al. (1996). For the Gin watershed, the calibration and validation of 4 years are selected for both models.

2.5 Objective Function

Model testing typically includes calibration and validation. Therefore, the complete dataset is divided into two components: calibration and validation length. The most important criterion for testing the overall performance of a model is the target characteristic, which in each case determines the scope of self-assurance of the model for use in a practical way, within the calibration and validation period (Guo & Wang, 2002). Researchers use their objective function to compare the simulated streamflow with the observed streamflow. Fleming et al. (2004) compared the observed and simulated flows using the objective function as shown in Table 2-3.

Table 2-3: List of statistics used to compare model output and observed data (Fleming & Neary, 2004)

Mean hourly flow (m^3/s)	$\left(\frac{1}{n}\right)\sum Q$	[2-2]
Standard deviation (m^3/s)	$\sqrt{\left(\frac{1}{n}\right)\sum (Q-\bar{Q})^2}$	[2-3]
Mean absolute error (m^3/s)	$\left(\frac{1}{n}\right)\sum \lfloor Q_o - Q_s \rfloor$	[2-4]
Root mean square error (m^3/s)	$\sqrt{\left[\sum \lfloor Q_o - Q_s \rfloor^2\right]/n}$	[2-5]
Baseline-adjusted coefficient of efficiency	$1.0 - \left[\sum \lfloor Q_o - Q_s \rfloor\right] / \left[\sum \left\lfloor Q_o - \bar{Q} \right\rfloor\right]$	[2-6]
Error in volume (%)	$[(V_o - V_s)/V_o] * 100$	[2-7]
The average error in time to peaks (h)	$\left(\frac{1}{n}\right)\sum \lvert T_s - T_o \rvert$	[2-8]
The average error in magnitude of peaks (%)	$\left[\left(\frac{1}{n}\right)\sum \lvert (Q_o - Q_s)/Q_o \rvert\right] * 100$	[2-9]

In the above table (Table 2-3), Q = hourly streamflow, $\bar{Q}$ = average streamflow Q_o = observed hourly streamflow, Q_s = hourly simulated streamflow, $\bar{Q}$ = baseline streamflow, V_o= observed streamflow volume, V_s = simulated streamflow volume, T_s= simulated hour of peak flow, and T_0 = observed hour of peak flow.

2.5.1 Percent Streamflow Volume Error (PVE) or Percent Bias (PBIAS)

PBIAS or PVE suggests the overall settlement between the observed flow and simulated flow over a certain time interval (Samady, 2017). The PVE is used as a primary metric for the objective function in maximum hydrologic models (Jain & Singh, 2003).

$$PVE\,\% = \frac{Qobs\ -\ Qsim}{Q_{Obs}} \times 100 \qquad [2\text{-}10]$$

In this equation, Q_{obs} is the determined streamflow (m³⁄s) and Q_{sim} is the simulated streamflow (m³⁄s) at the watershed outlet. Percent bias compares the average tendency of the simulated flows to be larger or smaller than the observed flow values (Gupta et al., 1999). It measures the unfairness/bias of model performance. The most reliable rate is zero, which means that the model has an unbiased flow simulation. Positive values indicate a tendency toward overestimation; negative values imply a tendency towards underestimation (Yu & Yang, 2000).

2.5.2 Nash Sutcliffe Efficiency (NSE)

The NSE is used to evaluate the performance of a model (Nash & Sutcliffe, 1970). The term is defined as 1 minus the sum of the absolute squared differences between the estimated and observed values normalized by using the variance of the localized values during the study (P. Krause et al., 2005). It is determined by the following equation.

$$NSE = \frac{1 - [\sum (Qobsi - Qsim)^2]}{[\sum (Qobsi - \bar{Q}sim)]} \quad [2\text{-}11]$$

Within the above equation, Q_{obsi} is the observed streamflow and $\bar{Q}_{sim}$ is the simulated streamflow. The NSE (unitless) measures the relative value of the residual variance (‘‘noise’’) to the variance of the flows (‘‘information’’). The greatest value is 1.0, and values must be large than 0. The zero shows minimally proper overall performance. A rate equal to zero shows that the suggested observed flow is a better predictor than the model (Gupta et al., 1999).

2.5.3 Coefficient of Determination (R^2)

The coefficient of determination (R^2) is an idea in the evaluation of variance and regression evaluation. I measure the percentage of explained variance present inside the data. Consequently, the better the rate of R^2, the better the model describes the information. It is also defined because of the squared value of the coefficient of correlation (P. Krause et al., 2005). R^2 is determined as:

$$R^2 = 1 - \frac{\sum_{i=1}^{n}(yi - \hat{y}i)^2}{\sum_{i=1}^{n}(yi - \bar{y})^2} \qquad [2\text{-}12]$$

Here $\bar{y}$ denotes the mean of the observations and $\hat{yi}$ is the prediction of yi using the approximate model. If there is no relationship between the predictor and response variables, $\bar{y}$ is a sufficient "model" to explain the data. Hence, the term $yi - \bar{y}$ describes the deviation when there is no relationship between the predictor variable(s) and the reaction variable. The variety of values of R^2 depends on the type of model to be fitted; in popular cases like linear least-squares regression fashions, they lie among 0 and 1. A value of 0 indicates no correlation in any respect, while the value of 1 means that the dispersion of the prediction is identical to that of the observation.

2.5.4 Root Mean Square Error (RMSE)

The other validation degree is the root-mean-squared error basis (RMSE). It is described as the square root of the mean of the squared verse variations, among the corresponding factors of prediction and observation (Barnston & G., 1992). The RMSE is calculated as:

$$RMSE = \frac{\sqrt{\sum_{i=1}^{n}(Q_{obs,i} - Q_{model})^2}}{n} \qquad [2\text{-}13]$$

where Q_{obsi} is the observed value, Q_{model} is the simulated value, and n is the number of observations. It describes the mean model performance error and varies with the variability of the error magnitudes (or squared error) as well as with the total error or average-error magnitude (MAE) (Willmott & Matsuura, 2005).

2.5.5 Recommended Performance Ratings

The recommended overall performance evaluation of the basin model, based entirely on the above statistical parameters, is summarized in Table 2-4, adapted from Moriasi, Arnold, and Van Liew (2007), and Jain and Singh (2003). The PBIAS and NSE levels were suggested by Moriasi et al. (2007). MARE was proposed by Wijesekera and Abeynyake (2003), primarily for their literature studies. The rankings vary from very good to unsatisfactory.

Table 2-4: General performance ratings for watershed

Performance Rating	**R^2**	**PBIAS/PVE**	**NSE**
Very good	$0.75 < R^2 \leq 1$	PBIAS ≤ ±10	0.75 < NSE ≤ 1
Good	$0.65 < R^2 \leq 0.75$	±10 ≤ PBIAS < ±15	0.65 < NSE ≤ 0.75
Satisfactory	$0.75 < R^2 \leq 0.65$	±15 ≤ PBIAS < ±25	0.50 < NSE ≤ 0.65
Unsatisfactory	$R^2 \leq 0.5$	BIAS ≥ ±25	NSE ≤ 0.5

CHAPTER 3

3 METHODOLOGY

3.1 Methodology Briefed

Research questions were determined by conducting background research on current modelling practices of the Gin River basin in Sri Lanka. The main objectives are determined based on study area information and the results. The selection of the river basin mainly considers the availability of data and the possibility of high demand for water in the future, as well as the risks of urbanization and water scarcity of the wetlands of Sri Lanka because of climate change and the reconstruction of the hydrographic basin. By representing intermediate attainment that needs to be passed to attain the overall goal, a specific goal is defined and used as a benchmark for the overall goal.

Once the objective is determined, the key aspects to study are determined as per the specific objective, and then the literature survey is carried out. First, considering research problems, adequate time, availability of data, and suitable model, an appropriate model for the study with an adequate parameter was chosen mainly from the literature review. For the desired model, a more detailed literature survey was executed to determine a suitable data period. Afterward, going through literature surveys an adequate objective function was selected to assess the efficiency of the model and an adequate method to calculate the evapotranspiration. Additionally, an earlier task relevant to the lumped model was also and the range of model parameters was determined, which is useful for sensitivity analysis model and calibration of the parameters. The literature on the warming period of one year for the model was studied, and the initial soil moisture and simple canopy, simple surface, SCS (Soil Conservation Service) unit hydrograph, and recession parameter were established for the model.

Considering the input essential of the model and using recommended methods for verification and data collection. The methods identified in the literature review were used to perform sensitivity analysis on the parameters. The data set is divided into two groups, the data ranges from 2007/8- 2011/12 is used for calibration, 2011/12 -2014/15 is used for validation, and the hydrological lump model had developed and verified accordingly. After all the parameters of the lumped model have been set, the observation data is calibrated and subsequently similar tasks for TRMM and APHRODITE gridded data continue with the same parameters and time frame. Optimization of some parameters continues, and the obtained optimized parameters value were used for model validation. Important discussions and conclusions were described based on the results of the model. On the obtained model results, the appropriate points of recommendation are enlisted.

3.2 Methodology Flowchart

The methodology flowchart for the entire study area is in Figure 3-1.

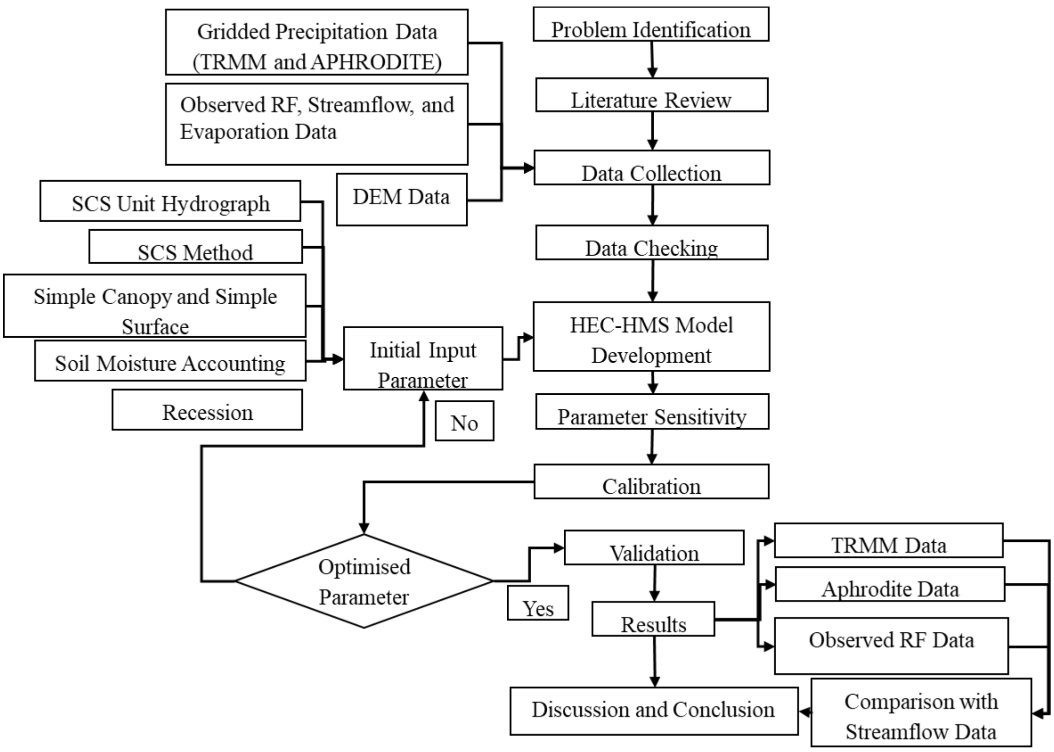

Figure 3-1: Methodology Flowchart

3.3 Project Study Area

The Gin River flows from the Gongara mountains of Deniyaya, which is over 1,300 m above sea level, and flows into the Indian Ocean in Ginthota, the Galle district of Sri Lanka. Precipitation samples in the basin are bimodal, with primary precipitation events occurring in May and September (southwest monsoon) and November and February (northeast monsoon), based on inter monsoon rainfall. The overall areas for the whole Gin Basin include natural forests and plantations, agriculture, and community settlements. Planting includes rice, tea, palm oil gum, and cinnamon.

The Gin River is the most important water resource in southern Sri Lanka, and it lies between 80°11'32.75"E, and latitudes 6°11'9.84" N. Rathnapura, Galle, Kalutara, and Matara are administrative divisions of the Gin River, with a basin area of about 716 km^2. Approximately 1.268 billion cubic meters of water are discharged from the Gin River into the sea every year (National Atlas, 2007). The mean temperature in the basin is 24℃～32℃ (Madhushankha & Wijesekera, 2021), with high humidity and sandy clay loam as the main soil texture. It is completely located in the humid region of the country and is surrounded by natural tropical rainforest.

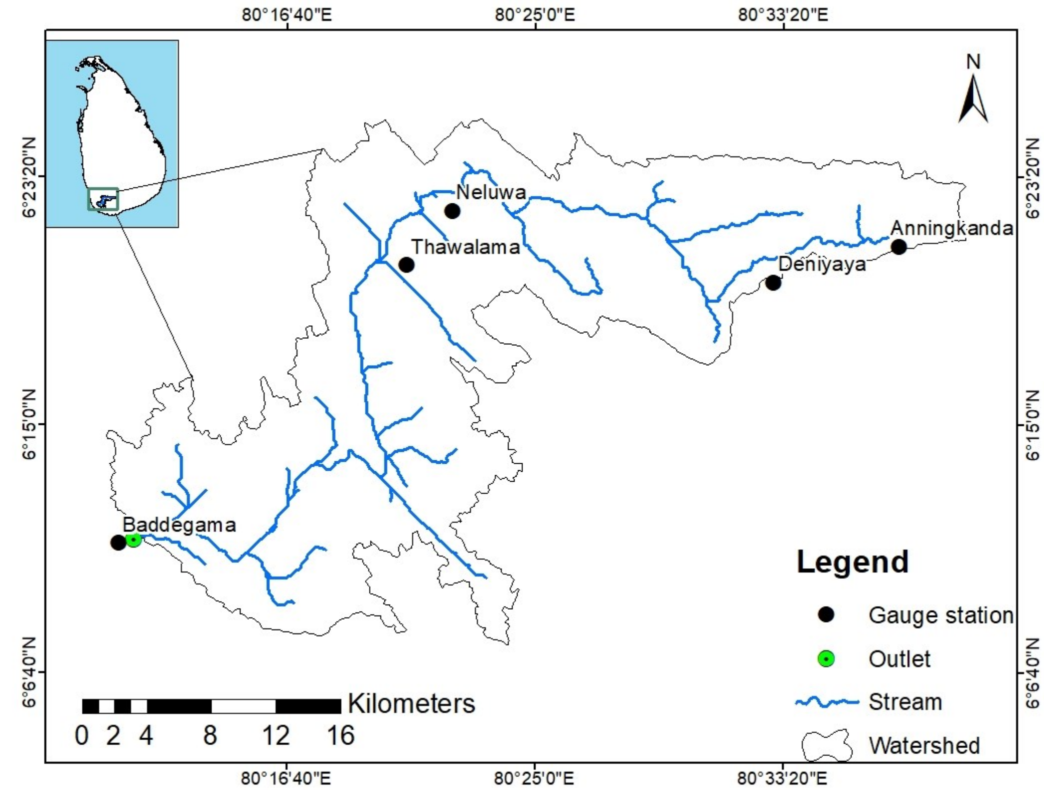

Figure 3-2: Study Area -Gin Watershed

The land-use dataset for 1998 was obtained from the Survey Department of Sri Lanka. Land use data was prepared in ARC GIS 10.5 version for the Gin Ganga watershed. Chena dominates the basin, representing 43.56%, while the area of all the pools is less coverage which represents 0.05% of the basin. When determining the curve number, the hydrological classification of the soil (Engineering Hydrology Subramanya). The weighted average CN (curve number) value 74 was calculated by averaging the CN value of each type of land use from the standard tables of the hydrological groups of soils AMC (Antecedent Moisture Conditions) II and C.

Table 3-1 shows a general summary of the watershed with a coverage area of 712 km^2 which is in the western province of Sri Lanka. It is placed in Galle and Matara district with a mainstream length of 95.9 km and a drainage density of 0.15 sq. km.

Table 3-1: Summary of Gin Watershed

Gin Watershed (sq. km)	712
Province	Southern province
District	Galle and Matara
Mainstream Length (km)	95.9
Drainage Density (km/sq.km)	0.15

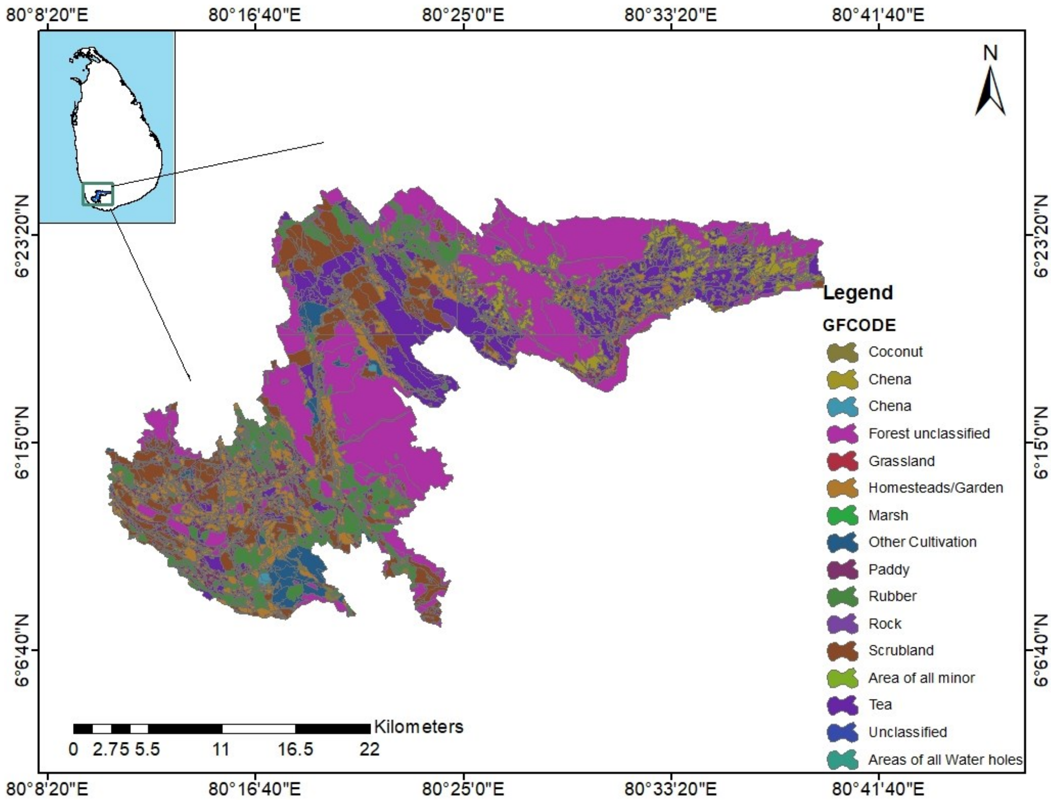

Figure 3-3: Land use (*Source: Survey Department,1998*)

3.4 General Data Collection

Precipitation, evaporation, and flow data collection were carried out according to the guidelines of the World Meteorological Organization (WMO), from the Department of Meteorology and the Department of Irrigation of Sri Lanka. These national organizations are responsible for maintaining water-based data from the above-mentioned data.

Five rainfall stations were selected for the study, namely Baddegama, Aningkanda, Deniyaya, Niluwa, and Tawalama, which are in the Gin watershed, as shown in Figure 3-2. The selected evaporation station is at Kottawa, which is nearby to the watershed. The main selection criteria for stations are data availability for the selected period and the watershed location. The verification time for data is selected from October 2007 to September 2015 (8 years).

Table 3-2: Data collected and its source

Sl. No.	Data	Year	Source of Data Collection
1	Daily rainfall data	2007 - 2015	Department of Meteorology and the Natural Resource Management Centre in Sri Lanka
2	Discharge data	2007 - 2015	Irrigation Department of Sri Lanka
3	Precipitation data	2007 - 2015	TRMM (3B42 V7) and APHRODITE (V1801R1) satellite rainfall data with a daily resolution.
4	Land Use	1998	Survey Department, Sri Lanka
5	Evaporation	2007 - 2015	Department of Meteorology and the Natural Resource Management Centre in Sri Lanka

3.5 BIAS CORRECTION

3.5.1 Linear Scaling

There are several methods to correct for distortions in precipitation projections (Schmidli et al., 2006). The purpose of the bias correction approach is to rectify the mean, variance, and/or quintile of the model time series variables using a specific correction aspect so that the time series of the corrected version closely matches the observed variables. Other methods are more complex and require a separate precipitation model. Some accurate precipitation methods are based entirely on empirical methods (Horton et al., 2006; Ines & Hansen, 2006; Leander & Buishand, 2007). In this study, a unique distortion correction technique, linear scaling (LS), and CDF (Cumulative Distribution Function) are used to correct for APHRODITE and TRMM data distortions on a daily time scale.

The following equations are used for the linear scale factor method:

$$P_{his}\ (d) * = \ P_{his}\ (d)\ X\ [\mu_m\ (P_{Obs}\ (d))/\mu_m\ (P_{his}\ \ (d))] \qquad [3\text{-}1]$$

$$P_{sim}\ (d) * = \ P_{sim}\ (d)\ X\ \left[\mu_m \frac{P_{Obs}\ (d)}{\mu_m}\left(P_{his}\ \ (d)\right)\right] \qquad [3\text{-}2]$$

where P is precipitation, d is daily, μm is the long-term monthly average, an asterisk indicates corrected bias, *his* refers to raw APHRODITE/TRMM data, and *obs* is observed data.

3.5.2 Cumulative Distribution Function

The most common and widely practiced method of bias correction (BC) is entirely on the quantile-mapping technique (Déqué, 2007; Gudmundsson et al., 2012; Haddad & Rosenfeld, 1997; Panofsky, H., 1958; Piani et al., 2010; Wood et al., 2004), mapping a model output x with cumulative distribution function (CDF) F_X, to an observation y, with CDF F_Y, through a function h, such that the two distributions are equivalent (Piani et al., 2010).

$$Y = h\ (x)\ such\ that\ F_Y\ (y) = F_X\ (x) \qquad [3\text{-}3]$$

Although h can be modeled through either parametric or nonparametric distributions and regression-like transformations [e.g., (Gudmundsson et al., 2012)], the so-called "Empirical Quantile Mapping" (EQM)—a distribution-derived nonparametric approach [e.g., (Déqué, 2007)]—is one of the most applied methods, directly deriving the corrected value y from the modelled value x:

$$Y = F_Y^{-1}(F_{X\,(x)}) \qquad [3\text{-}4]$$

3.6 Lumped Model

A lumped model was developed for the Gin Ganga watershed as it can be a great opportunity for complex physically-based models when the primary purpose is solely for streamflow prediction (Gebre, 2015). The model element, objective function, evaluation of thresholds, model evaluation criteria, calibration, and validation requirements were determined for this task by comparing other options with their relevance to the present study area. As a model structure, the whole Gin watershed represents to lumped model. The reach and junction were ignored since river routing was not considered for the lumped model.

3.6.1 Canopy Model

The model user manual states that canopy interception needs to be integrated into continuous modeling using techniques that are consistent with the soil moisture accounting (Feldman, 2000a; Scharfenberg, 2016). To view interception and evapotranspiration, one can choose a canopy component from available three strategies such as gridded simple, simple, and dynamic canopy (Feldman, 2000a). The Simple canopy is ideal for this study because of its compatibility with loss methods and its applicability to continuous methods (Feldman, 2000a).

3.6.2 Precipitation Loss Model

Various techniques are available to simulate the losses. Event modeling consists of several options such as Initial Steady, SCS CN (Soil Conservation Service Curve Number), Exponential, Green Ampt, Smith Parlange, and more. The principal in continuous modeling usually uses a loss technique that is consistent with soil moisture accounting.

3.6.3 Soil Moisture Accounting

Soil moisture calculation methods differ from other methods such as various whole-based SCS curves, using five layers: retention layers, depression storage surface, soil, upper groundwater, and under groundwater. One can simulate the movement of water. SCS curve number-based model focuses most on soil technology but ignores soil properties that are rarely implemented due to estimation and performance challenges, popular for parametric (Tramblay et al., 2010). The initial status of these five layers should be defined as the water content in each storage layer before simulation.

Using the Soil Moisture Accounting (SMA) algorithm, it considers the long-term watershed soil moisture balance and is suitable for simulating daily, monthly, and seasonal flows. The SMA algorithm explicitly considers all components of runoff, including direct runoff (surface flow) and indirect runoff (interflow and groundwater flow) (Ponce, 1989).

The model requires an input of daily rainfall, soil conditions, and other hydrometeorological data. The HEC-HMS SMA algorithm represents a watershed with five aquifers, namely canopy interception, surface depression, soil profile, groundwater storage, which includes twelve parameters, namely canopy interception water storage, water storage in surface depressions, maximum penetration. Storage rate, tension zone storage, soil storage, soil zone permeability and groundwater storage depth 1 and 2, storage coefficient, and permeability. Layer entrance, exit, and capacity rate control the amount of water lost or added to individual storage layers. The present storage content is determined during the simulation and is constantly changing during and between storms. Apart from precipitation, the only other input to the SMA algorithm is the evapotranspiration rate (Feldman, 2000a).

The recession curve, or receding limb of a hydrograph, can be described by Equation [3-5],

$$q_1 = q_o K_r = q_o * \exp(- \propto t) \qquad [3\text{-}5]$$

where q_0 is the initial streamflow, q_1 is the streamflow at a later time, t, K_r is a recession constant less than 1, and $\alpha = -In\ K_r$. The endorsed time stop for streamflow regression analysis is 1 day. By using the area of the shallowest slope of the streamflow hydrograph and Equation [3-6], Groundwater 2 α-value can be calculated. If the calculation consequences in any negative α-values, it can be ignored or deleted. The average of remaining α-values can be calculated for Groundwater 2 Recession Coefficient by using Equation [3-6],

$$Recession\ of\ Coefficient = \frac{1}{\propto} \qquad [3\text{-}7]$$

Using the same section of the streamflow hydrograph and Equation [3-6], the Groundwater 2 Storage depth for each step can be determined. By averaging the values for final Groundwater 2 Storage Depth can be calculated.

$$S_t = \frac{q_t}{\propto} \qquad [3\text{-}8]$$

S_t is the storage in the basin at a time, t. Repeating the same calculations using the Runoff + Interflow graph to decide the Groundwater 1 Recession Coefficient and Groundwater 1 storage depth

Table 3-3: SMA model parameter

Canopy	Initial canopy storage (%) Maximum canopy storage (mm) Crop coefficient
Surface	Initial surface storage (%) Maximum surface storage (mm)
SMA	Soil (%) Groundwater 1 (%) Groundwater 2 (%) Max infiltration rate (mm/h) Impervious (%) Soil storage (mm) Tension storage (mm) Soil percolation (mm/h) GW 1 storage (mm) GW 1 percolation (mm/h) GW 1 coefficient (h) GW 2 storage (mm) GW 2 percolation (mm/h) GW 2 coefficient (h)

3.6.4 Transform Model

HEC-HMS offers seven options for converting excess precipitation into direct runoff (Scharffenberg, 2016). The SCS approach was used because i) The SCS method adaptation is used in many environments and gives higher results. ii) The two most practical types of parameters allow for simple calculations. iii) Adequate and the supreme outcome can be generated as same as complex models (Salvadore et al., 2015).

3.6.5 Baseflow Model

Hydrograph recession analysis is popularly used in water resources planning, hydrological studies, and management (V. U. Smakhtin, 2001; Tallaksen, 1995). The most familiar applications are low water level prediction, groundwater resource estimation in catchment areas, hydrograph analysis, and precipitation runoff models. Vogel and Kroll (1992) estimated low runoff using the baseline runoff retreat parameters of the regional forecast model. Groundwater balance factors such as loss, new formation, and storage can be identified and measured based on nonlinear storage algorithms (Wittenberg & Sivapalan, 1999).

In step with the literature evaluation, calculations baseflow in many hydrological models across the sector are achieved using an exponential recession approach (Arnold et al., 1995). Before calculating the base flow, the HEC-HMS model requires two parameters, and they are the ratio of threshold discharge to K and peak. A set of rainfall and runoff data is used to estimate these two parameters.

Baseflow can be represented in five strategies for an available model. The base flow was calculated using the exponential regression method for continuous process (Ali et al., 2011) applicability, smaller parameter range, and compatibility with loss models. A study in Sri Lanka took advantage of the baseflow recession because it can be automatically reset each time a storm event occurs (Jayadeera & Wijesekera, 2019; Sampath et al., 2015; Siriwardana & Wijesekera, 2020).

3.7 Model Evaluation

The evaluation of the model is investigated on two criteria. They are 1) Annual water balance. 2) Flow duration curve (FDC) matching.

3.7.1 Annual Water Balance

For a watershed, in an interval of time Δt, continuity equation can be written as,

Mass Inflow – Mass Outflow = Change in Mass Storage

$$P - R - G - E - T = \Delta S \tag{3-9}$$

P- Precipitation, *R*- Surface Runoff, *G*- Net Ground-Water Flow, *E*- Evaporation, *T*-Transpiration, and *ΔS*- Change of Storage (Subramanya, 2008).

The above equation can be rearranged neglecting the change of storage (ΔS) in annual cycles as,

$$P - (R+G) - E - T = 0 \tag{3-10}$$

Rainfall - Stream flow = Evapotranspiration

Therefore, the Thiessen averaged rainfall minus streamflow was calculated and plotted against the annual pan evaporation to check the annual water balance for the Gin watershed.

3.7.2 Flow Duration Curve

The drift length curve characterizes the ability of the basin to absorb currents of varying amplitudes. The shape of the upper and lower flow-duration curve is especially important for assessing the characteristics of catchments and running water. The profile of the curve in the high flow area shows the type of flood regime in the basin, and the shape of the low flow zone characterizes the ability of the basin to support low flow at certain points during the dry spell. A very steep curve, showing short-term heavy runoff, is expected to cause rain-induced flooding over small catchments.

When constructing the flow duration curve, the monthly flow data are rearranged in descending order and sorted starting at one. The excess probability is calculated as follows.

$$P = 100 * [\frac{M}{(n+1)}] \qquad [3\text{-}11]$$

where, *P* = the probability that a given flow will be equalled or exceeded (% of the time), *M* = the ranked position on the listing (dimensionless), and *n* = the number of events for a period of record (dimensionless).

The probability of exceedance indicates how much percentage of a discharge value has been exceeded.

CHAPTER 4

4 DATA CHECKING AND ANALYSIS

4.1 General

For the data period considered by Gin Ganga, standard data verification methods are used to verify rainfall data, streamflow data, and evaporation data. Under data verification, visual data verification, identification and filling of missing data, consistency verification, seasonal rainfall variation, and runoff coefficient verification are performed.

4.2 Data Source

The main statistics used in this study were rainfall, runoff, evaporation, land use, and data of soil map. Precipitation and runoff datasets for the study area were retrieved from the Irrigation Department between 2007 and 2015. The data sources for the Gin River basin are shown in Table 4-1.

Table 4-1: Data source and availability

Data	Year	Source of Data Collection
Daily rainfall data	2007 -2015	Department of Meteorology and the Natural Resource Management Center in Sri Lanka
Discharge data	2007 - 2015	Irrigation Department of Sri Lanka
Precipitation data	2007 -2015	TRMM (3B42 V7) and APHRODITE (V1801R1) satellite rainfall data with a daily resolution.
Land Use	1998	Survey Department, Sri Lanka
Evaporation	2007 - 2015	Department of Meteorology and the Natural Resource Management Center in Sri Lanka

4.2.1 Thiessen Averaged Rainfall

The Thiessen polygon, also known as a Voronoi polygon, is generated around a series of points in a particular space by assigning all the locations in that space to the closest member of the set of points. Any place in the Thiessen polygon is closer than other members near the corresponding point.

This method is a graphical representation that calculates the seasonal rainfall basically on the comparative field of individual measuring stations in the Thiessen polygon network. The method proposed by Theisen (1911) assigns weighted values to each rain gauge station mainly on the rate of areas that represent the total area of the area. The depth of the precipitation of the area derived by the method represents the depth of weight.

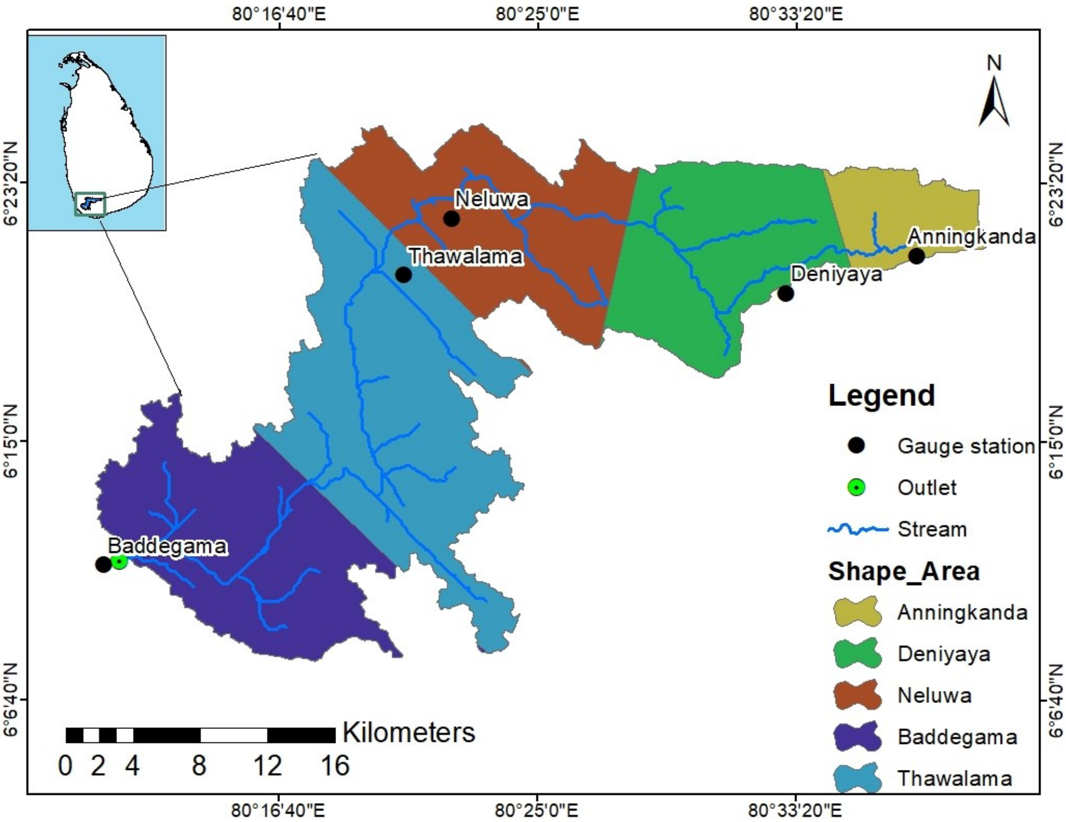

Figure 4-1: Thiessen Polygon for Gin Watershed

Table 4-2: Thiessen Polygon and its Weights for Gin watershed

Sl. No	**Station**	**Thiessen Weight for RF**
1	Anningkanda	0.20
2	Tawalama	0.25
3	Neluwa	0.17
4	Baddegama	0.20
5	Deniyaya	0.18

4.2.2 Rainfall and Streamflow

In this study, daily rainfall and discharge data were used as the primary input for a model for simulating runoff in the Gin watershed. The locations of all stations are shown in Table 4-3. The locations of precipitation and runoff stations are also shown in the location maps in Figure 3-2.

Table 4-3: Gauge station detail

Gauge Station	**Location**	**Data Type**
Baddegama	Lat: 6º 11' 03" N Lon: 80º 11' 01" E	Rainfall and Streamflow
Tawalama	Lat: 6º 20' 10" N Lon: 80º 20' 11" E	Rainfall
Anningkanda	Lat: 6 º 21' 12" N Lon: 80º 36' 53" E	Rainfall
Deniyaya	Lat: 6º 19' 48" N Lon: 80º 33' 00" E	Rainfall
Neluwa	Lat: 6º 22' 12" N Lon: 80º 22' 12" E	Rainfall

4.3 Visual Data Checking

The primary purpose of visual inspection of a dataset is to verify the response of the streamflow to rainfall, which is regarded as the significant condition of water balance modelling. The visual inspection of data is carried out in the study.

Firstly, the rainfall dataset is examined to determine the number of missing digits. According to the consensus, for a considered site, the amount of missing data must be below 10% of the total value. The percentage of missing data for the Gin watersheds shows that the percentage of missing data for all stations is less than 10%.

For the years 2007/8, 2009/10, 2013/14, and 2014/15 for water year the streamflow and rainfall were observed good responding where maximum rainfall was observed in June. For 2008/9 year it shows unmatching of streamflow and rainfall in February. The rest of the remaining graphs are included in Annexure 1.

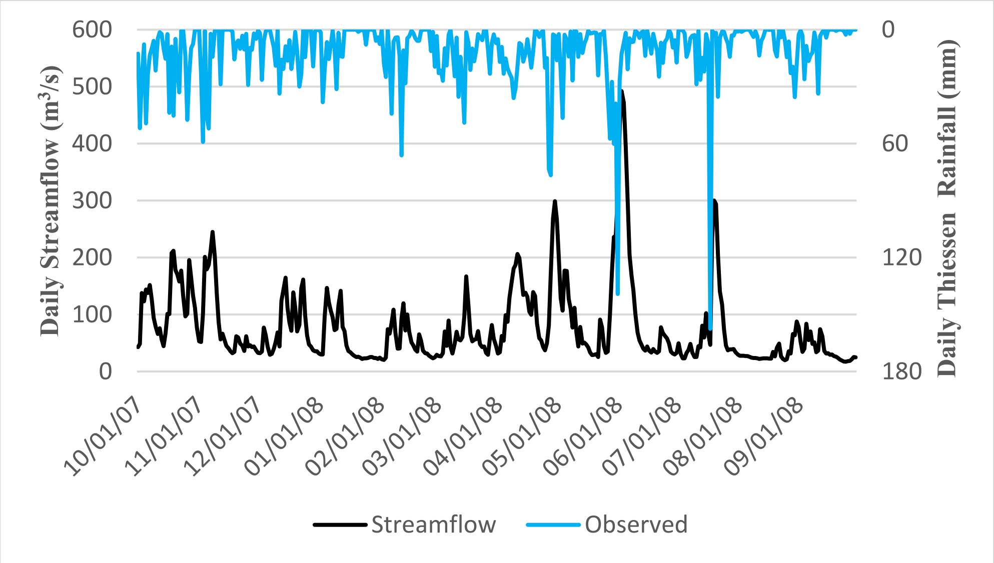

Figure 4-2: Comparison of streamflow and rainfall for 2007/8 water year

4.4 Evaporation and Runoff Coefficient

The runoff coefficient for the Gin watershed varies from 0.30 to 0.50 for the eight years for the water year of Sri Lanka. The maximum runoff coefficient was observed in 2011/12 years with a low on 2014/15 years. The evaporation record ranges from 595 mm to 914 mm for the same year as above. The maximum evaporation is illustrated in the below graph on 2011/12 with a low on 2007/8. The low evaporation is due to streamflow does not respond well to the rainfall for the particular year.

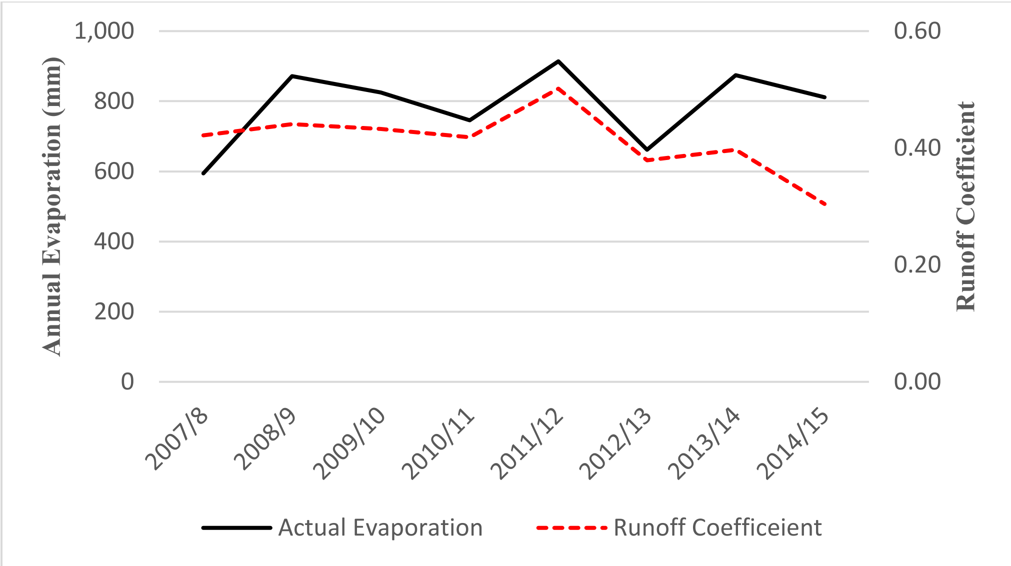

Figure 4-3: Comparison of pan evaporation and runoff coefficient

4.5 Consistency Check

All rainfall information is examined for continuity and consistency before use. Double and single mass curves were utilized as a common tool for all stations (Nalaka Gunasekara & Lanka, 2018). The double mass curve represents the cumulative total of rain gauge for the total of all gauge stations. The double mass curve of the present study is shown in Figure 4-9 and the rest are shown in Annexure 3. For a double mass curve, for a straight line, it shows consistency across all precipitation stations and shows reliable data. Conversely, if the line does not follow a straight-line pattern, Consistency shows adequate data. The generated double mass curve shows the best information consistency by following a straight sample. The individual mass curves generated also emphasize the consistency of individual precipitation stations over the entire duration of the study. From literature, the main purpose of the singles mass curve is an addition to check precipitation consistency, mass curves supplement the missing dataset. The single mass curve shows the consistency of each gauge compared to other gauges. station. As a result of these two tests, the available precipitation dataset is adequate.

Table 4-4: Summary of missing value

Station Name	Missing Value	Missing Data (%)
Precipitation		
Anningkanda	1	0.03
Tawalama	0	0
Baddegama	30	1.03
Deniyaya	155	5.31
Neluwa	183	6.26
Gridded Data		
TRMM data	0	0
APHRODITE data	0	0
Discharge		
Baddegama	1	0.03
Evaporation		
Ratnapura	261	8.93

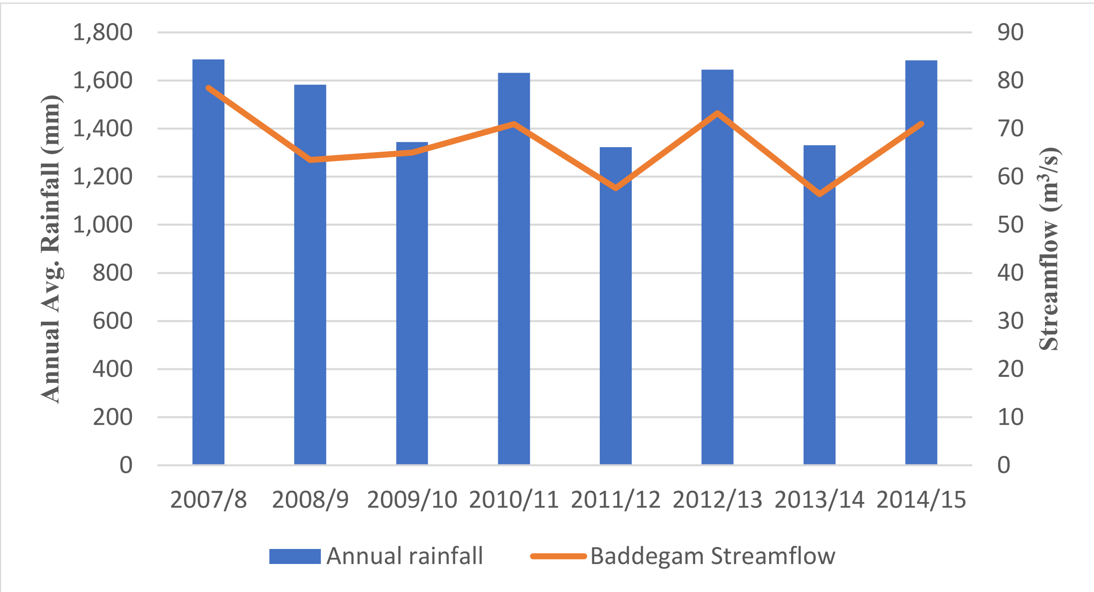

Figure 4-4: Comparison of annual streamflow and rainfall - Gin Watershed

As per the annual visual inspection of the annual river flow data, in 2009/10 it was observed a decrease in rainfall compared to the rest of the year. In 2014/15 it was observed exceeding the observed streamflow as per the rainfall for the same year. In the Anningkanda station, maximum rainfall was observed in November for 2012/13 with the least in January and February month. The maximum rainfall was observed in

2010 and minimum in the 2009 year for the Deniyaya station. In the Neluwa station, maximum rainfall was observed in December and minimum in February month. The missing data was observed from April till September. In the Tawalama station, the maximum rainfall was observed in October month and the minimum rainfall in January month. In the Baddegmaa station, the maximum rainfall was observed in May month and the minimum rainfall in January month. The rest of the remaining graphs are in Annexure 2.

Figure 4-5 shows a comparison of monthly rainfall for all the water years with two-line showing the maximum and minimum rainfall.

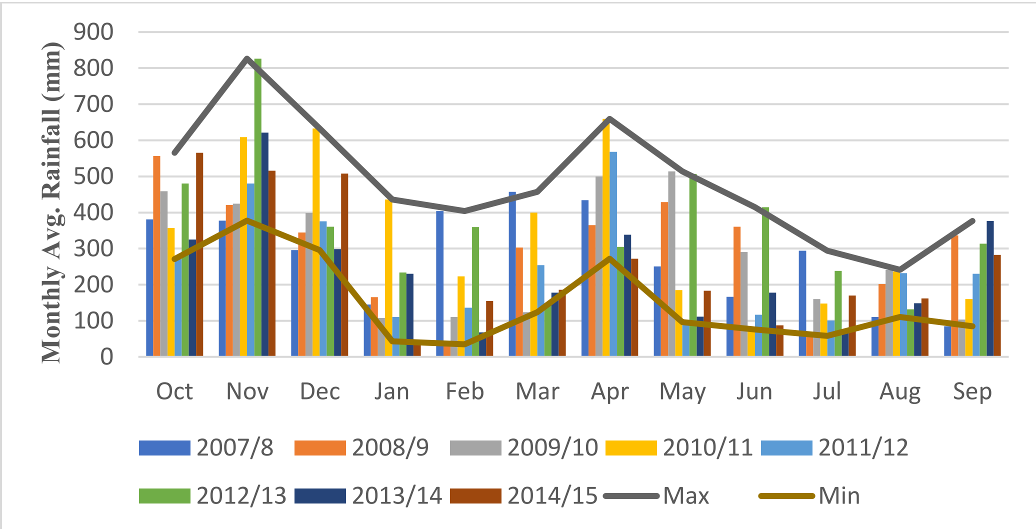

Figure 4-5: Rainfall distribution – Anningkanda station

4.6 Streamflow at Baddegama Station

The graph below shows the variation of rainfall in a water year, and it is visually compared with the maximum and minimum streamflow. The maximum rainfall was observed in November and with the least rainfall in January month.

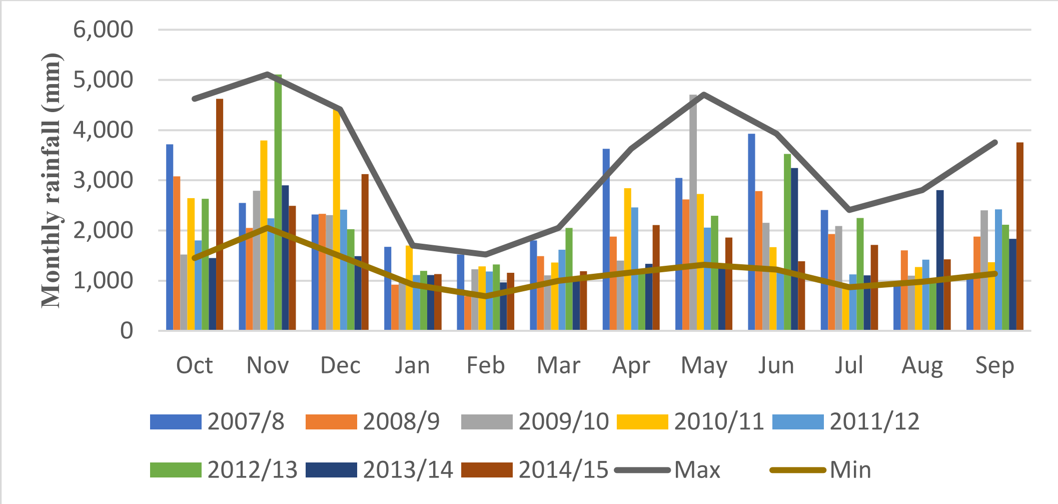

Figure 4-6: Streamflow distribution – Baddegama station

4.7 Linear Regression Method

Simple linear regression is popularly used as a statistical technique, it is a method of modelling the relationship between two sets of variables (Mao et al., 1999). The linear scaling method of bias correction was applied to the grid-based climate model data for rain gauge to predict the future climate in a decadal time frame (Shrestha et al., 2016).

Figure 4-7 shows major rainfall was observed on average of other stations compared to Anningkanda station. Among the five-station Tawalama station receive maximum rainfall. The rest of the correlations for an individual are in Annexure 3.

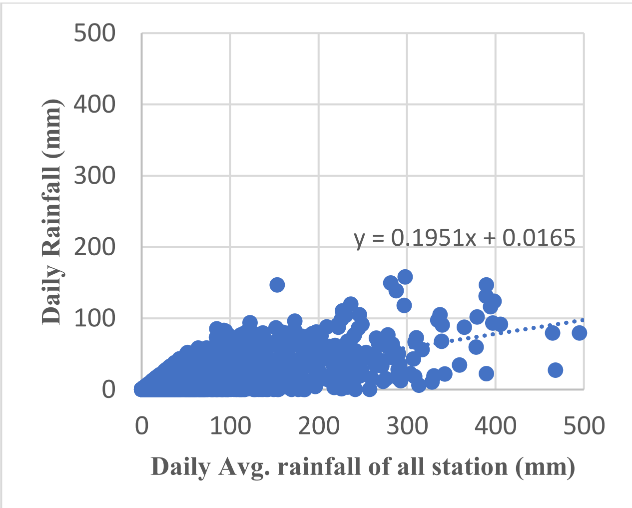

Figure 4-7: Correlation between daily observed of Anningkanda rainfall with all the average rainfall-Gin Ganga

Individual quality curves of all rainfall stations were plotted on the map to examine the consistency of the rainfall data and it was observed the maximum rainfall at Tawalama station, as shown below in Figure 4-8.

Moreover, the highest Thiessen weightage for rainfall of 0.32 was assigned as per the Thiessen polygon weightage obtained from ArcMap 10.5 GIS application. This leads to an impact on the overall consistency of Thiessen's averaged rainfall of the Thawalama station.

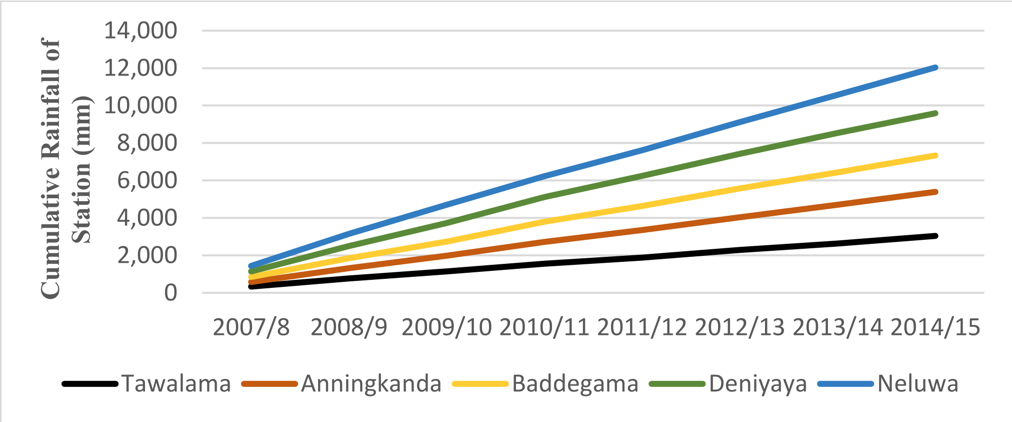

Figure 4-8: Single mass curves for all the gauging stations - Gin Ganga Watershed

4.8 Double Mass Curve Analysis

If the conditions associated with the precipitation station recording change significantly during the recording period, the station's precipitation recording may be inconsistent. The main reasons for the discrepancy could be rain gauge replacement at another suitable area, changes in the area around the station, changes in the area due to disasters, and observation errors from a certain date. The representation of the double mass curve shows discrepancies are mainly based on the double mass curve method. It is basically on the following principles. When individual measured data comes from the same parental population, they are consistent (Subramanya, 2008). Consistency if all recorded information is from the same parent population.

A double mass curve analysis was carried out for the entire rain gauge in the Gin watersheds shown in Figure 4-9. Appropriate consistent slopes were found almost everywhere except Badegama station. The rest of the double mass curve is in Annexure 4.

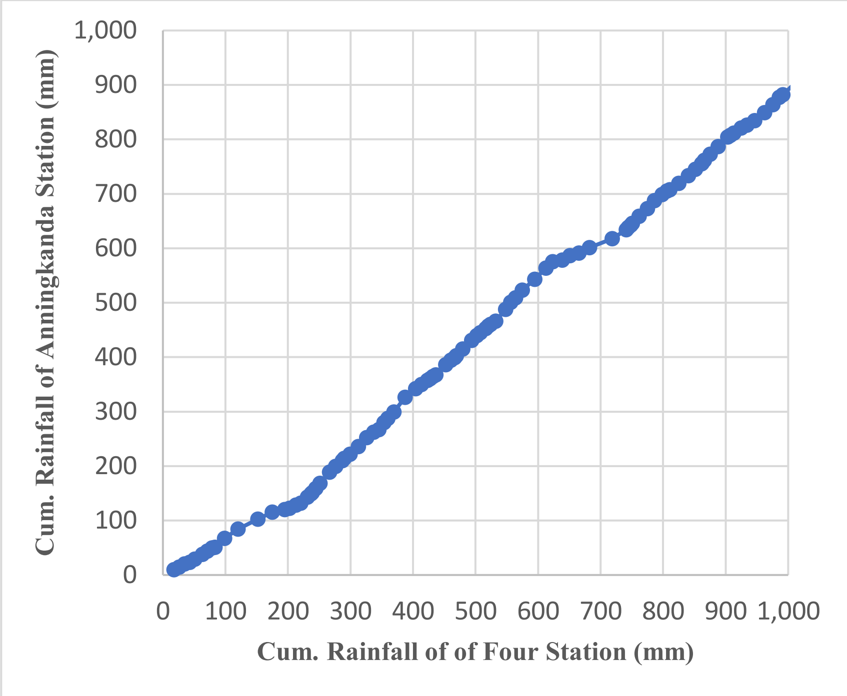

Figure 4-9: The double mass curve - Anningkanada station

Figure 4-10 shows underestimation for both gridded precipitation data while comparing for the monthly cumulative rain gauge, TRMM, and APHRODITE data.

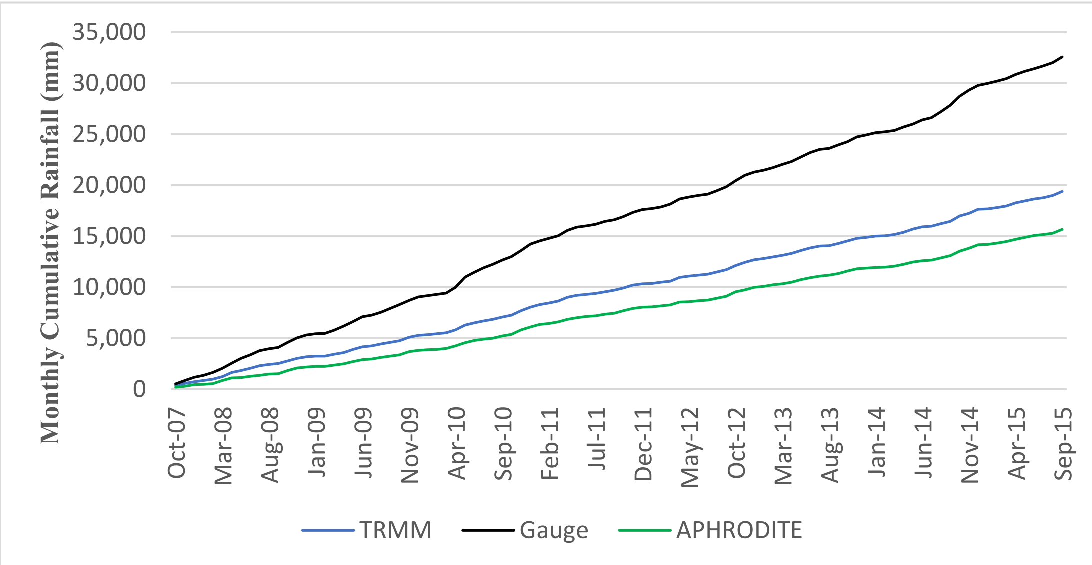

Figure 4-10: Comparison of cumulative gauge, TRMM, and APHRODITE data

Figure 4-11 is an alternative way to compare the gridded dataset against the observed data. The reflected graph below shows the variation when compared to observed data for raw gridded precipitation data.

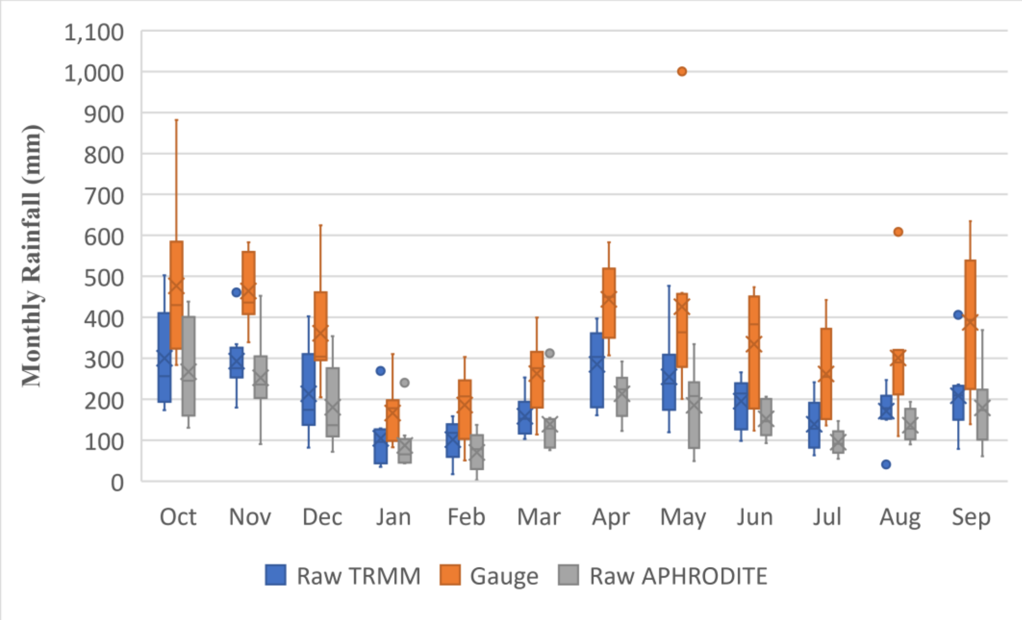

Figure 4-11: Comparison of monthly observed, TRMM, and APHRODITE data

4.9 Cumulative Distribution Function (CDF)

The two graphs below in Figure 4-12 and Figure 4-13**Error! Reference source not found.** show two gridded precipitation (TRMM and APHRODITE data) that get close to gauge data after bias correction.

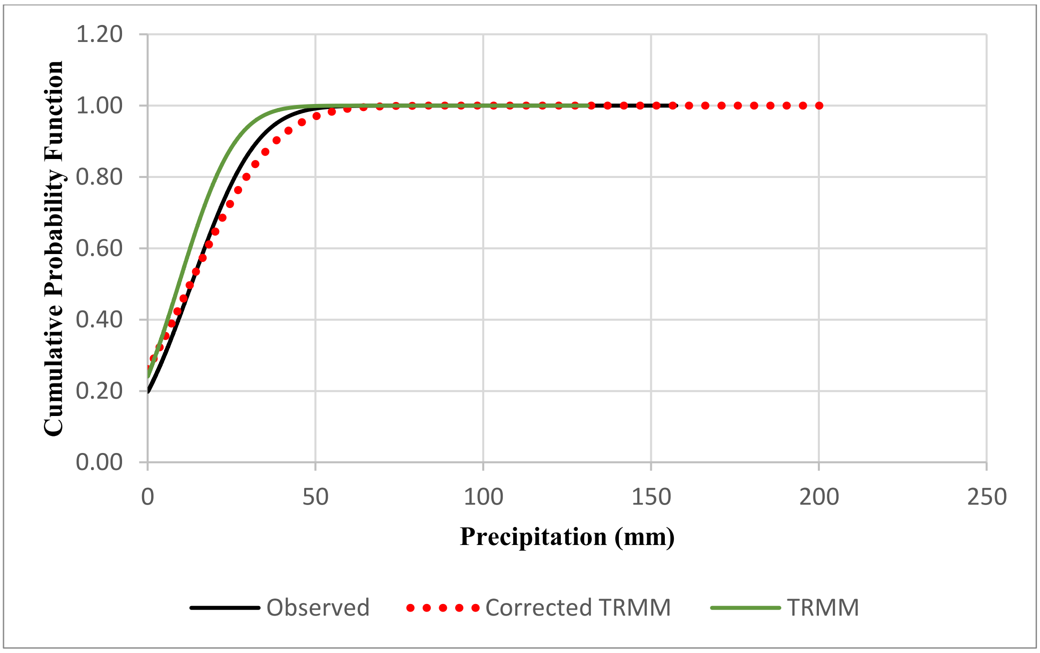

Figure 4-12: Corrected TRMM data get close to observed data after correction

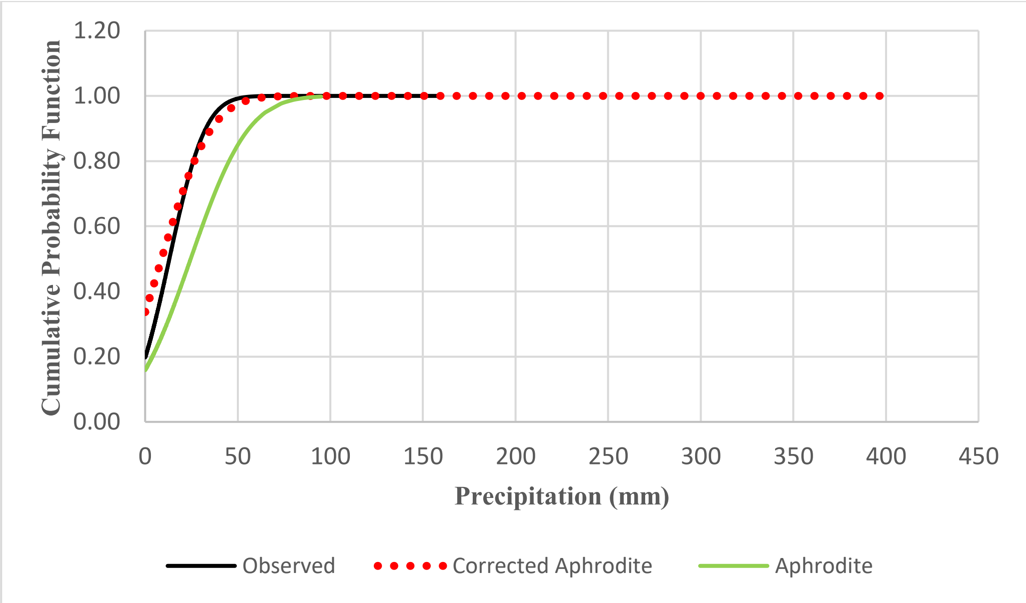

Figure 4-13: Corrected APHRODITE data get close to observed data after correction

4.10 Correlation Between Observed and Gridded Precipitation Data

The below normal graph is plotted for raw and corrected gridded precipitation data with observed data in a scatter plot. The correlation of determination improves from 0.76 to 0.78 on a monthly scale after bias correction of raw TRMM data shown in Figure 4-15. The APHRODITE data improves to 0.66 from 0.64 after bias correction as shown in Figure 4-17.

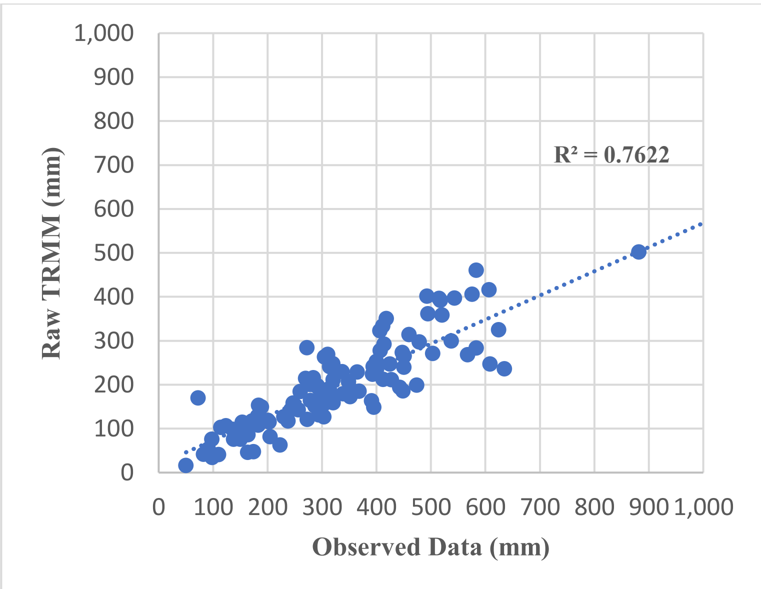

Figure 4-14: Correlation between observed and raw TRMM data

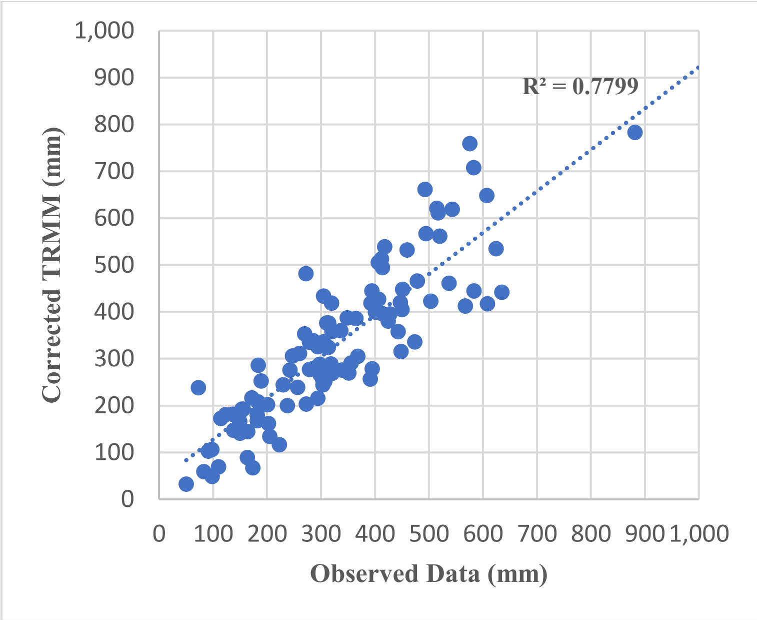

Figure 4-15: Correlation between observed and corrected TRMM data

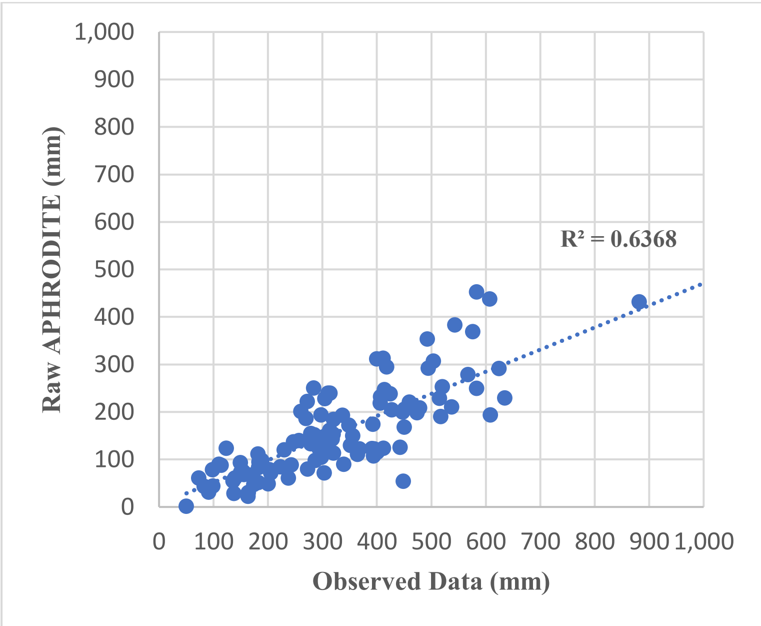

Figure 4-16: Correlation between observed and raw APHRODITE data

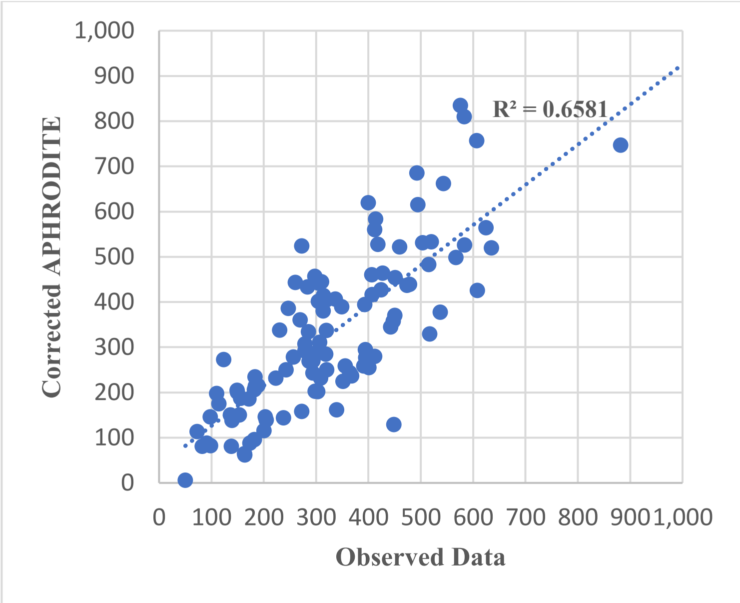

Figure 4-17: Correlation between observed and corrected APHRODITE data

4.11 Comparison of Raw Gridded Precipitation Data with Observed Station

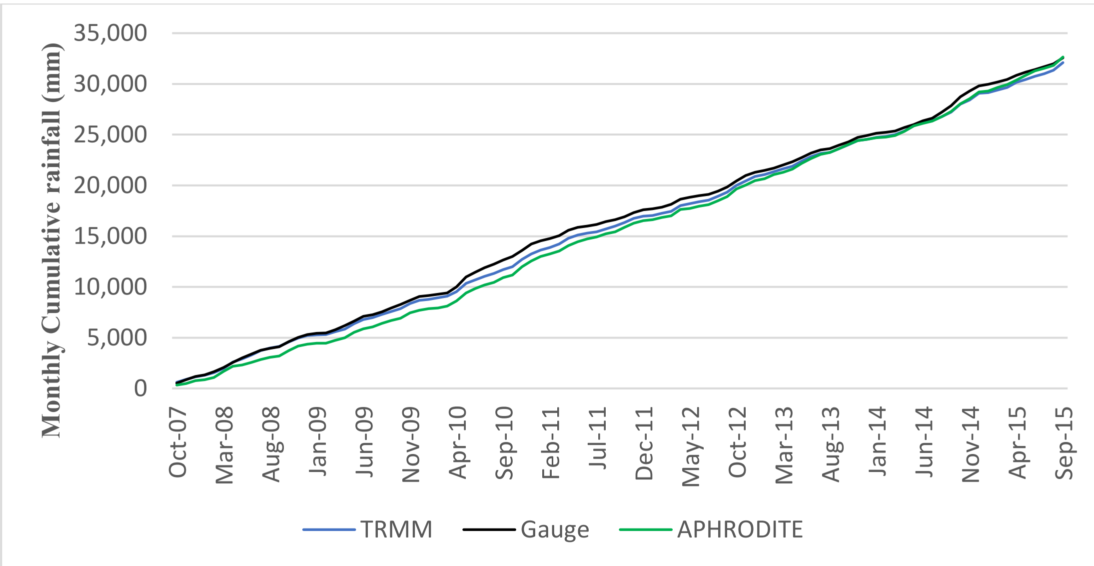

Figure 4-18: Comparison of monthly cumulative rainfall of gauge and gridded precipitation data

The overall graphs show improvement after using linear scaling and cumulative distribution function for the gridded precipitation data. The above graph represents TRMM data shows close approximate to observed rainfall data when compared to APHRODITE data. Figure 4-19 shows a comparison of corrected gridded precipitation data to observed rainfall data in a box plot.

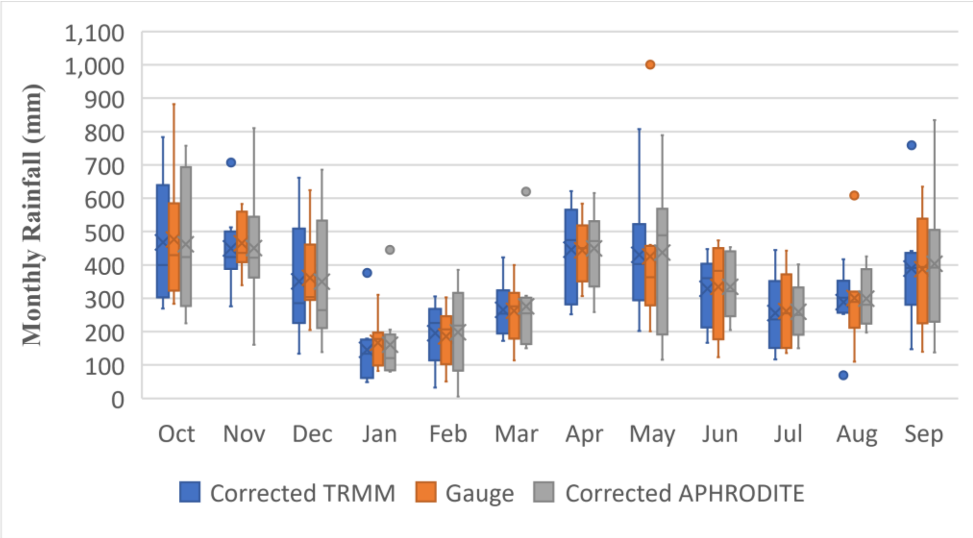

Figure 4-19: Comparison of monthly rainfall of observed and gridded precipitation data

4.12 Dry and Wet Spell Comparison

The dry spell is taken as less than one millimeter including zero from the rainfall data set obtained from the globe at the resolution of 0.25° x 0.25° for the study area. The graph below shows APHRODITE gridded data show close to approximate observed data when compared to TRMM gridded data as shown in Figure 4-20 and Figure 4-21.

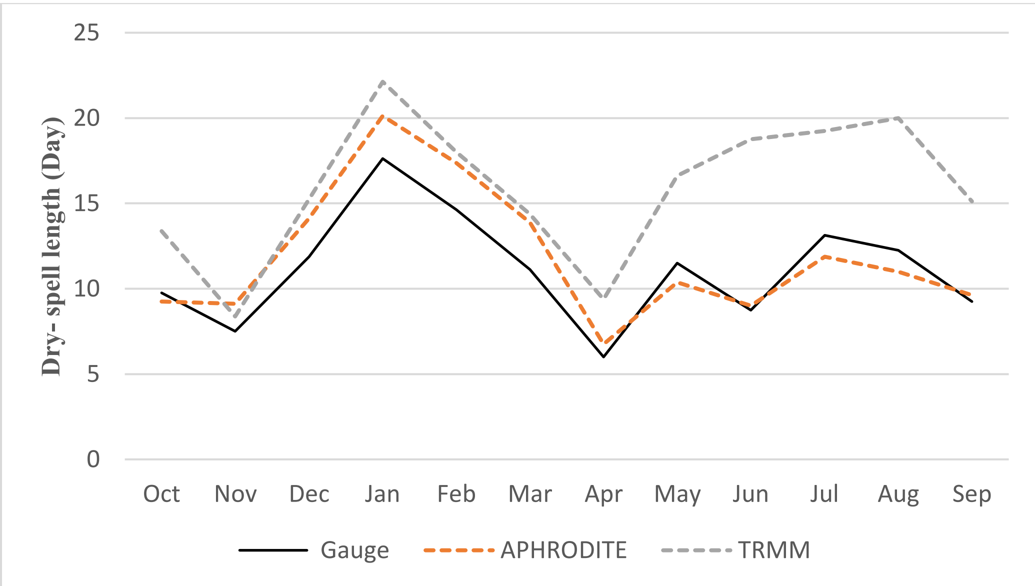

Figure 4-20: Monthly rainfall of rain gauges and gridded rainfall products in the 2007/8–2014/15 period -Dry spell length

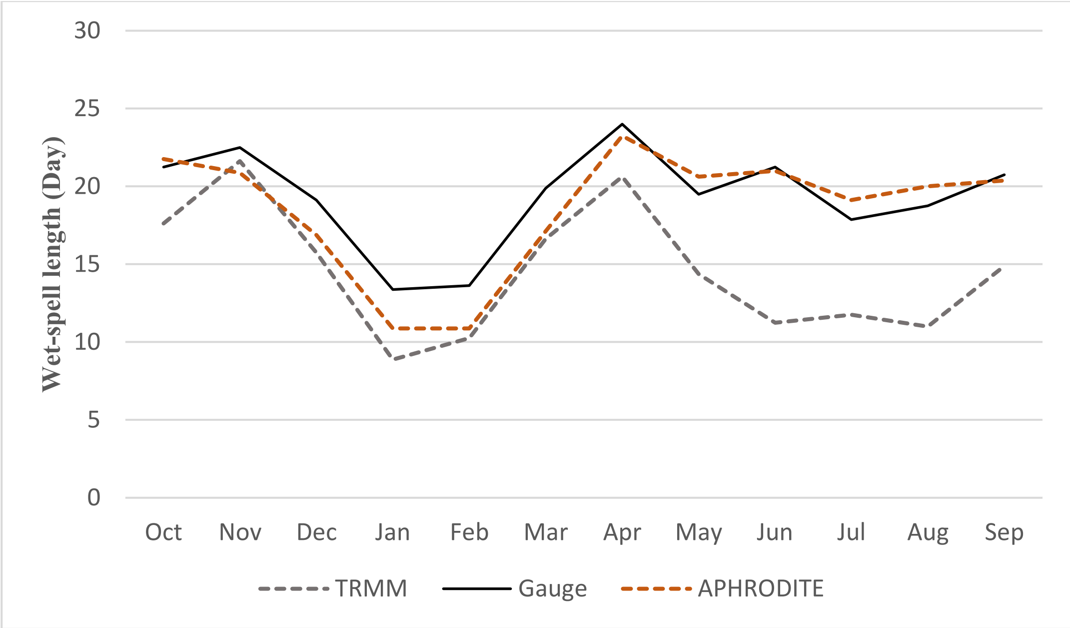

Figure 4-21: Monthly rainfall of rain gauges and gridded rainfall products in the 2007/8–2014/15 period - Wet spell length

Table 4-5 shows both gridded precipitation data shows close approximate to rain gauge in terms of average rainfall. The coefficient of determination and correlation is low on the daily scale.

Table 4-5: Summary of statical value comparison for observed and gridded precipitation data – Daily scale

Precipitation Product	Daily					
	Average (mm)	Stdv	Max. (mm)	Min. (mm)	R^2	Correlation
Observed RF	11.15	16.05	172.60	0		
TRMM	11.15	21.69	260.31	0	0.37	0.61
APHRODITE	11.18	16.81	168.87	0	0.10	0.31

Table 4-6 shows both gridded precipitation data shows close approximate to rain gauge in terms of average rainfall on a monthly scale. The coefficient of determination and correlation is good for the daily scale. The maximum precipitation obtained from two gridded precipitation show underestimation.

Table 4-6: Summary of statical value comparison for observed and gridded precipitation data – Monthly scale

Precipitation Product	Monthly					
	Average (mm)	Stdv	Max. (mm)	Min. (mm)	R^2	Correlation
Observed	339.29	167.62	1,000.33	50.26		
TRMM	339.29	167.72	798.94	30.53	0.76	0.88
APHRODITE	340.14	180.02	834.30	5.64	0.64	0.80

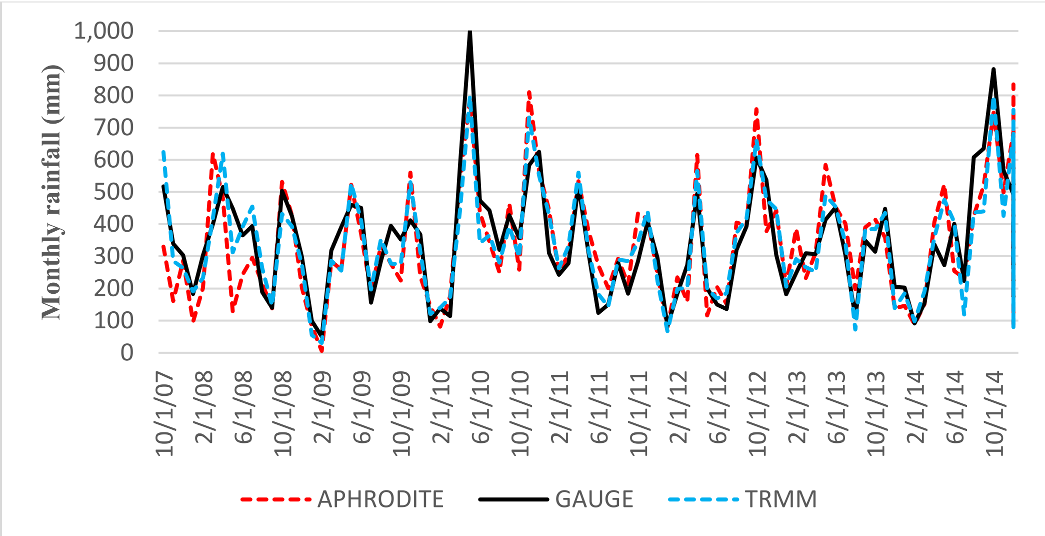

Figure 4-22: Comparison of observed and gridded precipitation data after bias correction

4.13 Annual Water Balance

Figure 4-23 shows the differences between annual rainfall and streamflow show over the entire period. Most of the years show overestimation of rainfall except 2014/15 year shows underestimation.

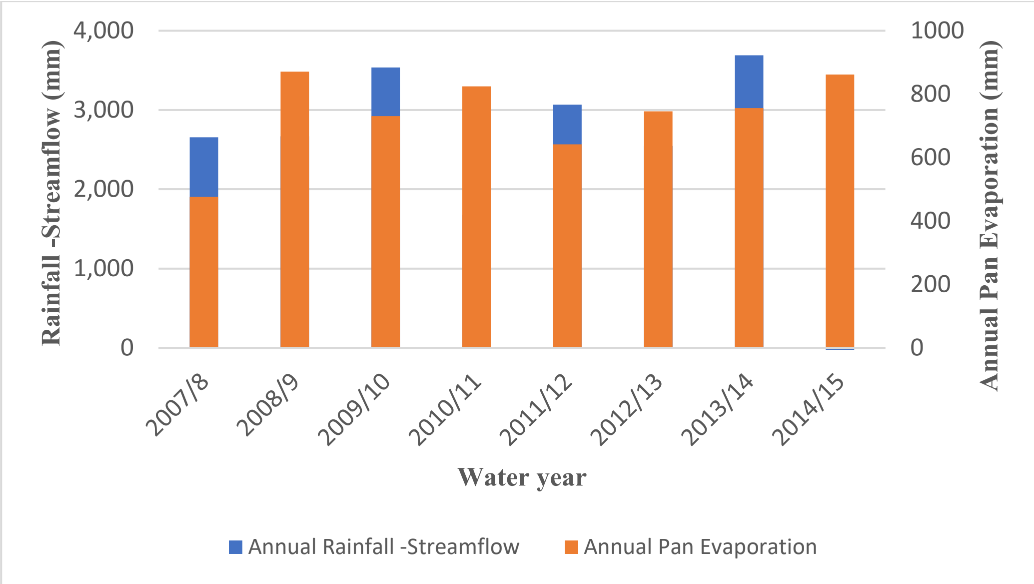

Figure 4-23: Annual water balance - Gin Watershed

Monthly and annual runoff coefficients were obtained by dividing streamflow by Thiessen averaged rainfall and plotted against the corresponding Thiessen averaged rainfall. The identified periods with data errors were further verified with the annual plot of the runoff coefficient as shown in Figure 4-24.

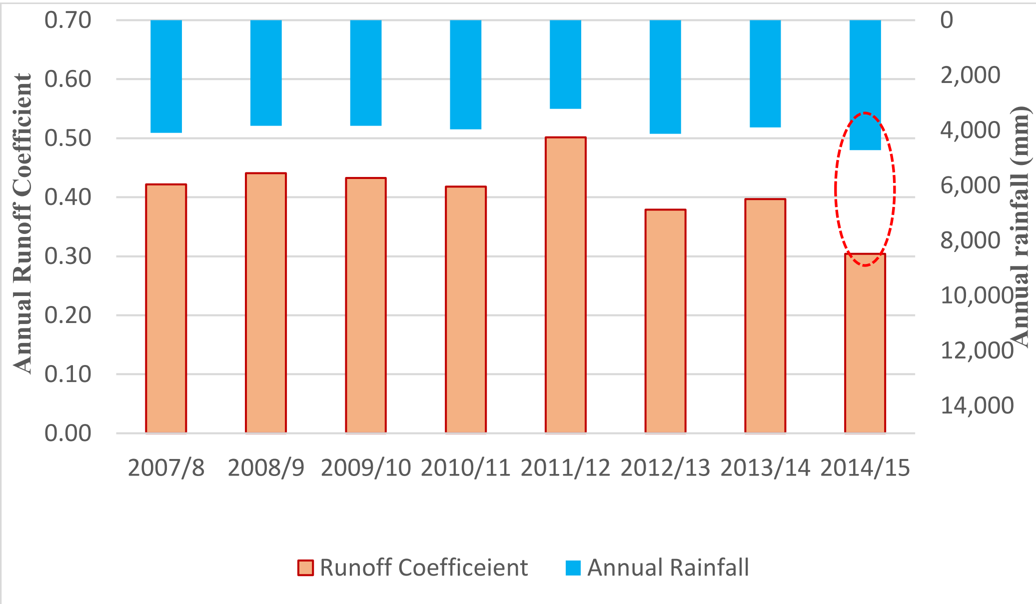

Figure 4-24: Annual runoff coefficient versus rainfall – Gin Watershed

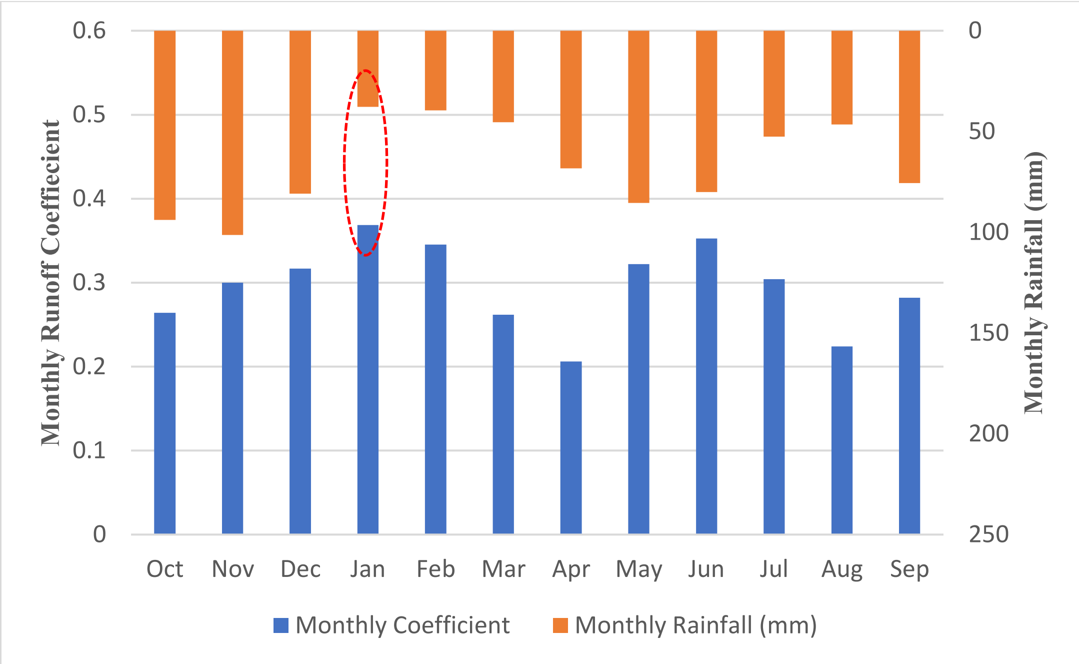

Figure 4-25: Monthly runoff coefficient vs. rainfall - Gin Watershed

Table 4-7 shows a comparison of the statical value calculated from the Gin watershed annually, monthly, and seasonally.

Table 4-7: Annually, monthly, and seasonally runoff coefficient

Runoff Coefficient	**Gin Watershed**			
	Annually	**Monthly**	**Season**	
			Maha	**Yala**
Average	0.41	0.30	0.37	0.39
Stdv	0.06	0.05	0.11	0.07
Max.	0.50	0.37	0.54	0.45
Min.	0.30	0.21	0.22	0.27

CHAPTER 5

5 MODEL DEVELOPMENT AND APPLICATIONS

The Hydrologic Modelling System (HEC-HMS) is developed for the simulation of streamflow from the watershed. The lumped model was chosen as it is aligned with my objective study. Based on the literature review, simple surface, simple canopy storage, soil moisture accounting, SCS unit hydrograph, and recession were selected for the study purpose.

5.1 Simple Surface

As per the HEC-HMS user's manual, this approach is a simple illustration of the soil surface. All precipitation or precipitation through -fall that reaches the soil surface is collected in a storage tank until the surface's storage capacity is filled. When water is present in the storage, water in surface storage infiltrate into the soil. This means that water will infiltrate even if the storage is not full. Surface runoff occurs when the storage capacity is full and the amount of precipitation through- the fall rate exceeds the infiltration rate. Equation 5-1 is used to generate maximum storage for the watershed.

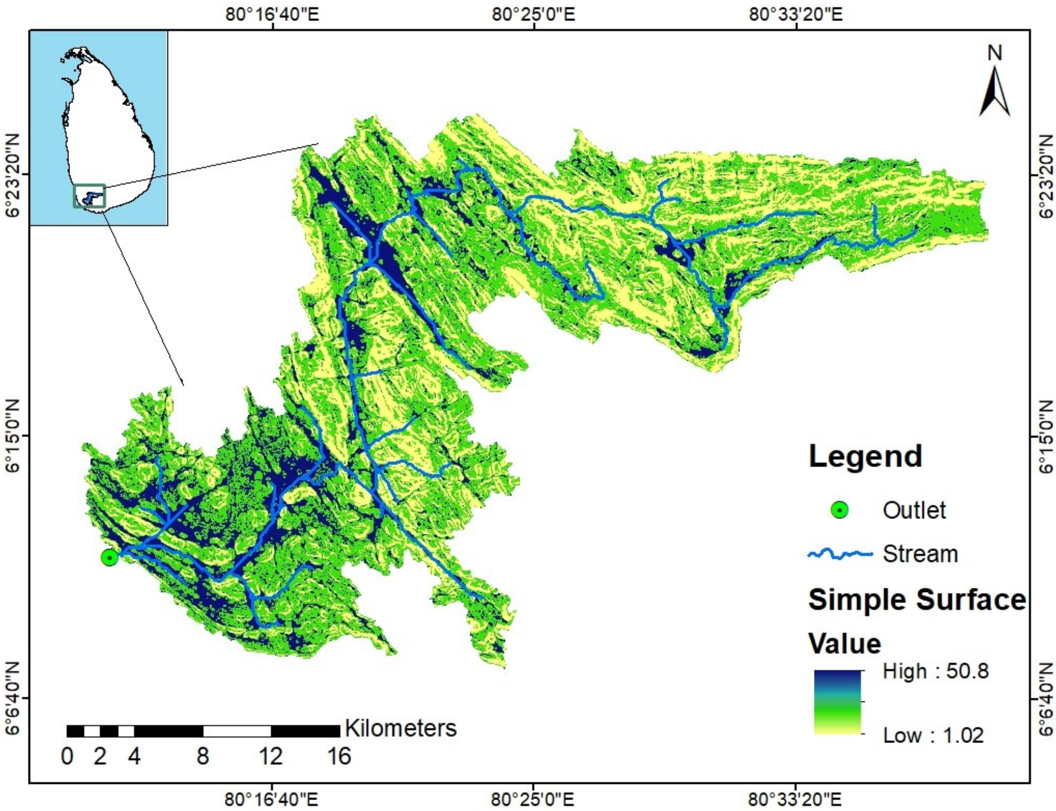

Figure 5-1: Canopy storage for the Gin Watershed (*Source: Esri 2020 Land Cover*)

Table 5-1 shows the calculation of the curve number for Gin watershed by using land use map, 1998 where forest unclassified have a maximum percentage with 202.35 km^2 and least with 0.25 km^2.

Table 5-1: Calculation of curve number - Gin Watershed

Description	Area (sq.km)	Curve no	C*A
Coconut	2.45	84.00	205.62
Chena	32.10	84.00	2,696.40
Forest - Unclassified	202.25	58.00	11,730.65
Grassland	0.50	74.00	37.08
Homesteads/Garden	72.80	79.00	5,751.05
Other cultivations	16.58	90.00	1,491.81
Paddy	46.49	95.00	4,416.48
Rubber	45.62	84.00	3,831.98
Rock	0.59	91.00	53.71
Scrub land	58.00	64.00	3,711.69
Areas of all Minor Streams	5.92	91.00	538.45
Tea	70.45	90.00	6,340.42
Areas of all Water holes	0.25	91.00	22.70
Grand Total	553.98	1,075.00	40,828.04
Curve number for watershed	74		

The potential abstraction for the simple surface was calculated by the following equation.

$$S = \frac{25{,}400}{CN - 254} \quad [5\text{-}1]$$

Where, S - potential abstraction (mm) and CN - Curve number

Table 5-2 shows the calculation of maximum storage of 89.2 mm and according to literature initial constant was taken 1.27 mm/hrs.

Table 5-2: Calculation of maximum storage for Gin watershed

Watershed	CN number	Maximum Storage (mm)	Initial constant rate (mm/hrs.)
Gin Watershed	74	89.24	1.27

5.2 Simple Canopy Storage

This value can be very small due to the Gin watershed's high impervious percentage of 44%. The initial retention of the canopy was estimated through optimization, considering both the dry and rainy seasons to determine evapotranspiration. The average canopy interception resulting for the study area is 1.01 mm as shown in Table 5-4.

Table 5-3: Calculation of maximum storage for Gin Watershed (Source: Bennett & Peters, 2004)

Vegetation Type	**Canopy Interception (mm)**
General vegetation	1.27
Grasses and deciduous trees	2.032
Trees and coniferous tree	2.54

Table 5-4: Calculation of canopy interception for Gin Watershed

Land Use Classification	**Canopy Interception (mm)**
Water	0
Tree	1.27
Grass	2.03
Flood Vegetation	1.27
Crop	2.03
Scrub/shrub	2.03
Built Area	0.00
Bare ground	0.00
Average (mm)	**1.08**

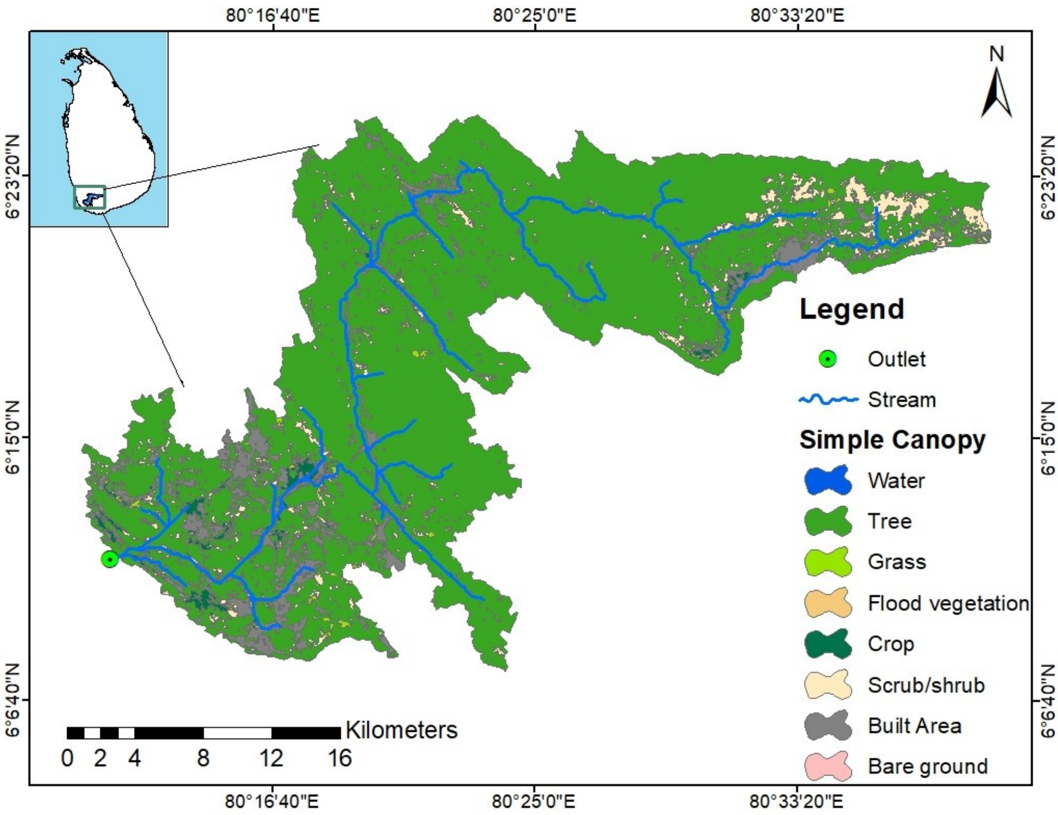

Figure 5-2: Simple canopy for Gin watershed

5.3 Baseflow Computation

According to Holberg (2014), three to four streamflow data for different storm events was chosen during the different months of the year. The storms are isolated where the streamflow hydrograph is allowed to return to normal for a few days earlier than runoff from the next storms occur. The free storm of three number analysis is taken from collected data as shown in Table 5-5. The optimum values for K and R were established by the calibration procedure.

Table 5-5: Chosen free storm period from a data set

Sl. No.	**Free Storm Data Set**
1	30th January 2010 till 2nd February 2010
2	29th January 2011 till 7th January 2011
3	18th December 2013 till 28th December 2013

The following three free storms were chosen from data collected for the calculation of baseflow for the study area.

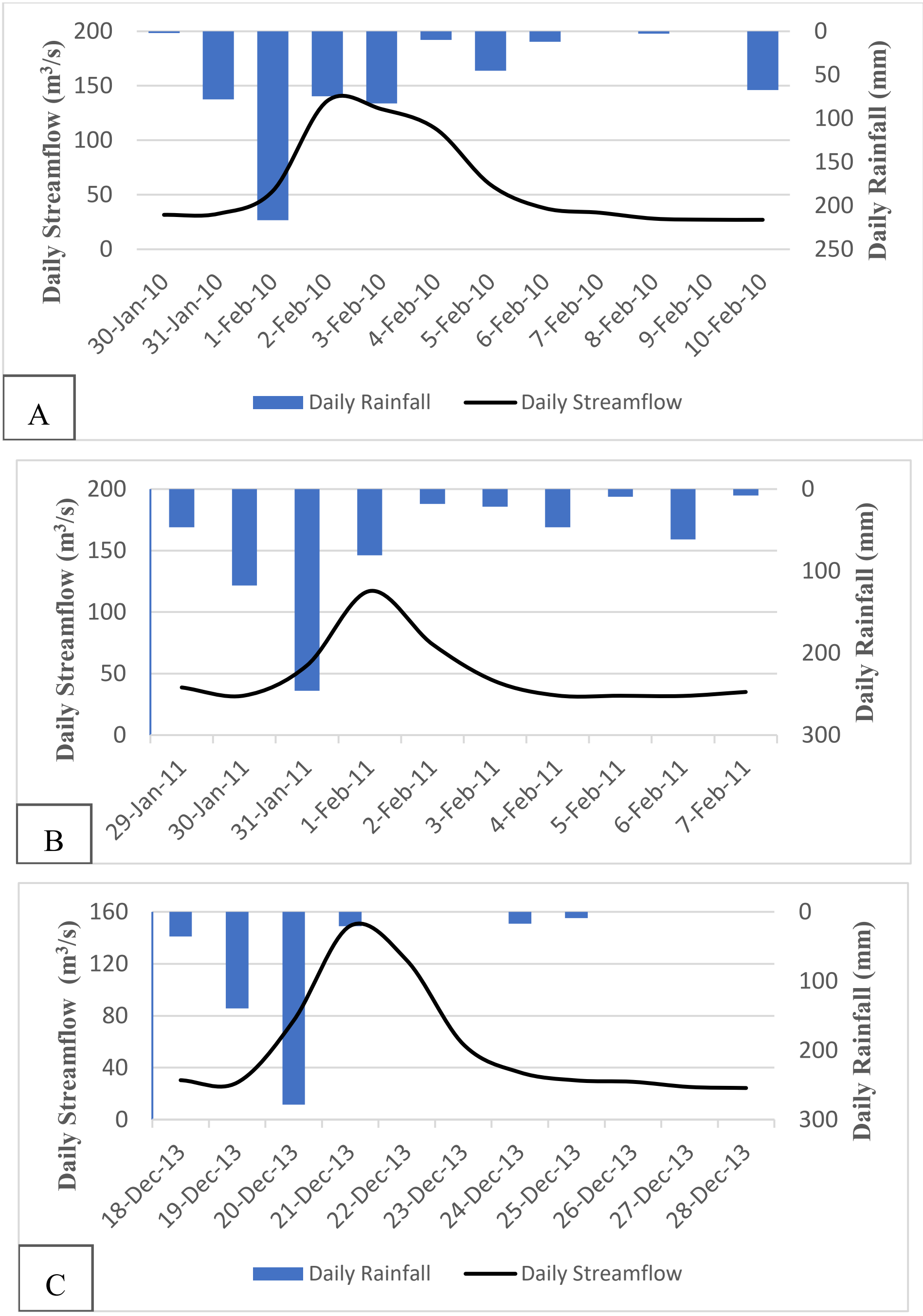

Figure 5-3: Selected hydrograph for baseflow computation – Gin Watershed

Table 5-6, Table 5-7, and Table 5-8 show the determination of groundwater 1 and 2 recession coefficient, and groundwater storage for all the chosen storms for the watershed. From the daily stream, baseflow and interflow were calculated.

Table 5-6: Calculation of groundwater 1 and 2 recession coefficient, groundwater 1 and 2 storages for storm A

Date	Daily Thiessen Rainfall (mm)	Daily Streamflow (m^3/s)	Baseflow (mm)	GW2 Recession Constant	GW2 storage (mm)	GW1 Recession coefficient	Interflow and Runoff (mm)	GW1 Recession constant	GW1 storage (mm)
30-Jan-10	1.90	31.60							
31-Jan-10	78.10	32.68	32.00				0.68		
1-Feb-10	216.50	53.54	43.00				10.54		
2-Feb-10	74.60	136.14	54.00				82.14		
3-Feb-10	82.80	128.54	56.00				72.54	0.29	52.14
4-Feb-10	10.00	110.33	49.00	0.13	366.95	1.00	61.33	1.00	5.48
5-Feb-10	45.30	59.24	40.00	0.20	197.10	1.21	19.24	0.83	2.89
6-Feb-10	12.00	37.68	37.00	0.08	474.59	1.09	0.68	0.92	1.05
7-Feb-10	0.00	33.58	33.00	0.11	288.44		0.58		
8-Feb-10	2.60	28.14	27.50	0.18	150.83		0.64		
9-Feb-10	0.00	27.17							
10-Feb-10	67.50	27.05							

Table 5-7: Calculation of groundwater 1 and 2 recession coefficient, groundwater 1 and 2 storages for storm B

Date	Daily Thiessen Rainfall (mm)	Daily Streamflow (m^3/s)	Baseflow (mm)	GW2 Recession Constant	GW2 storage (mm)	GW1 Recession coefficient	Interflow and Runoff (mm)	GW1 Recession constant	GW1 storage (mm)
29-Jan-11	46.50	38.75							
30-Jan-11	117.40	32.15	31.00				1.15		
31-Jan-11	245.90	56.69	30.00	0.03	914.92		26.69		
1-Feb-11	80.90	117.13	29.00	0.03	855.42		88.13		
2-Feb-11	18.00	73.90	28.00	0.04	797.92	0.96	45.90	1.04	18.19
3-Feb-11	21.50	43.77	27.00	0.04	742.42	0.93	16.77	1.07	6.06
4-Feb-11	46.70	32.15	26.00	0.04	688.92	0.90	6.15	1.11	1.95
5-Feb-11	9.50	32.00	25.00	0.04	637.42	0.89	7.00	1.12	0.62
6-Feb-11	61.40	31.84							
7-Feb-11	7.80	35.07							

Table 5-8: Calculation of groundwater 1 and 2 recession coefficient, groundwater 1 and 2 storages for storm C

Date	Daily Thiessen Rainfall (mm)	Daily Streamflow (m^3/s)	Base flow (mm)	GW2 Recession Constant	GW2 storage (mm)	GW1 Recession coefficient	Interflow and Runoff (mm)	GW1 Recession constant	GW1 storage (mm)
29-Jan-11	46.50	38.75							
30-Jan-11	117.40	32.15	31.00				1.15		
31-Jan-11	245.90	56.69	30.00	0.03	914.92		26.69		
1-Feb-11	80.90	117.13	29.00	0.03	855.42		88.13		
2-Feb-11	18.00	73.90	28.00	0.04	797.92	0.96	45.90	1.04	18.19
3-Feb-11	21.50	43.77	27.00	0.04	742.42	0.93	16.77	1.07	6.06
4-Feb-11	46.70	32.15	26.00	0.04	688.92	0.90	6.15	1.11	1.95
5-Feb-11	9.50	32.00	25.00	0.04	637.42	0.89	7.00	1.12	0.62
6-Feb-11	61.40	31.84							
7-Feb-11	7.80	35.07							

Saturated hydraulic conductivity and porosity based on soil texture were taken from Table 5-9 and the type of soil for the Gin watershed was taken from Table 5-10.

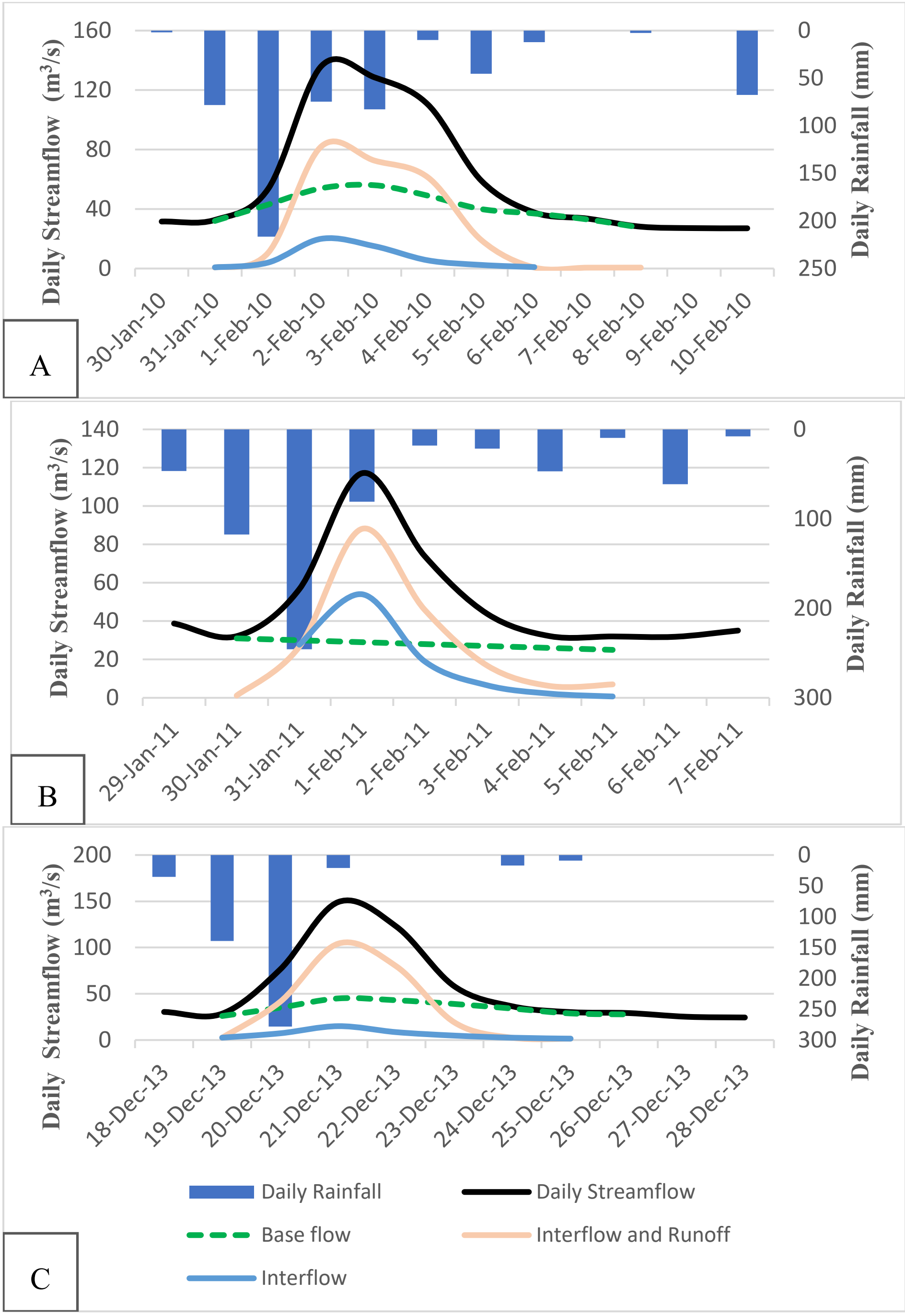

Figure 5-4: The three selected events for streamflow recession analysis

5.4 Soil Moisture Accounting

Soil maps of the Gin River basin to the Baddegama river station were obtained at a scale of 1: 50,000 by the Survey Department of Sri Lanka. From an agricultural point of view, the developed soil maps were divided into three soil types, as shown in Figure 5-5.

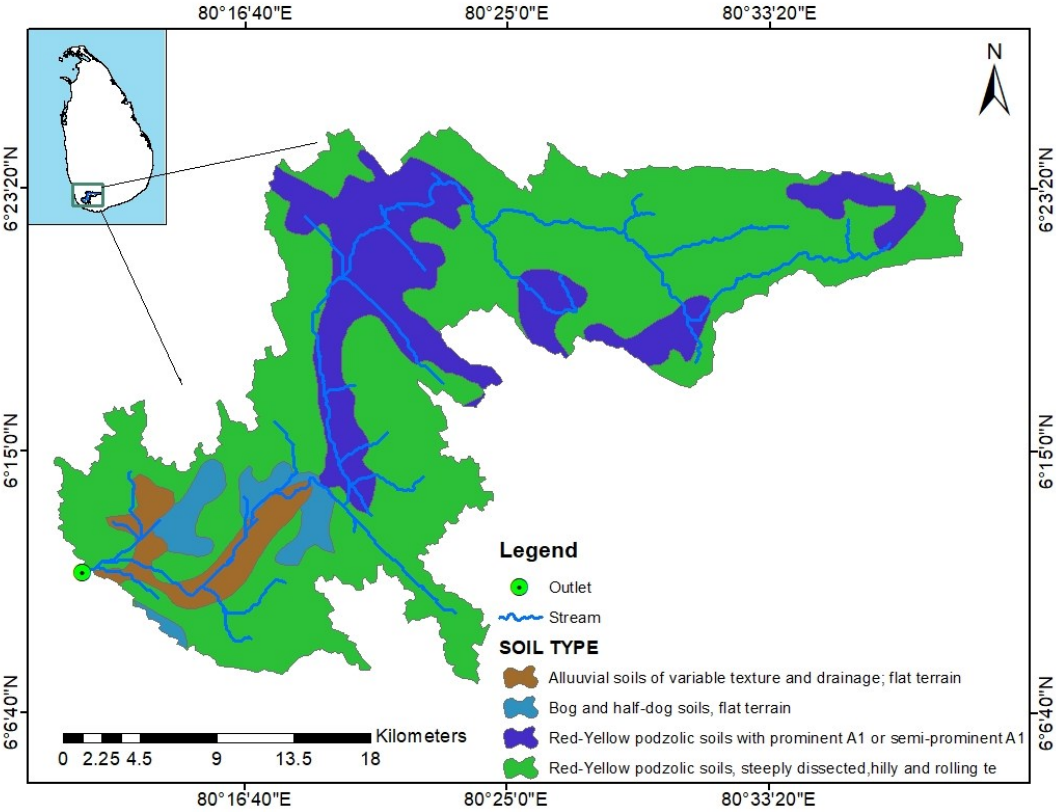

Figure 5-5: Soil map of Gin Watershed

Table 5-9: Saturated hydraulic conductivity and porosity based on the soil texture (Rawls et al., 1983)

Texture	**Saturated hydraulic conductivity (in/hr)**	**Porosity (in^3/in^3)**
Sand	4.6	0.42
Loamy Sand	1.2	0.4
Sandy Loam	0.4	0.41
Loam	0.1	0.43
Silt Loam	0.3	0.49
Sandy Clay Loam	0.06	0.33
Clay Loam	0.04	0.31
Silty Clay Loam	0.04	0.43
Sandy Clay	0.02	0.32
Silty Clay	0.02	0.42
Clay	0.01	0.39

The three types of soil were present in the Gin watershed and average porosity was calculated by taking information from Table 5-10.

Table 5-10: Soil type calculation (Rawls et al., 1983)

Soil Type	**Soil Horizons**	**Depth (in)**	**Soil Texture**	**Sat. HC (in/hr.)**	**Porosity (in^3/in^3)**	***Avg. K_{sat} (cm/hr.)***	***Avg. Porosity***
Bog and half-dog soils, flat terrain	Horizon 1	4	Sandy loam	0.40	0.41	*2.03*	*0.41*
	Horizon 2	48	Sandy loam	0.40	0.41		
Red, Yellow Podzolic	Horizon 1	3	Sandy clay loam	0.06	0.33	*0.06*	*0.32*
	Horizon 2	15	Sandy clay	0.02	0.32		
	Horizon 3	23	Sandy clay	0.02	0.32		
	Horizon 4	39	Clay	0.01	0.39		
Alluvial Soil	Horizon 1	15	Clay	0.01	0.39	*0.05*	*0.41*
	Horizon 2	24	Silty Clay Loam	0.04	0.43		

5.5 SCS Unit Hydrograph

$$T_c = \left[\frac{L}{VX60} + 15\right] \text{Minutes} \qquad [5\text{-}2]$$

Lag time is the most convenient parameter in the SCS-UH method and was determined by considering the relationship between lag time and a time of concentration. The time of concentration (T_C) is determined by using the Kirpich method. In Sri Lankan Equation [5-2] is widely used for the calculation of the time of concentration. The basin lag time was calculated to be 3,000 minutes.

5.6 Recession

The recession baseflow model contains three parameters such as the initial flow rate, recession constant, and peak ratio. On this, the ratio to the peak was assumed to be 0.06. The groundwater flow recession constant is 0.95 by choosing from the typical values proposed for the types of catchments of 300 km^2 to 1,600 km^2 (Feldman, 2000a). Initial streamflow at the beginning was taken as the initial baseflow value (Ahbari et al., 2018).

Table 5-11: Optimized value

	Parameter	**Unit**	**Initial value**	**Optimized value**
1	Recession - Ratio to Peak		0.06	0.08
2	SCS Unit Hydrograph - Lag Time	min	3,000.00	3,249.30
3	Simple Canopy - Max Storage	mm	1.08	1.20
4	Soil Moisture Accounting - GW1 Percolation	mm/hr.	0.10	0.10
5	Soil Moisture Accounting - GW1 Storage	mm	30.00	28.47
6	Soil Moisture Accounting - GW1 Storage Coefficient	hr.	1.00	1.03
7	Soil Moisture Accounting - GW2 Percolation	mm/hr.	0.10	0.11
8	Soil Moisture Accounting - GW2 Storage	mm	35.00	37.43
9	Soil Moisture Accounting - GW2 Storage Coefficient	hr.	1.00	1.05
10	Soil Moisture Accounting - Initial GW1 Content	%	30.30	32.16
11	Soil Moisture Accounting - Initial GW2 Content	%	9.00	9.88
12	Soil Moisture Accounting - Initial Soil Content	%	10.00	10.99
13	Soil Moisture Accounting - Max Infiltration	mm/hr.	0.91	0.80
14	Soil Moisture Accounting - Soil Percolation	mm/hr.	0.18	0.24
15	Soil Moisture Accounting - Soil Storage	mm	300.00	321.21
16	Soil Moisture Accounting - Tension Storage	mm	1.00	1.07
17	Recession - Initial Discharge	m^3/s	21.00	22.62
18	Recession - Recession Constant		0.89	0.95

Table 5-11 values are obtained after calibration and selection of a suitable range for eighteen parameters as in the table. In the objective part, minimization and root mean square error was chosen for goal and statistics respectively. The period was selected the same as the calibration period for the model. The optimized value is used in the validation of the model.

CHAPTER 6

6 RESULTS AND ANALYSIS

6.1 Model Calibration for Simulated Observed Rainfall

6.1.1 Overall Calibration Comparison of Simulated Observed Rainfall Against Gauge Data (2007/8 -2010/11)

Figure 6-1 shows the comparison of simulation flow against gauge data of streamflow for the calibration period. The observed simulation flow shows a similar pattern to the gauge station of streamflow with some variation. The peak flow for simulated observed rainfall exceeds to gauge streamflow. A possible reason may be due to the overestimation of precipitation at the local rain gauge. A possible reason is that the local sparse rain gauge network may not completely capture the center of the precipitation storm, which may lead to the underestimation of high runoff.

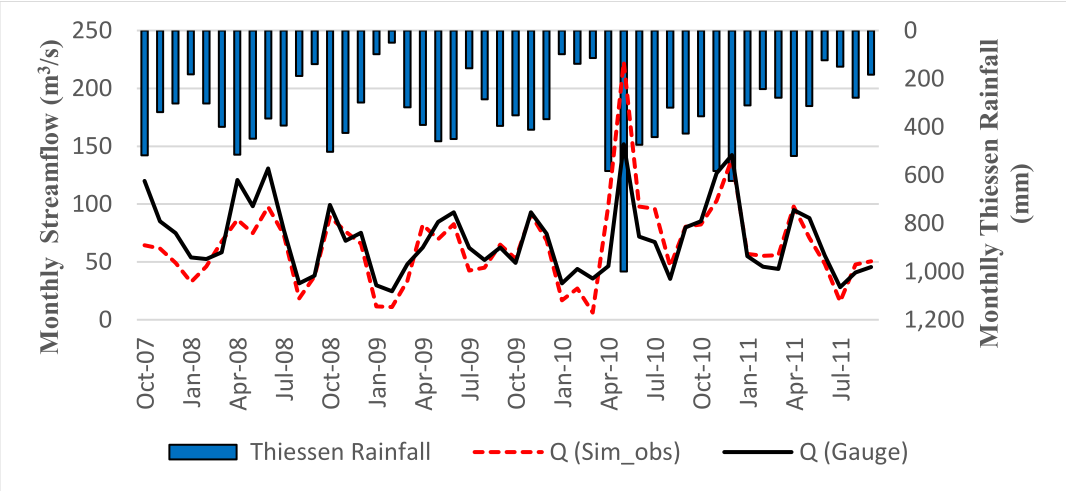

Figure 6-1: Monthly calibration for simulated of observed rainfall against gauge data – Gin Watershed

6.1.1.1 Daily Comparison of Simulated Flow from Thiessen Rainfall Against Gauge Data – Normal Plot

Figure 6-2 and Figure 6-3 show the comparison of monthly calibration for simulated observed flow against gauge streamflow data annually. The graph is compared to a single water year from 2007/8 till 2010/11. In Figure 6-2, observed simulated flow for both graphs shows a similar pattern to gauge station of streamflow with underestimation on a few months. This may be due to being the only point source of rainfall gauge stations in the study area. Even the observed streamflow data may have some errors while recording the data. Figure 6-3 (D) shows the best fit to gauge station among the calibration period for simulated of observed rainfall while graph (C) shows least match to the gauge data due to the local rain gauge network can be very sparse. If the rainfall measurement network is sparse, the systems may not be properly recorded at the gauge station which may lead to underestimation of either rainfall or streamflow.

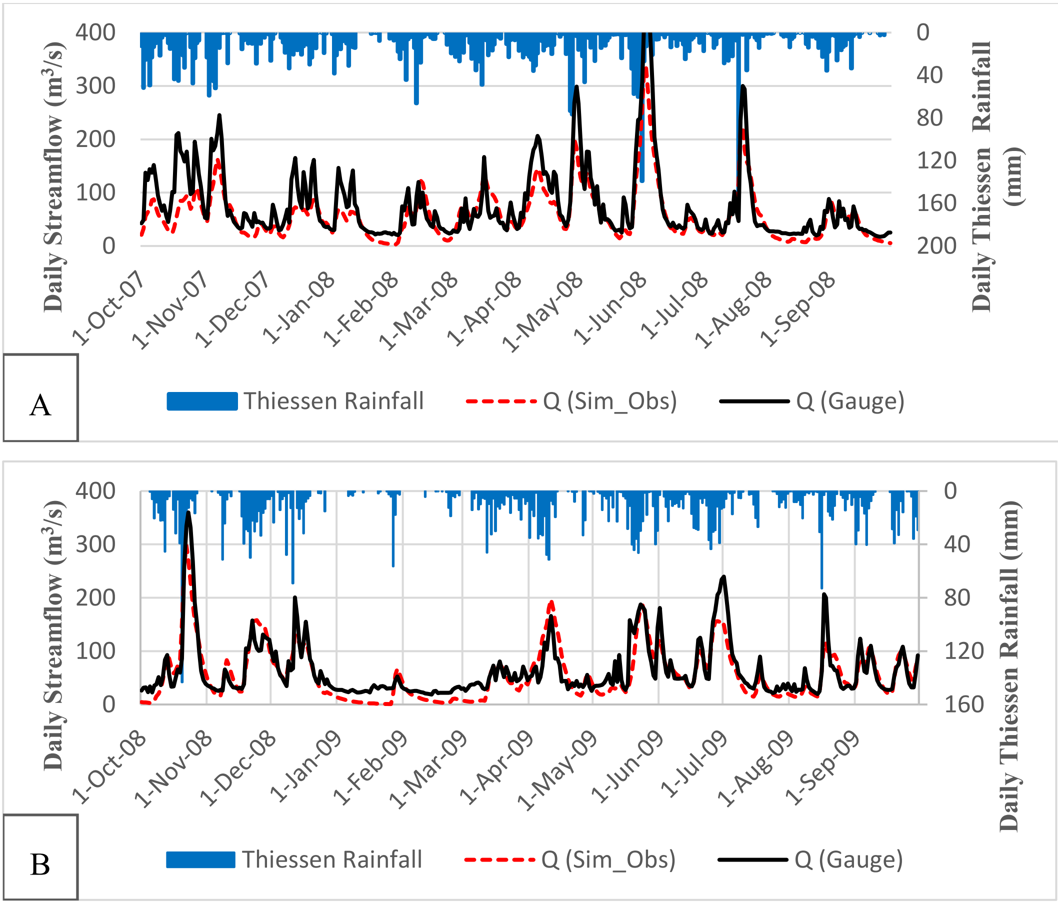

Figure 6-2: Calibration for simulated observed rainfall against gauge data (2007/8 and 2008/9)

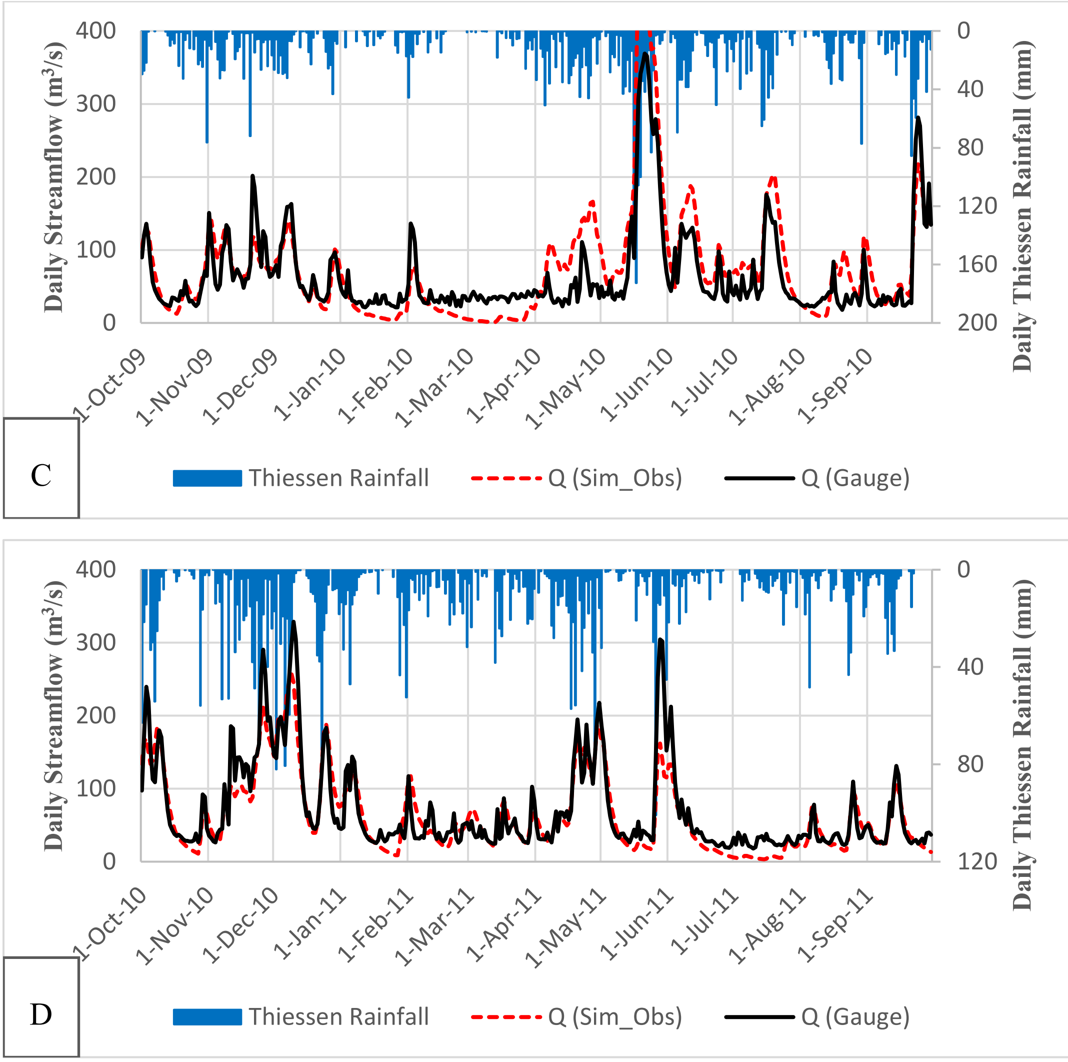

Figure 6-3: Calibration for simulated of observed rainfall against gauge data (2009/10 and 2010/11)

6.1.2 Flow Duration Curve – Calibration period

The normal flow duration curves were created for the entire calibration period (2007/8 – 2010/11). The simulated observed rainfall is underestimated in the high region and in a medium region the flow matches up to a certain extent. And the low flow is underestimated in the low regions shown in Figure 6-4 and Figure 6-5. The inconsistency in the lower streamflow maybe since the model spins-up time is short relative to the initial soil moisture.

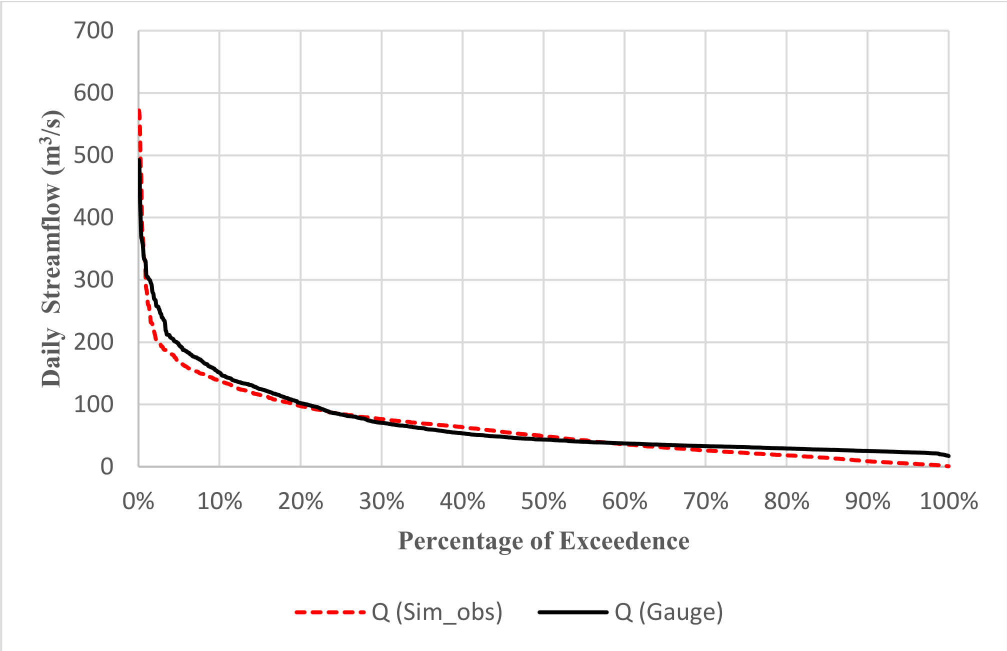

Figure 6-4: Flow duration curve for simulated of observed rainfall against gauge data for calibration period – Daily scale

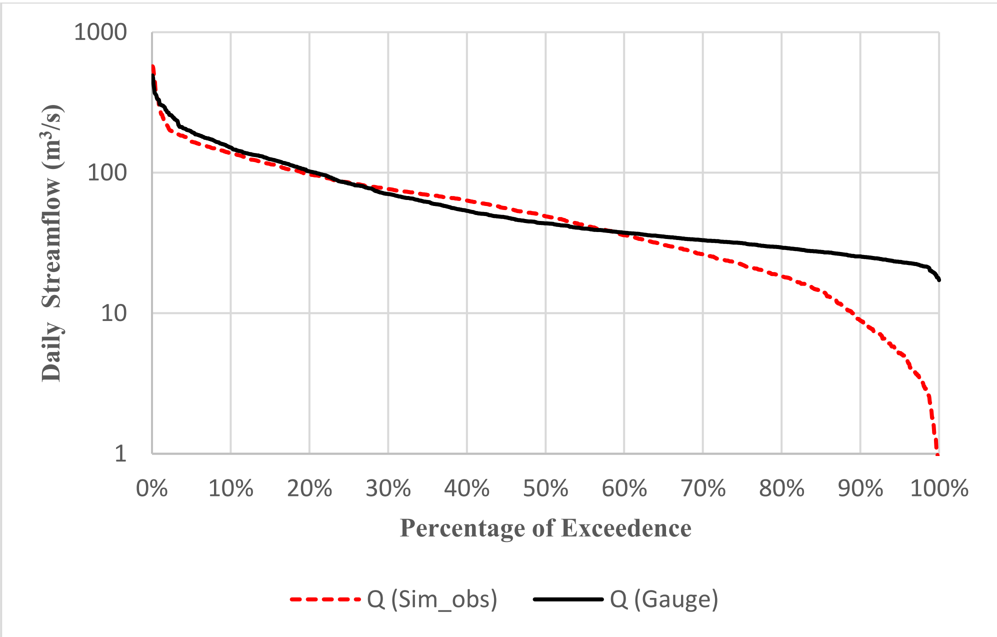

Figure 6-5: Semi log form comparison for simulated observed rainfall against stream gauge-Calibration period

The normal and semi-log scale for calibration length (2007/8 – 2010/11) for observed and simulated flow is shown in Figure 6-6 and Figure 6-7 for daily scale.

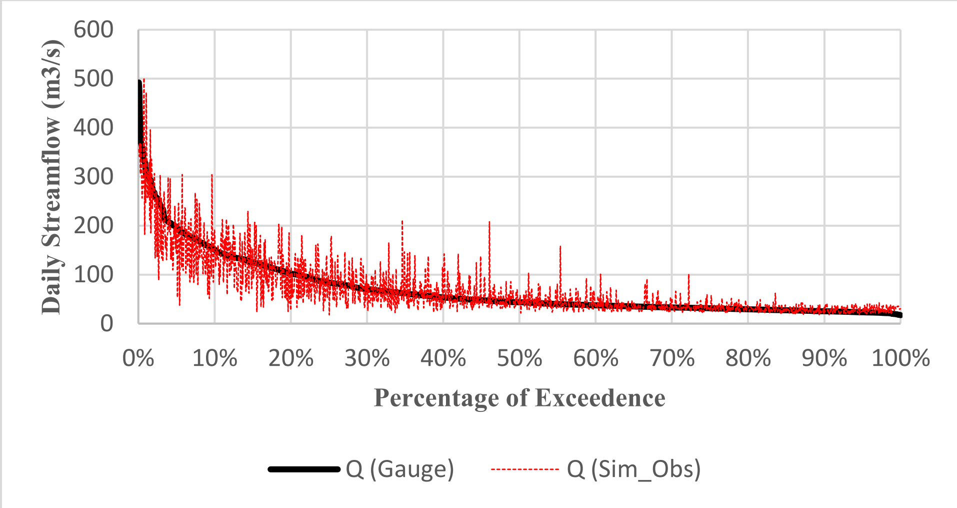

Figure 6-6: Normal FDC comparison for simulated observed rainfall against stream gauge – Calibration

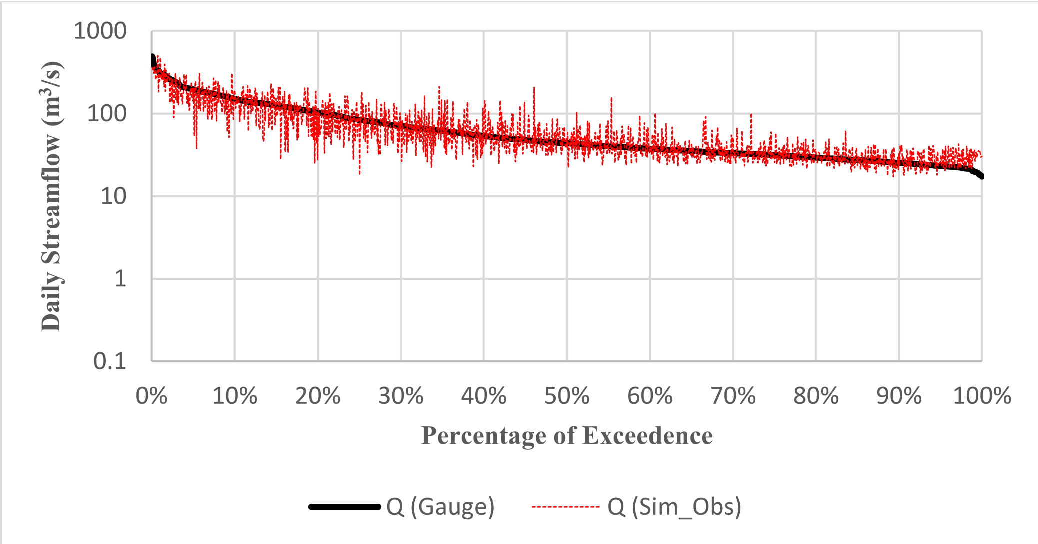

Figure 6-7: Logarithmic plot of flow duration curve for simulated of observed rainfall against gauge data (2007/8 - 2010/11)

6.1.3 Annual Water Balance – Calibration Period

The results of the annual water balance over the model's calibration period are shown in Table 6-1 and Figure 6-8. Table 6-1 shows annual water difference for 2009/10 years has resulted in underestimation and overestimation for the rest of the calibration period.

Table 6-1 shows the calculation of significance for determining the level of accuracy of calculated and observed flows in the year. The annual water balance differences were underestimated in 2009/10 years while for the rest of the year it overestimates. Table 6-1 shows annual water difference for 2009/10 years has resulted in underestimation and overestimation for the rest of the calibration period.

Table 6-1: Annual water balance calculation for calibration period for observed data (2007/8 – 2011/12)

Calibration						
Water Year	**Sim. SF (mm)**	**Thiessen Avg. RF (mm)**	**Obs. SF (mm)**	**Obs. WB (mm)**	**Sim. WB (mm)**	**Annual WB Diff. (mm)**
2007/8	1,085.63	4,094.87	1,438.45	2,656.42	3,009.24	352.82
2008/9	1,030.00	3,830.69	1,163.44	2,667.25	2,800.69	133.44
2009/10	1,383.41	4,729.62	1,192.16	3,537.46	3,346.21	-191.25
2010/11	1,169.20	2,980.48	1,301.20	1,679.29	1,811.28	131.99

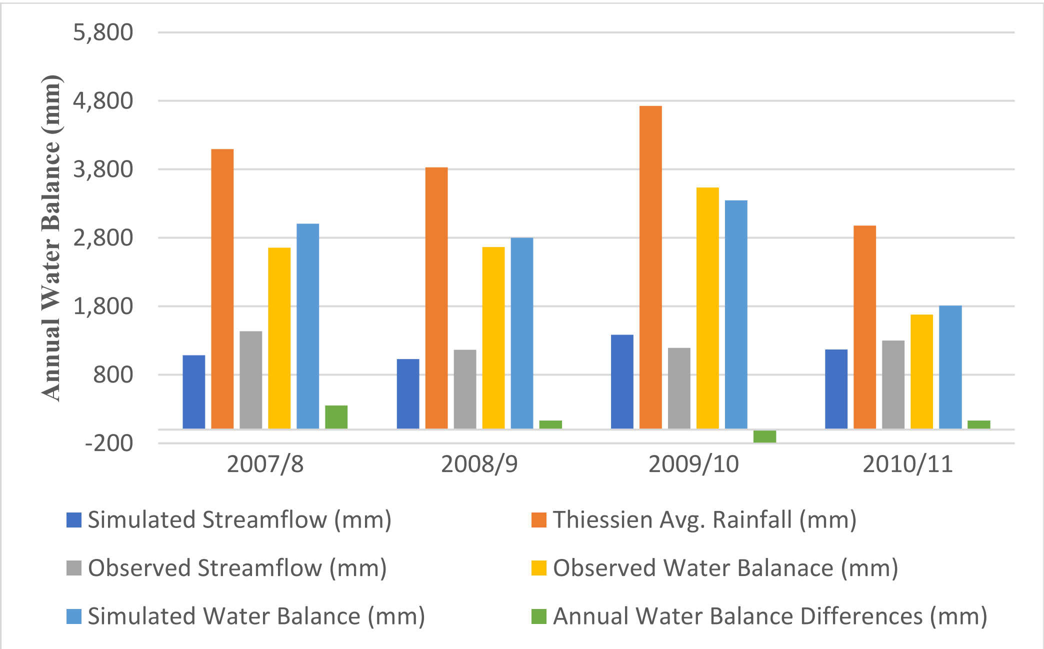

Figure 6-8: Annual water balance plot for calibration period for observed data (2007/8 – 2011/12)

6.1.4 Sensitivity Analysis

The calibration changes analysis was carried from 50% to -50% in 10% increments, keeping all other parameters constant. The following figure is used for sensitivity analysis of soil moisture accounting parameters (SMA) and other parameters. The most sensitive parameters are tension storage, simple surface, and soil storage. Figure 6-9 shows the deviation in percentage as per change in runoff volume.

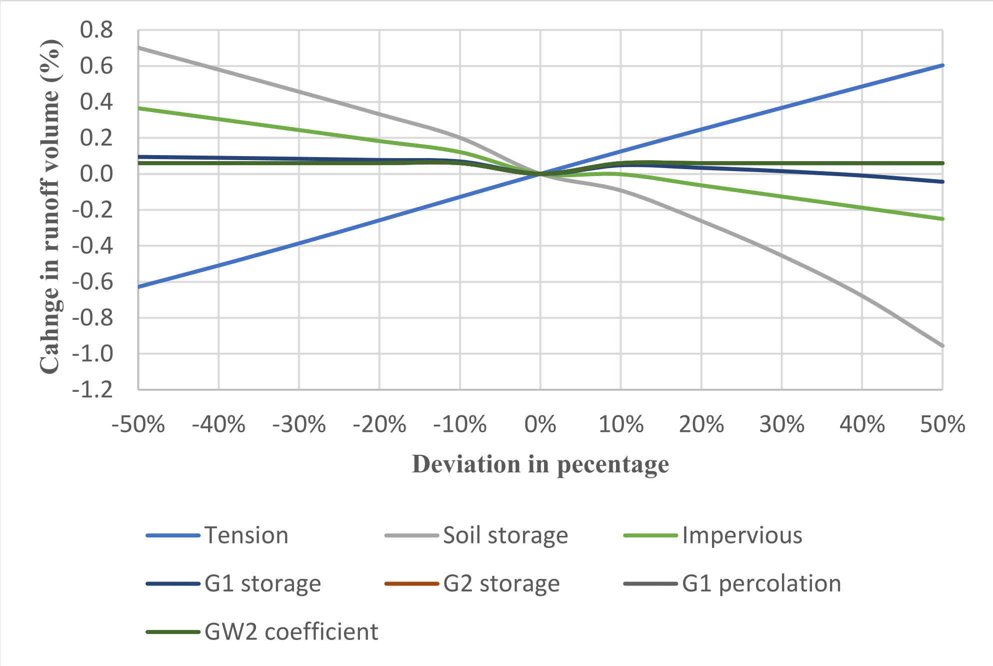

Figure 6-9: Sensitivity Analysis for SMA

6.2 Model Validation for Simulated Observed Rainfall

6.2.1 Overall Validation Comparison of Simulated Observed Rainfall with Gauge data (2011/12- 2014/15)

Figure 6-10 shows the comparison of monthly simulated observed rainfall against gauge data of streamflow for the validation period. The simulated observed rainfall follows a pattern to gauge flow. The peak flow for observed simulation exceeds to gauge data as in Figure 6-10. A possible reason may be due to the overestimation of precipitation at the local rain gauge. The inconsistency in the lower streamflow maybe since the model spins-up time is short relative to the initial soil moisture.

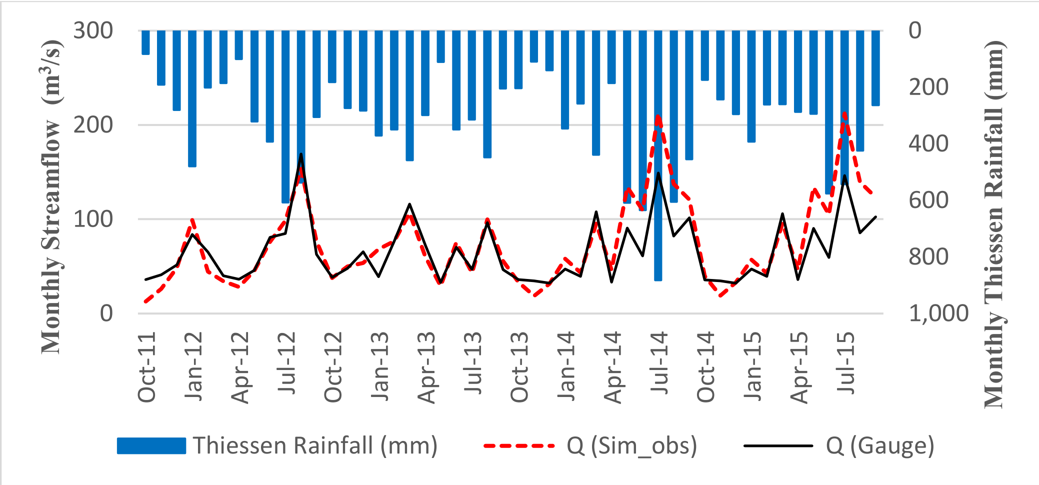

Figure 6-10: Monthly validation for simulated of observed rainfall against gauge data – Gin watershed

6.2.1.1 Daily Comparison of Observed Simulated Flow with Gauge Data – Normal Plot

The below four graph shows the comparison of monthly validation for simulated observed flow against gauge data annually. The graph is compared to a single water year from 2011/12 till 2014/15 as shown in Figure 6-11 and Figure 6-12. The peak flow for simulated observed flow exceeds to gauge data (Figure 6-12 (C) and (D)). A possible reason may be due to the overestimation of precipitation at the local rain gauge. A possible reason is that the local sparse rain gauge network may not completely capture the center of the precipitation storm, which may lead to the underestimation of high runoff.

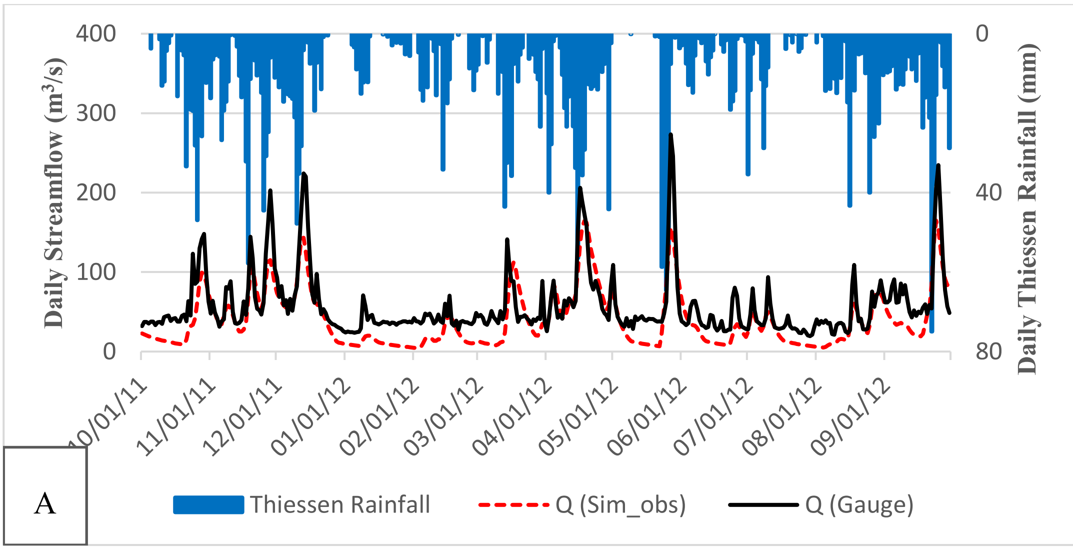

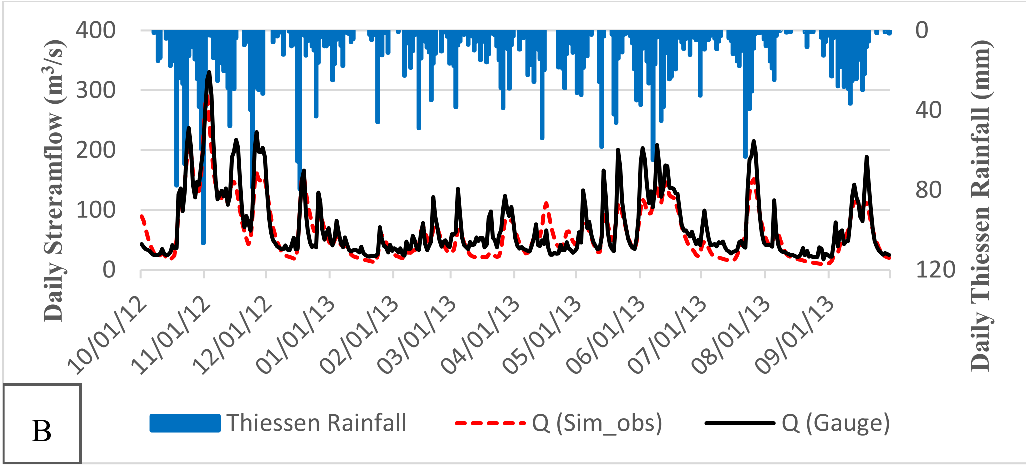

Figure 6-11: Comparison of simulated observed rainfall against gauge data for validation period – (2011/12 and 2012/13)

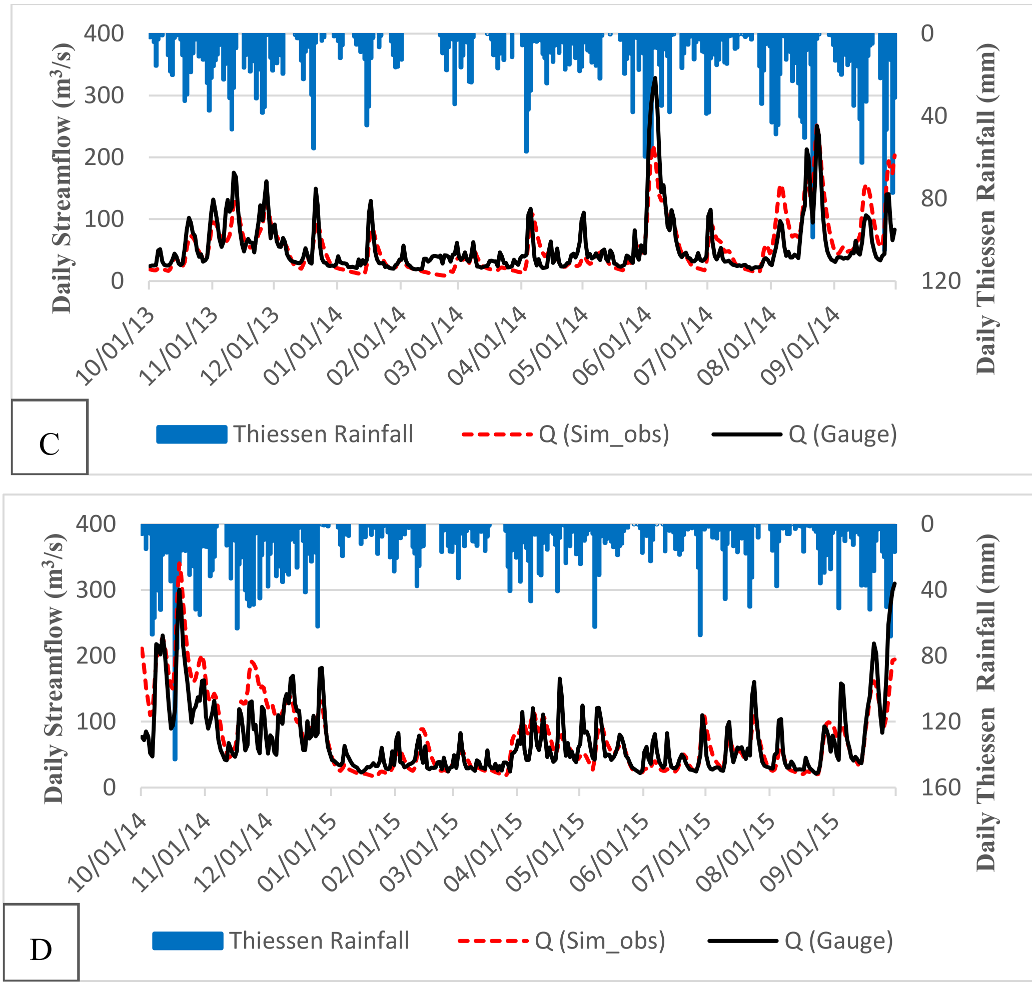

Figure 6-12: Comparison of simulated observed rainfall against gauge data for validation period – (2013/14 and 2014/15)

6.2.2 Flow Duration Curve – Validation Period

The normal flow duration curves were created for the entire validation period (2011/12 -2014/15). The simulated observed flow is overestimated in the medium region while the low flow is underestimated in the low region as shown in Figure 6-13 and Figure 6-14.

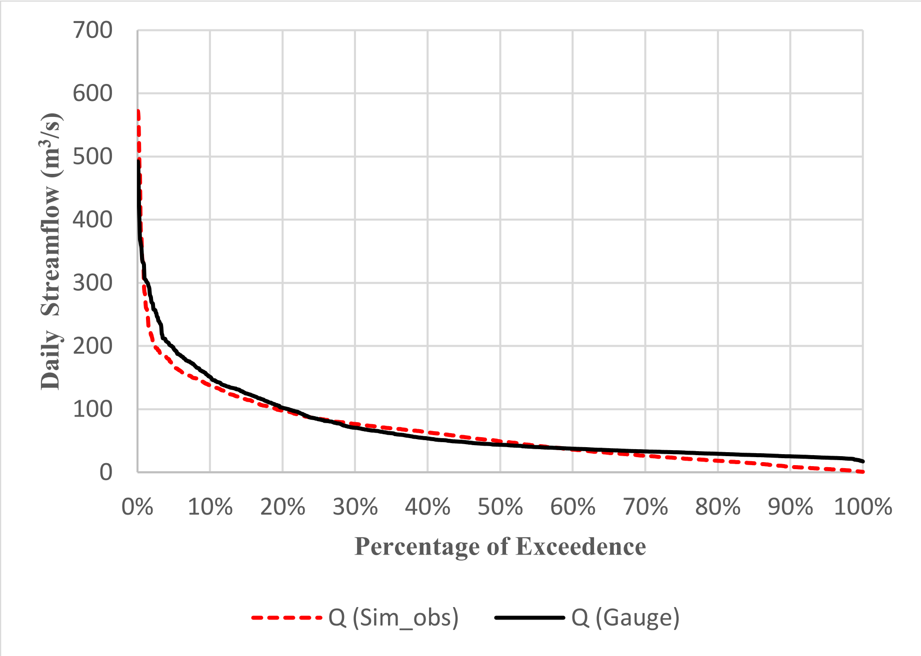

Figure 6-13: Flow duration curve of simulated observed rainfall against gauge data for validation period (2011/12 -2014/15)

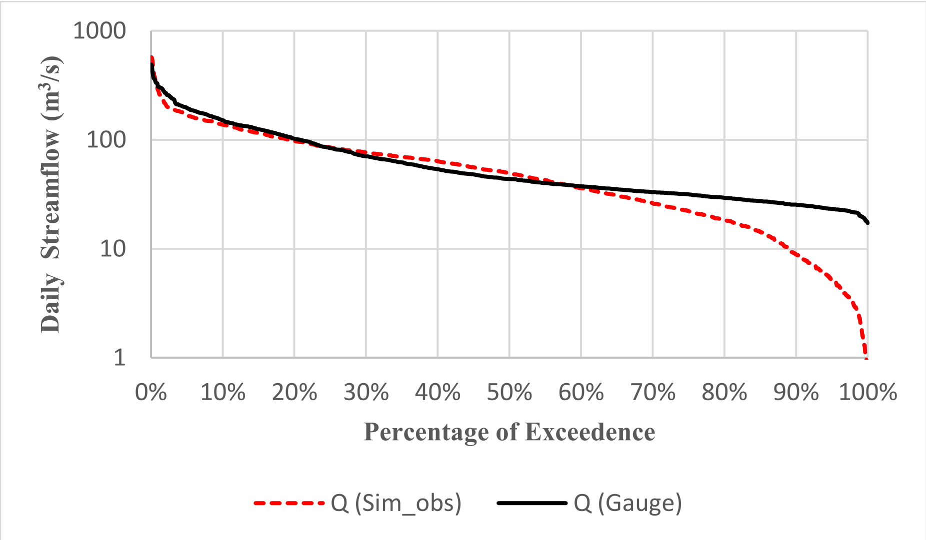

Figure 6-14: Semi log form comparison for simulated observed rainfall against stream gauge - Validation period

The normal and semi-log scale for validation length (2011/12 -2014/15) for observed and simulated flow is shown in Figure 6-15 and Figure 6-16 for daily scale with the flow period curve divided into a high, medium, and low flow based on the possibility of exceedance.

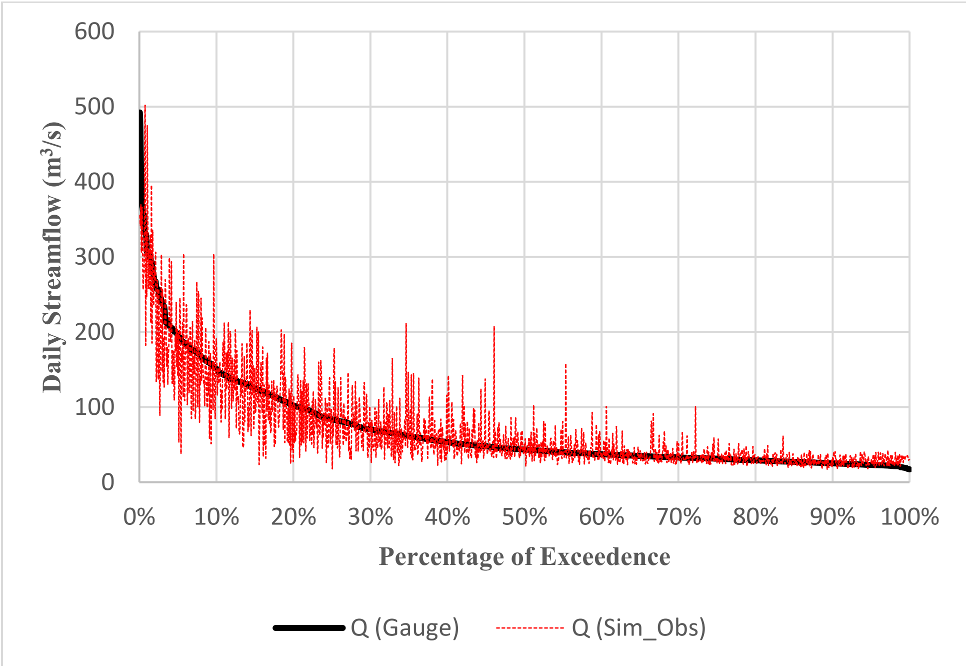

Figure 6-15: Normal FDC for simulated observed rainfall against stream gauge -Validation period

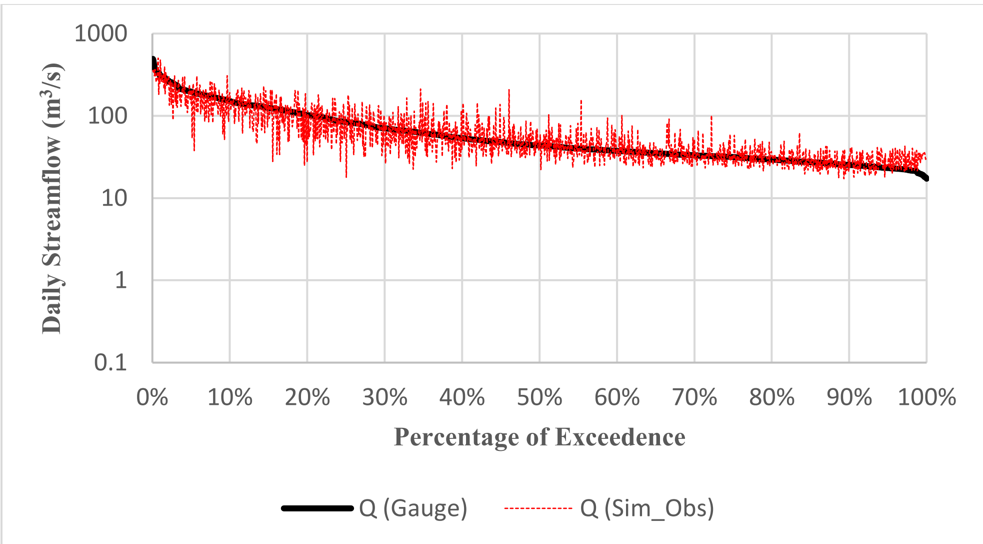

Figure 6-16: Logarithmic plot of flow duration curve for simulated observed rainfall against gauge data (2011/12 -2014/15)

6.2.3 Annual Water Balance – Validation Period

The results of the annual water balance over the model's validation period are shown in Table 6-2 and Figure 6-17. This calculation is significant for determining the level of accuracy of calculated and observed flows in the year. The annual water balance differences were underestimated in 2013/14 and 2014/15 years while for the rest of the year it overestimates.

Table 6-2: Annual water balance calculation for validation period for simulated observed rainfall against gauge data (2011/12 – 2014/15)

Validation						
Water Year	**Sim. SF (mm)**	**Thiessen Avg. RF (mm)**	**Obs. SF (mm)**	**Obs. WB (mm)**	**Sim. WB (mm)**	**Annual WB Diff. (mm)**
2011/12	922.12	3,681.25	1,218.47	2,462.78	2,759.13	296.35
2012/13	964.47	3,639.47	1,145.50	2,493.97	2,675.00	181.03
2013/14	1,400.22	4,865.15	1,245.90	3,619.25	3,464.93	-154.32
2014/15	1,425.91	4,012.16	1,246.10	2,766.06	2,586.25	-179.81

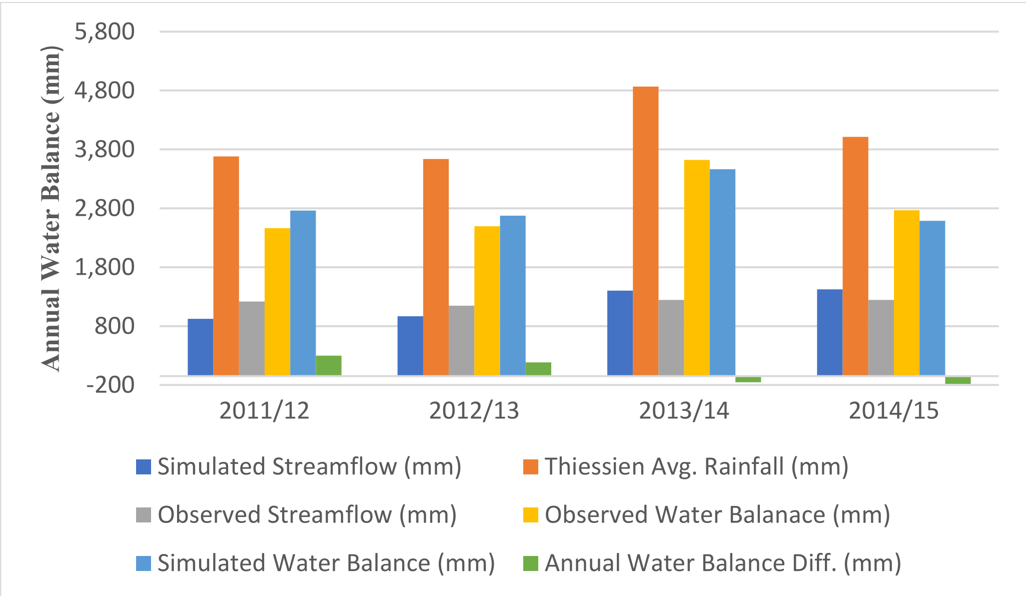

Figure 6-17: Annual water balance graph for calibration period for simulated observed rainfall against gauge data (2011/12 – 2014/15)

6.3 Model Calibration for Simulated TRMM Gridded Data

6.3.1 Overall Calibration Comparison of TRMM data with Gauge data (2007/8 - 2010/11)

The graph below shows the comparison of monthly (Figure 6-18). TRMM simulation flow against gauge data of streamflow for the calibration period. The peak flow for observed simulation matches to gauge data as in Figure 6-18. The inconsistency in the lower streamflow maybe since the model spins-up time is short relative to the initial soil moisture. It could also be due to using global datasets in a relatively small watershed.

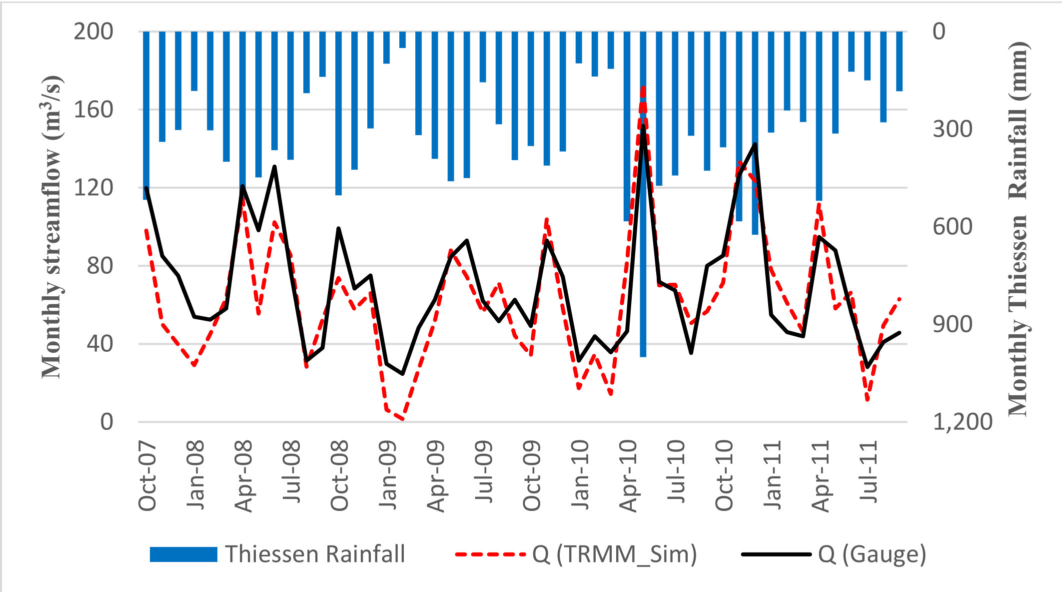

Figure 6-18: Monthly calibration from TRMM simulation against gauge data

6.3.1.1 Daily Comparison of TRMM Simulated Flow with Gauge Data – Normal Plot

The below four graph shows the comparison of monthly calibration for TRMM simulation flow against gauge data annually. The graph is compared to a single water year from 2007/8 till 2010/11 as shown in Figure 6-19 and Figure 6-20. **Error! Reference source not found.**The inconsistency in the lower streamflow maybe since the model spins-up time is short relative to the initial soil moisture. It could also be due to using global datasets in a relatively small watershed.

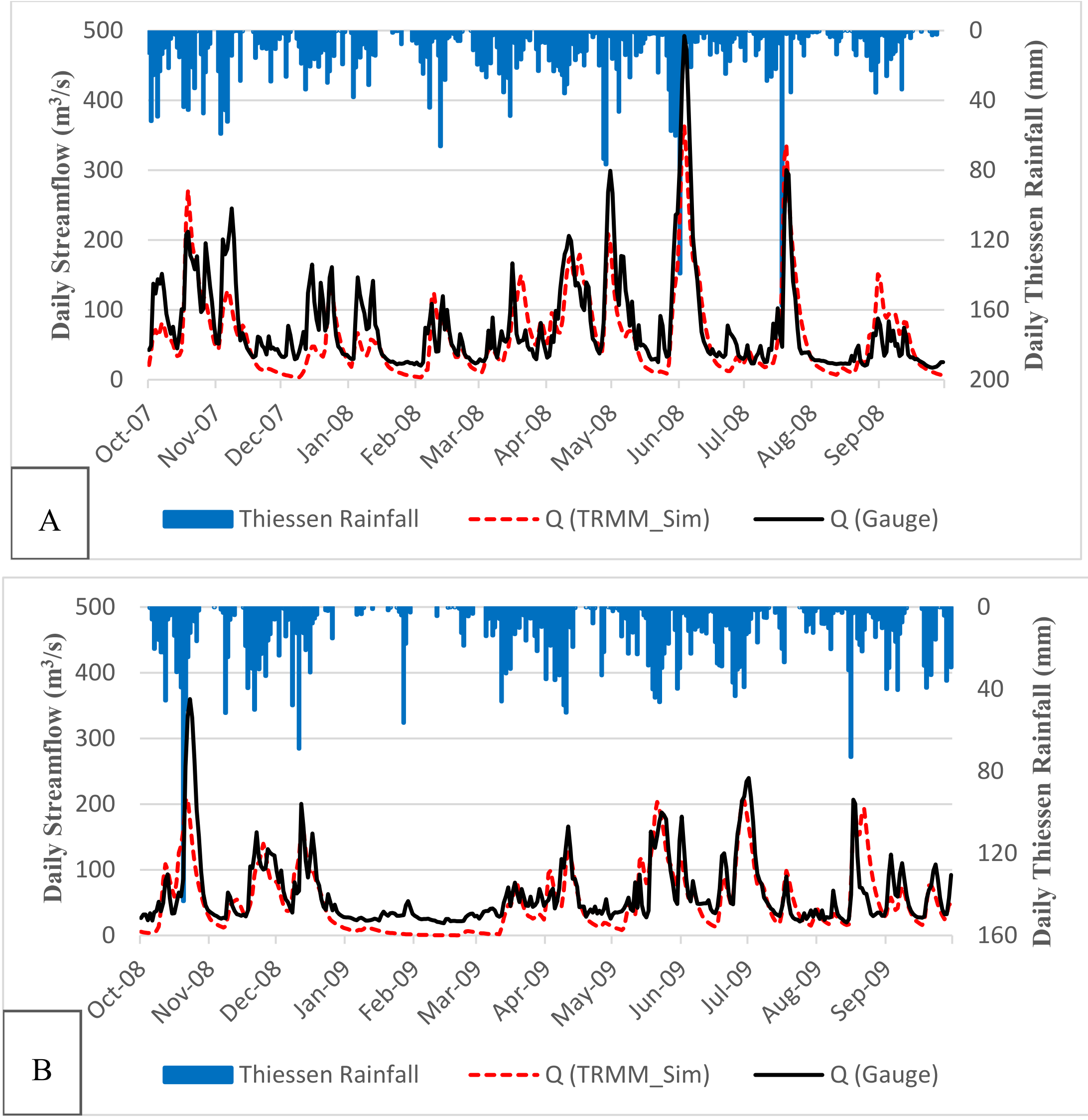

Figure 6-19: Comparison of TRMM and gauge data for calibration period (2007/8 and 2008/9)

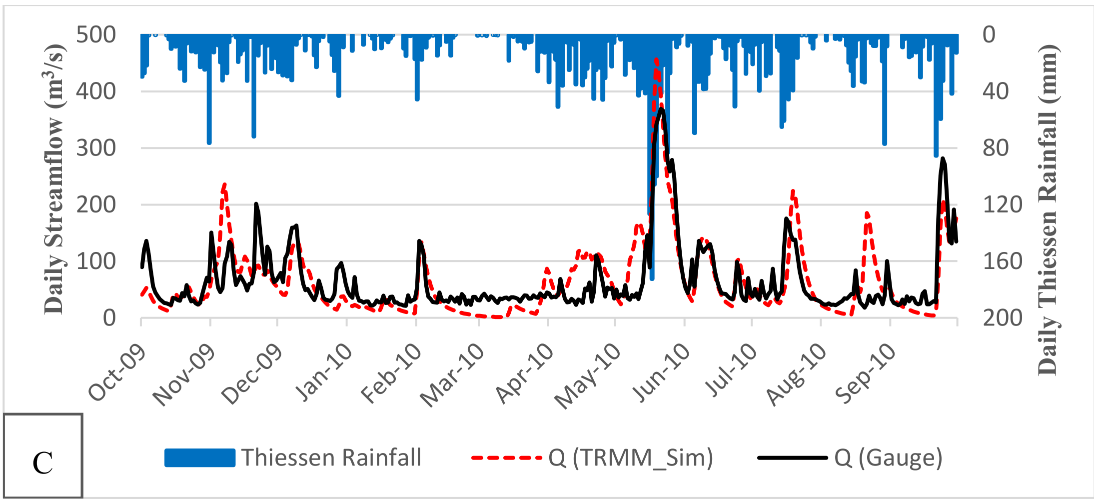

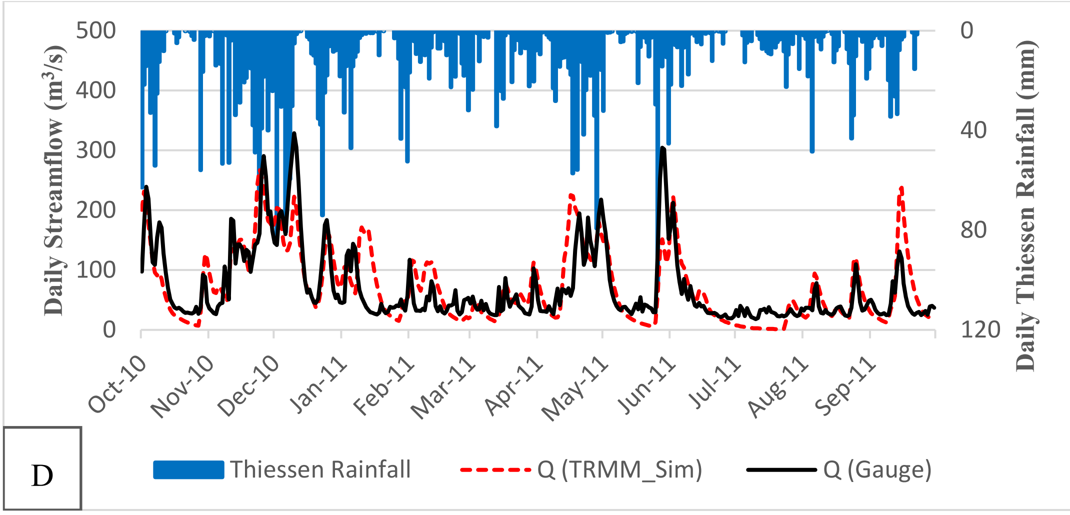

Figure 6-20: Comparison of TRMM and gauge data for calibration period (2009/10 and 2010/11)

6.3.2 Flow Duration Curve – Calibration Period

The normal flow duration curves were created for the entire calibration period (2007/8 – 2010/11). The simulated observed flow is underestimated in both high and low region regions shown in Figure 6-21 and Figure 6-22.

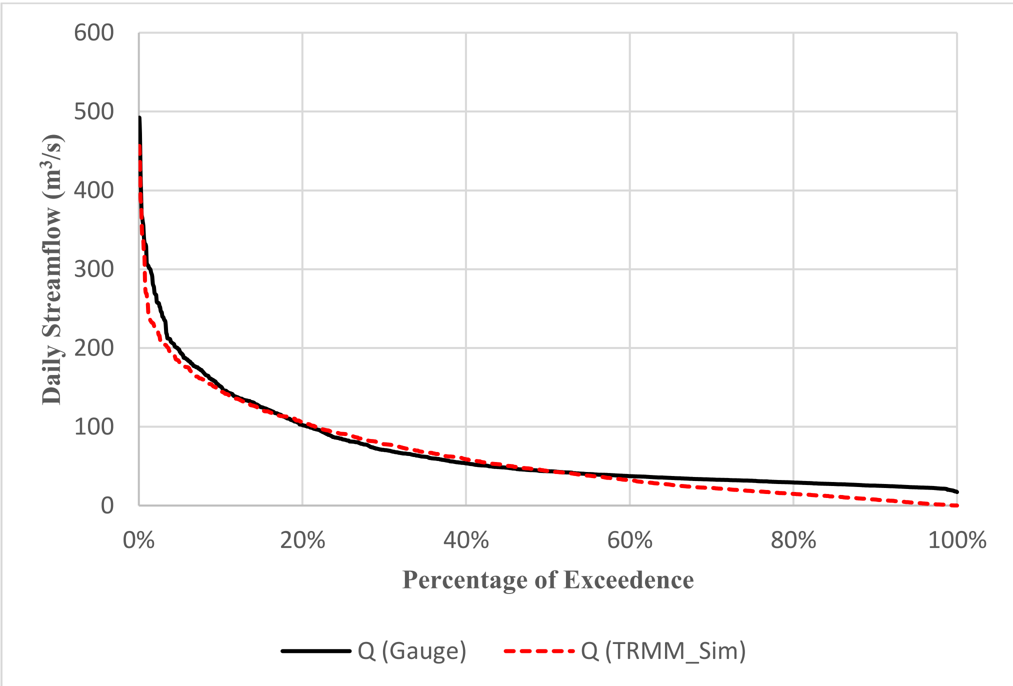

Figure 6-21: Flow duration curve for TRMM simulated streamflow against gauge data for calibration period – Daily scale

The overestimation of flow within the execution of the gridded precipitation-controlled model is especially due to the systematic overestimation of precipitation. Another clarification is that the execution of the gridded precipitation data-driven model runs adopted the rain gauge-based model parameters that are likely to be distorted by actual hydrological characteristics or features.

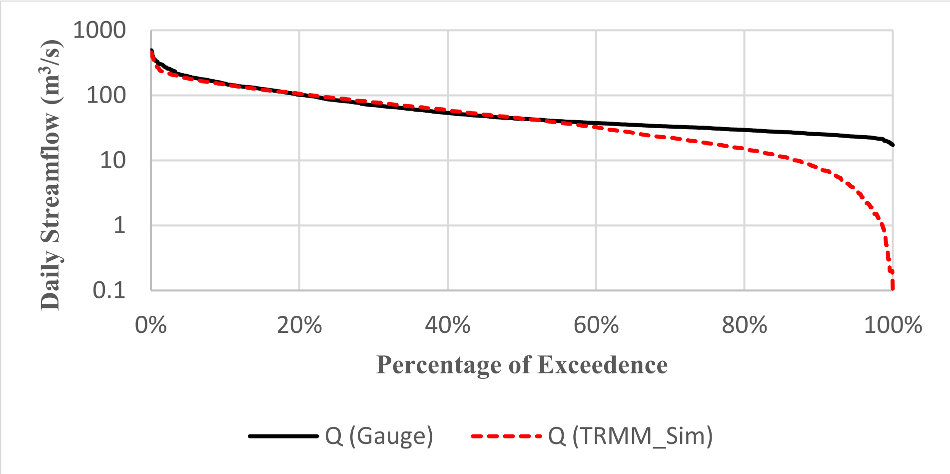

Figure 6-22: Semi log form comparison for simulated TRMM data against stream gauge - Calibration period

The normal and semi-log scale for calibration length (2007/8 – 2010/11) for TRMM and simulated flow is shown in Figure 6-23 and Figure 6-24 for the daily scale. It also highlights the underestimation of precipitation in the lower region due to the underestimation of precipitation by TRMM gridded data.

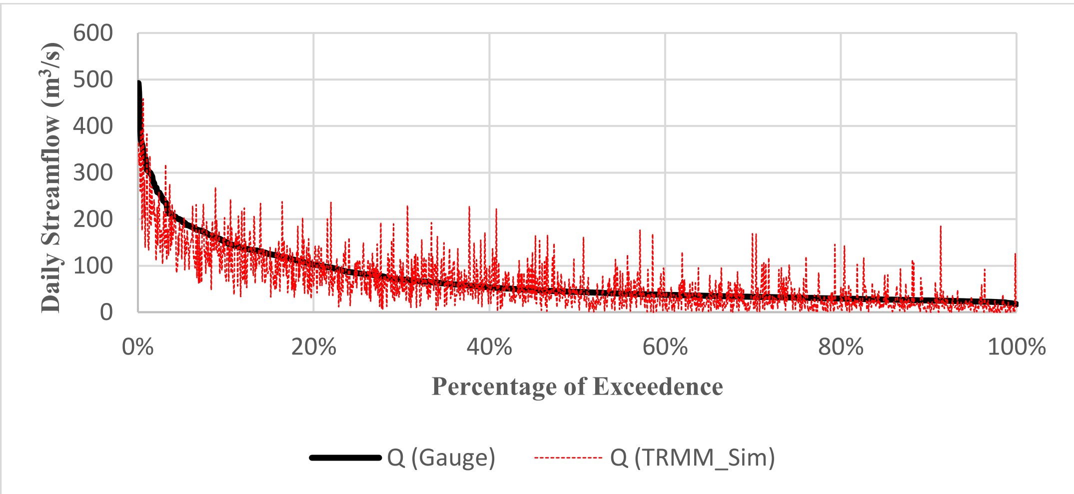

Figure 6-23: Normal FDC comparison for simulated TRMM data against stream gauge – Calibration period

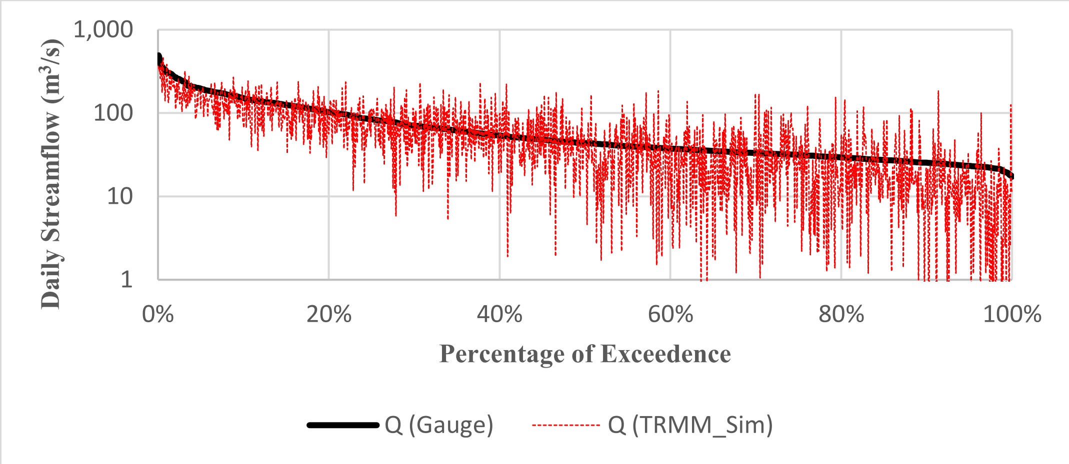

Figure 6-24: Logarithmic plot of flow duration curve for the calibration period (2007/8 – 2011/12)

6.3.1 Annual Water Balance – Calibration Period

The results of the annual water balance over the model's calibration period are shown in Table 6-3 and Figure 6-25. This calculation is significant for determining the level of accuracy of calculated and observed flows in the year. The annual water balance differences were underestimated in 2010/11 years while for the rest of the year it overestimates.

Table 6-3: Annual water balance calculation for calibration period for TRMM data (2007/8 – 2011/12)

Calibration						
Water Year	**Sim. SF (mm)**	**Thiessen Avg. RF (mm)**	**Obs. SF (mm)**	**Obs. WB (mm)**	**Sim. WB (mm)**	**Annual WB Diff. (mm)**
2007/8	1,167.39	4,094.87	1,438.45	2,656.42	2,927.48	271.06
2008/9	943.94	3,830.69	1,163.44	2,667.25	2,886.75	219.50
2009/10	1,170.29	4,729.62	1,192.16	3,537.46	3,559.33	21.87
2010/11	1,335.20	2,980.48	1,301.20	1,679.29	1,645.28	-34.01

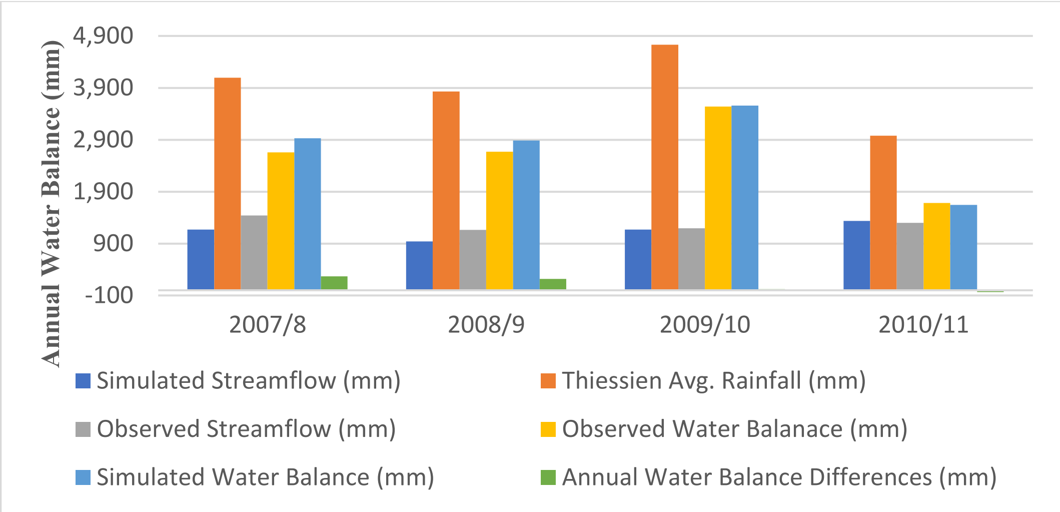

Figure 6-25: Annual water balance graph for calibration period for TRMM data (2007/8 – 2011/12)

6.4 Model Validation for TRMM Data

6.4.1 Overall Validation Comparison of TRMM Data with Gauge Data (2011/12- 2014/15)

Figure 6-26 shows the comparison of monthly and daily TRMM simulation flow against gauge data of streamflow for the validation period. The peak flow for TRMM simulation exceeds to gauge data as in Figure 6-26. The overestimation of peak flow within the execution of the gridded precipitation-controlled model is especially due to the systematic overestimation of precipitation by gridded data.

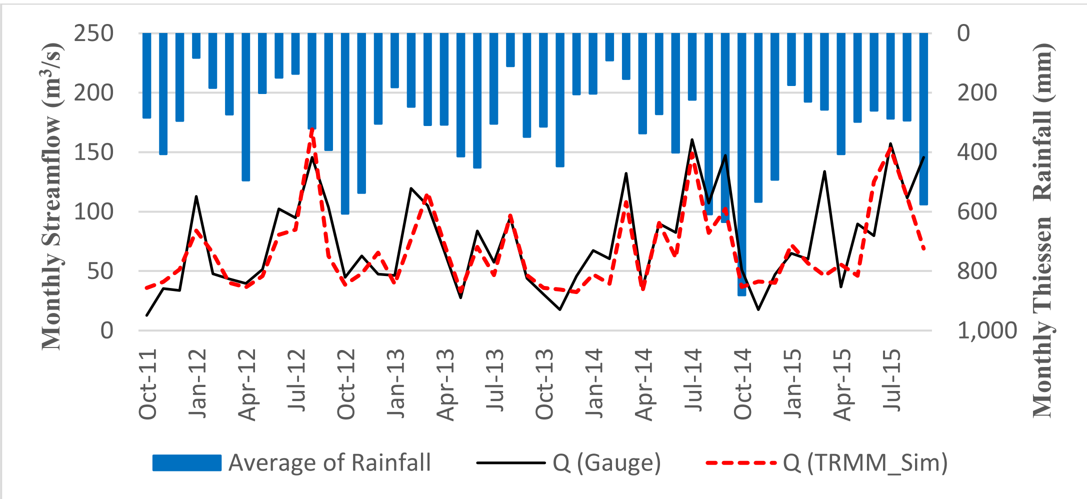

Figure 6-26: Comparison of monthly simulated TRMM flow with gauge data for validation period (2011/12 – 2014/15)

6.4.1.1 *Overall Comparison of TRMM Simulated Flow with Gauge Data – Normal Plot*

The below four graph shows the comparison of monthly validation for simulated TRMM flow against gauge data annually. The graph is compared to a single water year from 2011/12 till 2014/15 as shown in Figure 6-27 and Figure 6-28. The inconsistency in the lower streamflow maybe since the model spins-up time is short relative to the initial soil moisture. It could also be due to using global datasets in a relatively small watershed.

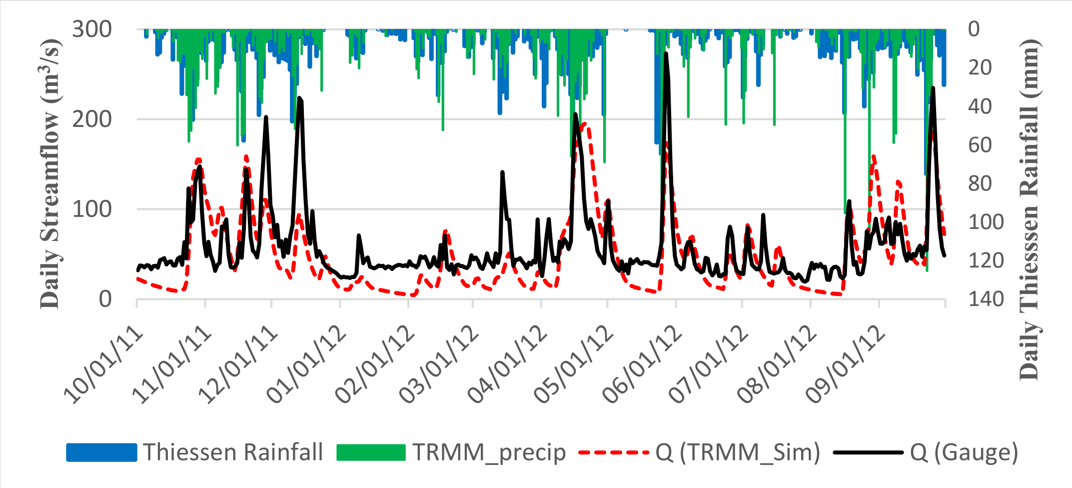

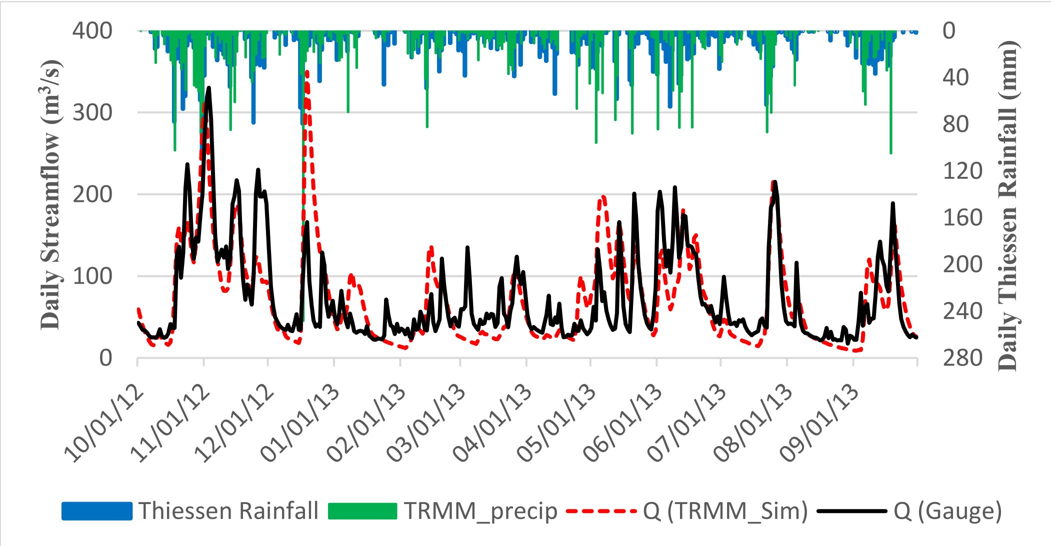

Figure 6-27: Comparison of daily TRMM simulated flow against gauge data (2011/12 and 2012/13)

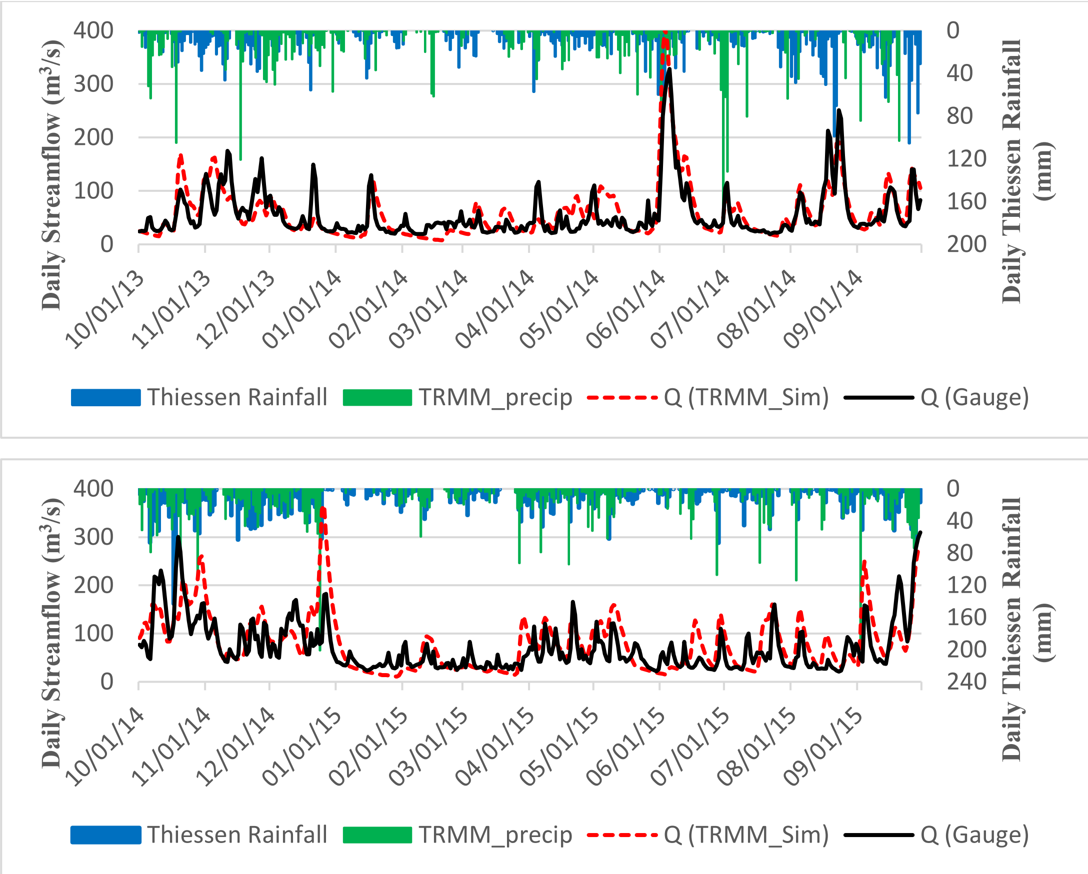

Figure 6-28: Comparison of daily TRMM simulated flow against gauge data (2013/14 and 2014/15)

6.4.2 Flow Duration Curve – Validation Period

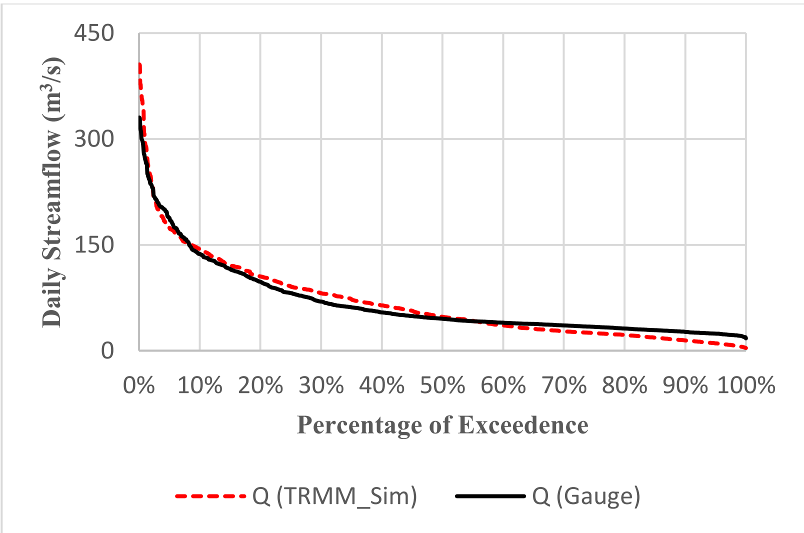

Figure 6-29: Flow duration curve for TRMM simulated streamflow against gauge data for validation period (2011/12 -2014/15)

The normal and semi-log flow duration curves (FDC) were created for the entire validation period (2011/12 - 2014/15). The observed simulated flow is overestimated in the medium region while the low flow is underestimated in the low regions shown in Figure 6-29 and Figure 6-30.

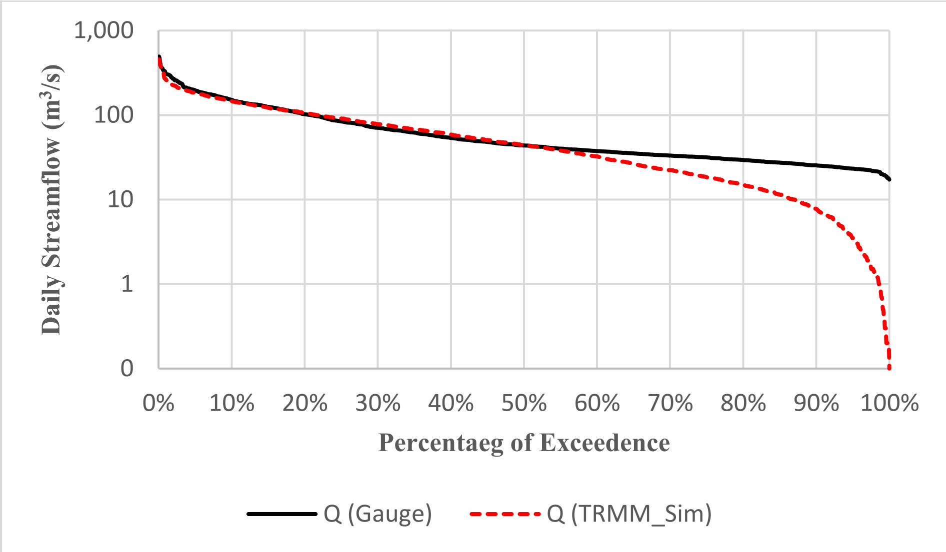

Figure 6-30: Semi log form comparison for simulated TRMM data against stream gauge - Validation period

The normal and semi-log scale for validation length (2011/12 -2014/15) for TRMM and simulated flow is shown in

Figure 6-31 and Figure 6-32 for the daily scale comparison and the graphs also reflect the underestimation in the high region by TRMM data due to using global datasets in a relatively too small watershed.

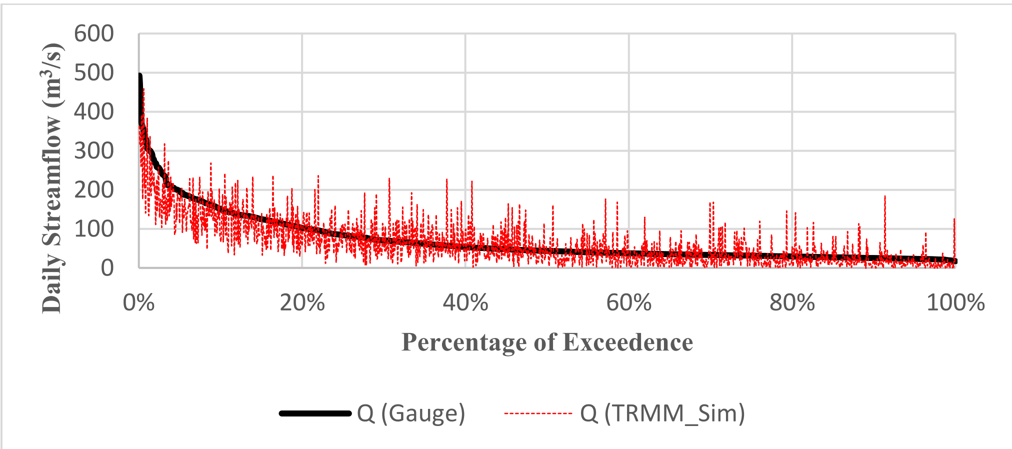

Figure 6-31: Normal FDC comparison for simulated TRMM data against stream gauge – Validation period

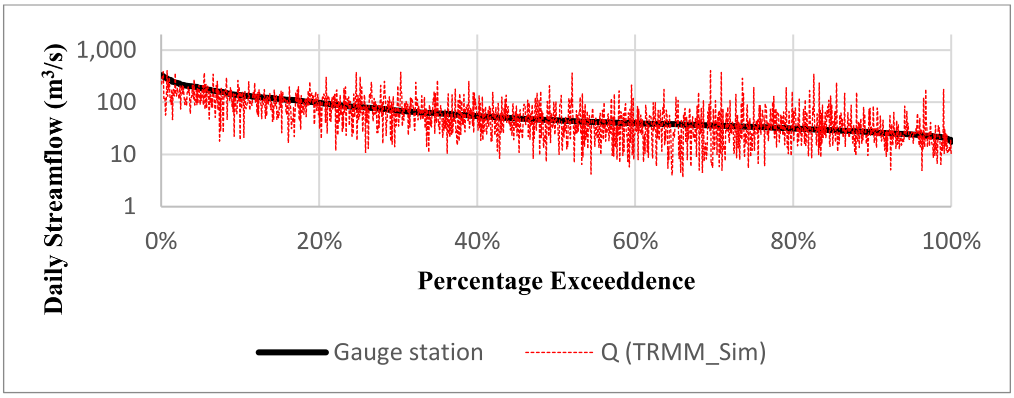

Figure 6-32: Logarithmic plot of flow duration curve for the validation period (2011/12 – 2014/15)

6.4.3 Annual Water Balance – Validation Period

The results of the annual water balance over the model's calibration period are shown in Table 6-4 and Figure 6-33 each. This calculation is significant for determining the level of accuracy of calculated and observed flows in the year. The annual water balance differences were underestimated in 2012/13, 2013/14, and 2014/15 years while 2011/12 years it overestimates.

Table 6-4: Annual water balance calculation for validation period for TRMM data (2011/12 – 2014/15)

Validation						
Water Year	**Sim. SF (mm)**	**Thiessen Avg. RF (mm)**	**Obs. SF (mm)**	**Obs. WB (mm)**	**Sim. WB (mm)**	**Annual WB Diff. (mm)**
2011/12	1,021.06	3,681.25	1,218.47	2,462.78	2,660.20	197.42
2012/13	1,164.49	3,639.47	1,145.50	2,493.97	2,474.98	-18.99
2013/14	1,338.01	4,865.15	1,245.90	3,619.25	3,527.14	-92.11
2014/15	1,374.65	4,012.16	1,246.10	2,766.06	2,637.51	-128.55

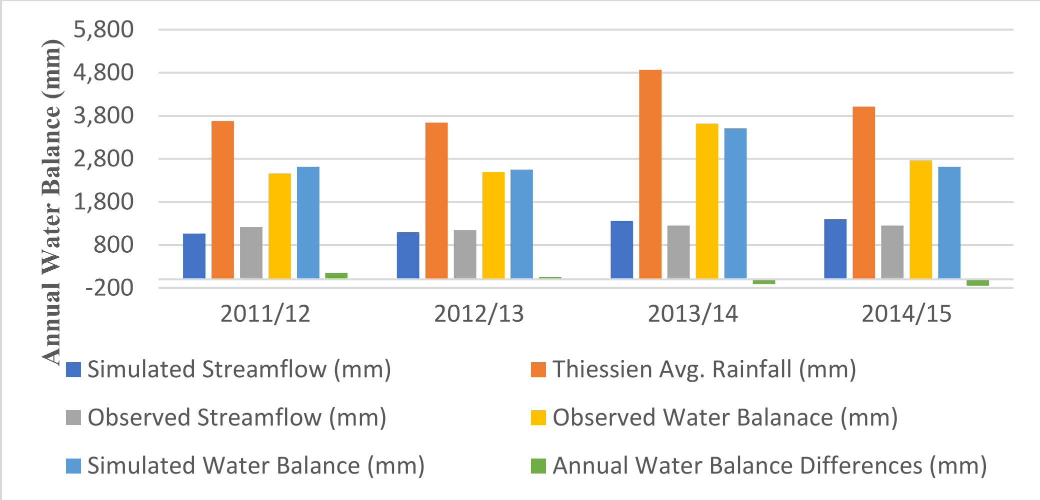

Figure 6-33: Annual water balance graph for calibration period for TRMM data (2011/12 – 2014/15)

6.5 Model Calibration for APHRODITE Data

6.5.1 Overall Calibration Comparison of APHRODITE simulation flow with Gauge Data (2007/8 -2010/11)

Figure 6-34 shows the comparison of monthly **Error! Reference source not found.**APHRODITE simulation flow against gauge data of streamflow for the calibration period. The peak flow for the simulated APHRODITE matches to gauge data as in Figure 6-34**Error! Reference source not found.**. The overestimation of peak flow within the execution of the gridded precipitation-controlled model is especially due to the systematic overestimation of precipitation.

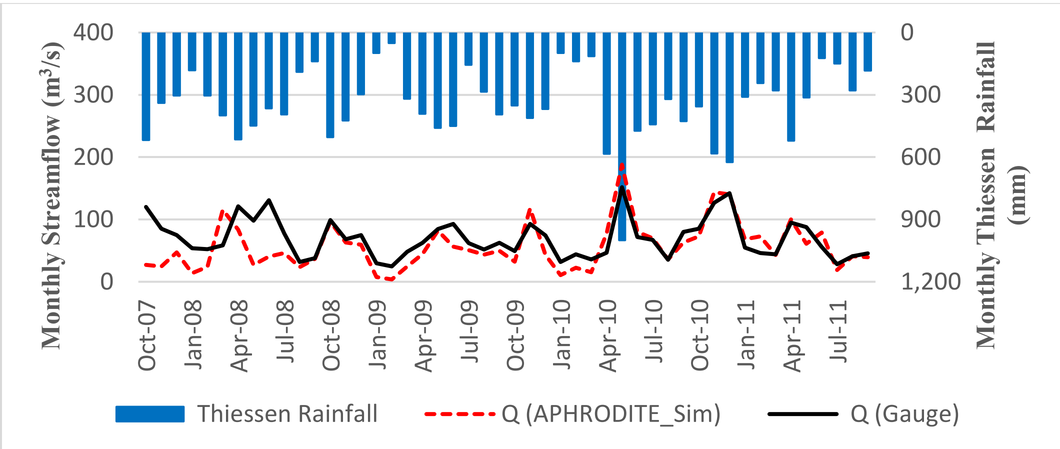

Figure 6-34: Monthly comparison of APHRODITE with gauge data for calibration period (2007/8 – 2010/11)

6.5.1.1 Daily Comparison of Observed Simulated Flow with Gauge Data – Normal Plot

The below four graph shows the comparison of monthly calibration for simulated APHRODITE flow against gauge data annually. The graph is compared to a single water year from 2007/8 till 2010/11 as shown in Figure 6-35 and Figure 6-36. The inconsistency in the lower streamflow maybe since the model spins-up time is short relative to the initial soil moisture. It could also be due to using global datasets in a relatively small watershed. It could be because the APHRODITE cannot depict small-scale changes because of its moderate resolution (0.25°).

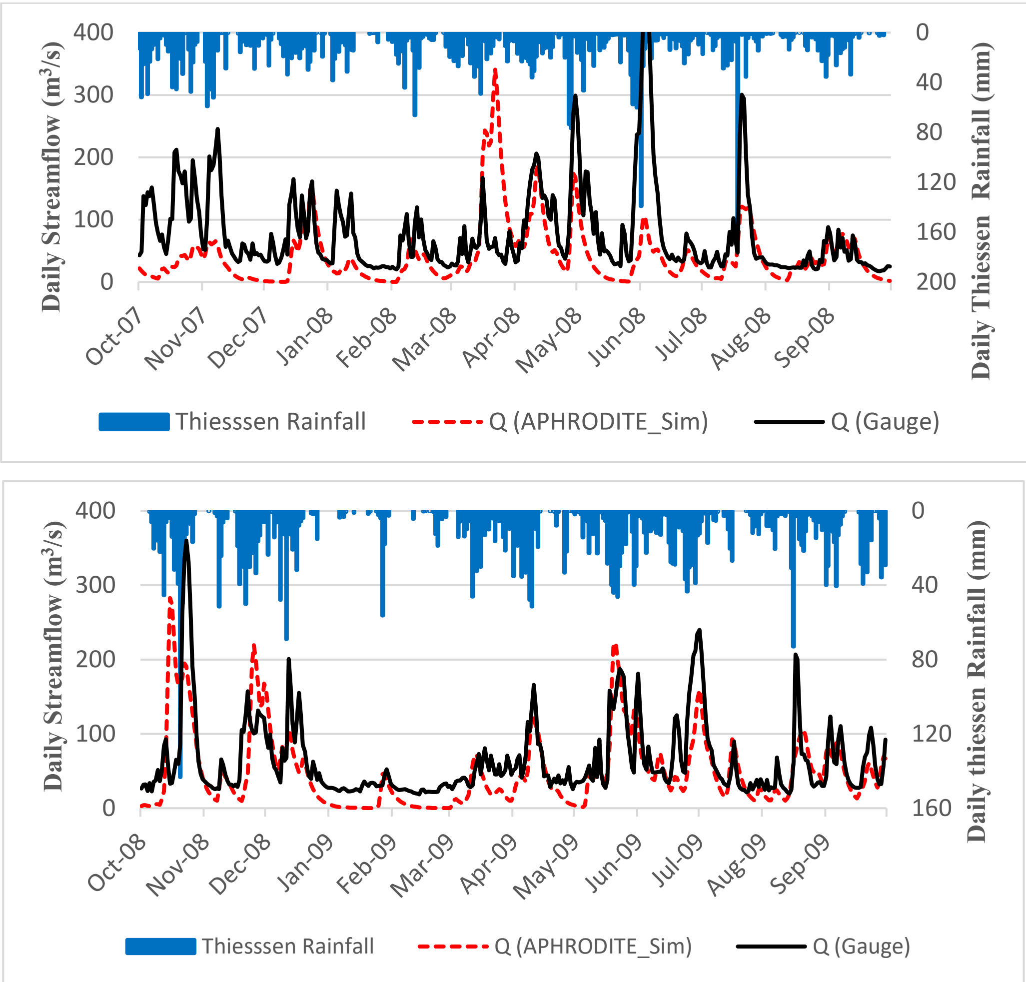

Figure 6-35: Comparison of APHRODITE and gauge data for calibration period (2007/8 and 2008/9)

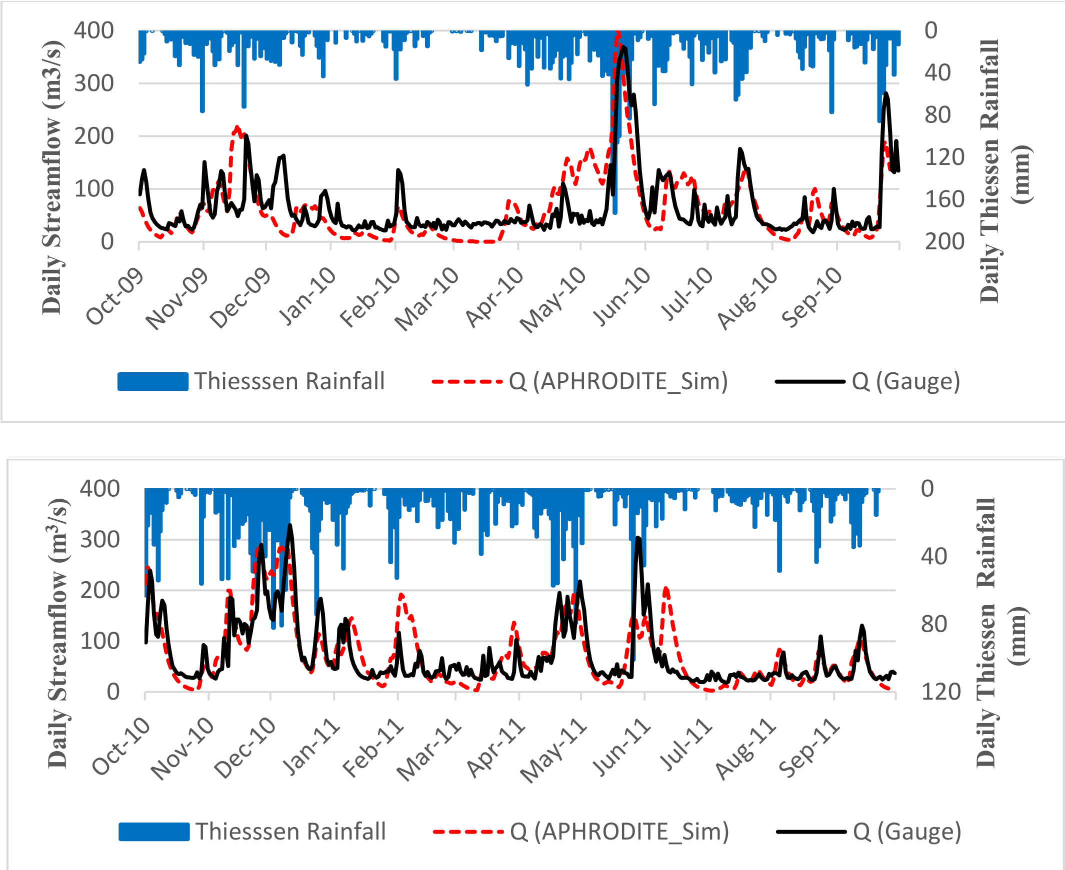

Figure 6-36. Comparison of APHRODITE and gauge data for calibration period (2009/10 and 2010/11)

6.5.2 Flow Duration Curve – Calibration Period

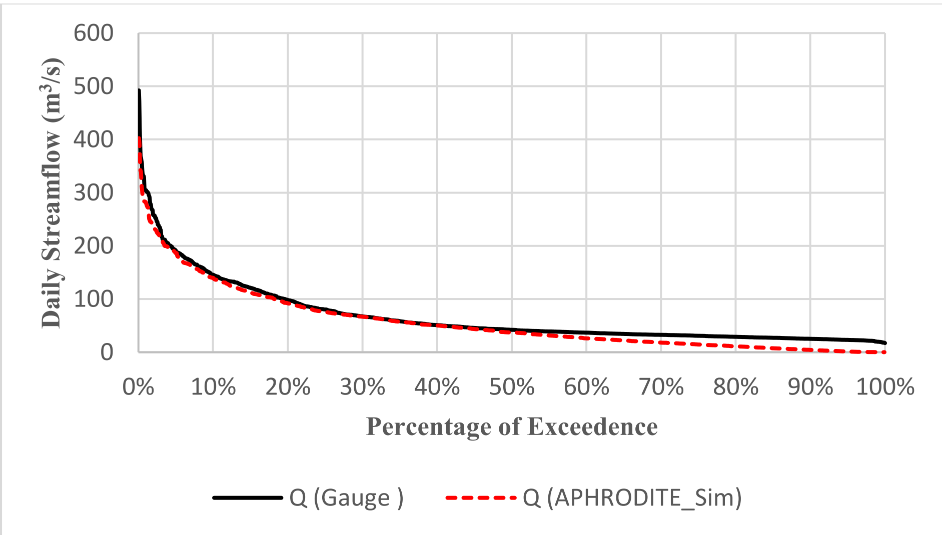

Figure 6-37: Flow duration curve for APHRODITE simulated streamflow against gauge data for calibration period – Daily scale

The normal flow duration curves were created for the entire validation period (2007/8 – 2011/12). The simulated APHRODITE flow is matched in the medium region while the low flow is underestimated in the low regions shown in Figure 6-37 and Figure 6-38.

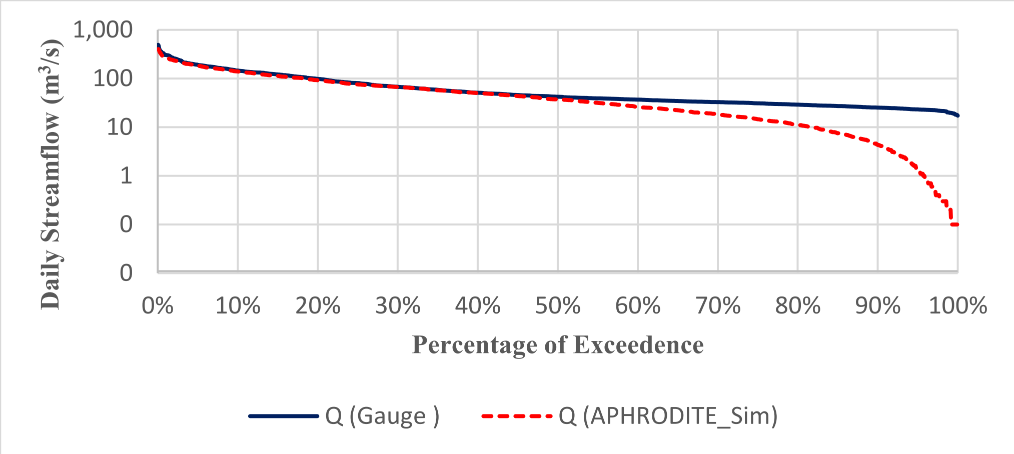

Figure 6-38: Semi log form comparison for simulated APHRODITE data against stream gauge - Calibration period

The normal and semi-log scale for calibration length (2007/8 – 2011/12) for simulated APHRODITE and gauge flow is shown in Figure 6-39 and Figure 6-40 for the daily scale. It also projects the underestimates in the lower region.

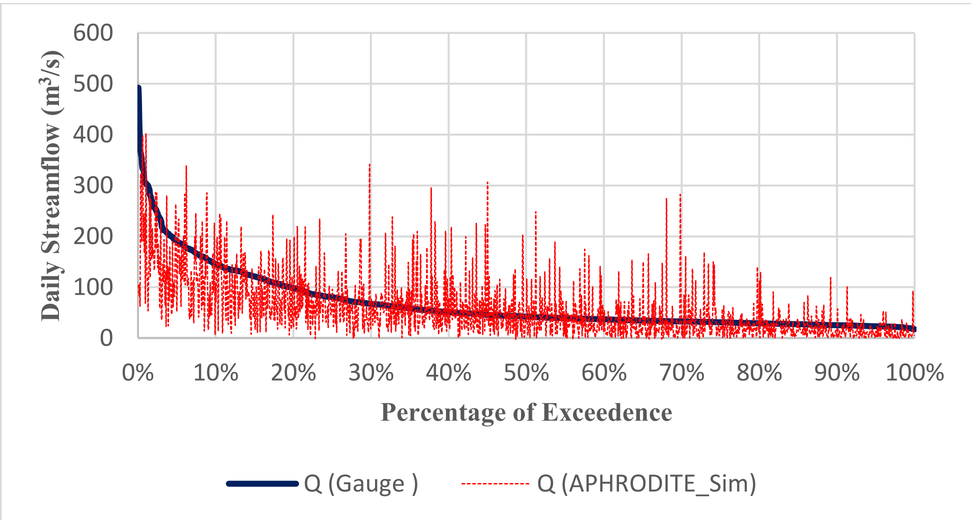

Figure 6-39: Normal FDC comparison for simulated APHRODITE data against stream gauge – Calibration period

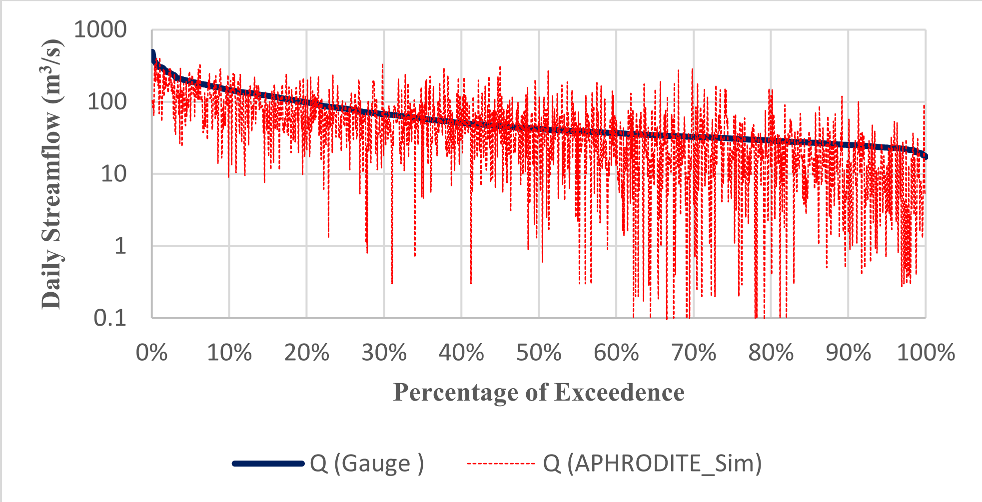

Figure 6-40: Logarithmic plot of flow duration curve for the calibration period (2007/8 – 2011/12)

6.5.3 Annual Water Balance – Calibration Period

The results of the annual water balance over the model's calibration period are shown in Table 6-5 and Figure 6-41 each. This calculation is significant for determining the level of accuracy of calculated and observed flows in the year. The annual water balance differences were underestimated in 2010/11 years while the rest of the year it overestimates.

Table 6-5: Annual water balance calculation for calibration period for APHRODITE data (2007/8 – 2011/12)

Calibration						
Water Year	**Sim. SF (mm)**	**Thiessen Avg.RF (mm)**	**Obs. SF (mm)**	**Obs. WB (mm)**	**Sim. WB (mm)**	**Annual WB Diff. (mm)**
2007/8	777.81	4,094.87	1,438.45	2,656.42	3,317.06	660.64
2008/9	889.96	3,830.69	1,163.44	2,667.25	2,940.73	273.48
2009/10	1,154.45	4,729.62	1,192.16	3,537.46	3,575.17	37.70
2010/11	1,345.08	2,980.48	1,301.20	1,679.29	1,635.40	-43.89

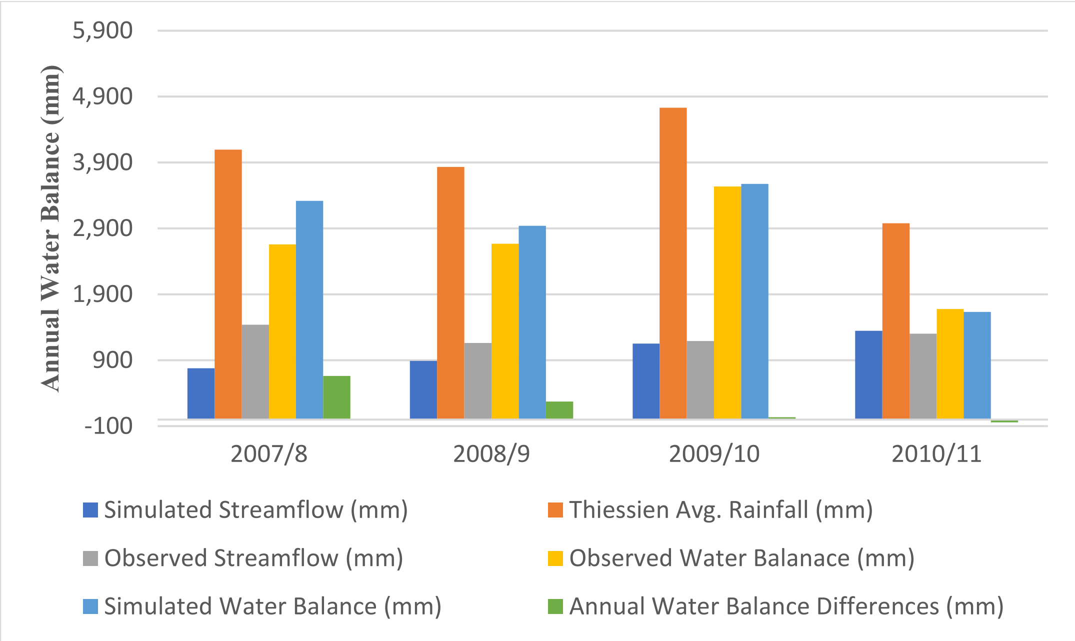

Figure 6-41: Annual water balance graph for calibration period APHRODITE data (2007/8 – 2011/12)

6.6 Model Validation – APHRODITE Data

6.6.1 Overall Validation Comparison of APHRODITE with Gauge Data (2011/12 – 2014/15)

Figure 6-42 shows**Error! Reference source not found.** the comparison of monthly and daily respectively for APHRODITE simulation flow against gauge data of streamflow for the validation period. The peak flow for APHRODITE simulation exceeds to gauge data as in Figure 6-42. The inconsistency in the lower streamflow maybe since the model spins-up time is short relative to the initial soil moisture. It could also be due to using global datasets in a relatively small watershed and APHRODITE cannot depict small-scale changes because of its moderate resolution (0.25°).

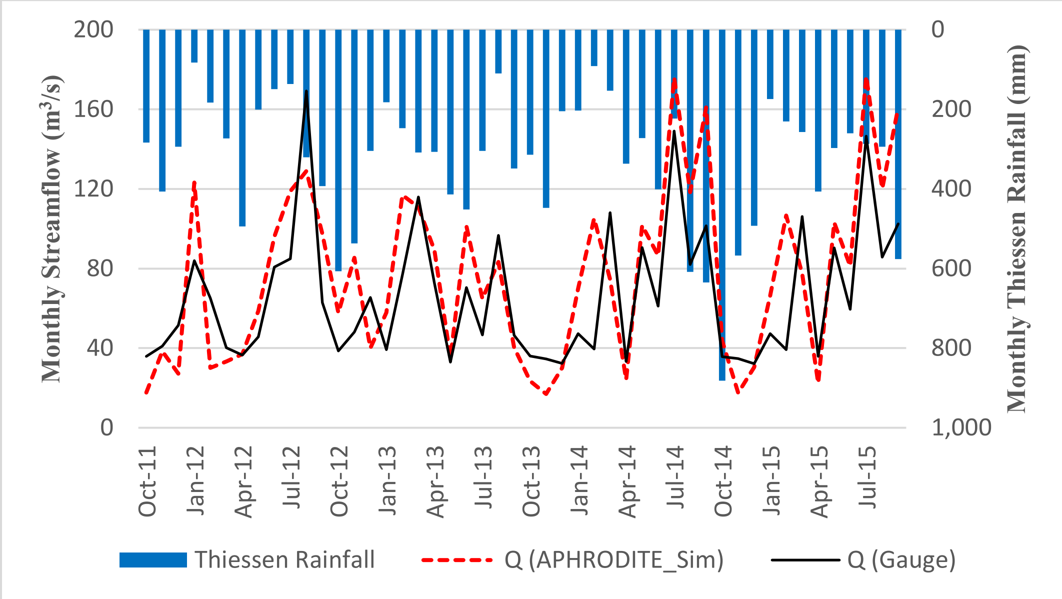

Figure 6-42: Monthly comparison of simulated APHRODITE flow with gauge data for validation period (2011/12 – 2014/15)

6.6.1.1 *Daily Comparison of APHRODITE Simulated Flow with Gauge Data – Normal Plot*

The below four graph shows the comparison of monthly validation for simulated APHRODITE flow against gauge data annually. The graph is compared to a single water year from 2011/12 till 2014/15 as shown in Figure 6-43 and Figure 6-44. The inconsistency in the lower streamflow maybe since the model spins-up time is short relative to the initial soil moisture. It could also be due to using global datasets in a relatively small watershed. It could be because APHRODITE cannot depict small-scale changes because of its moderate resolution (0.25°).

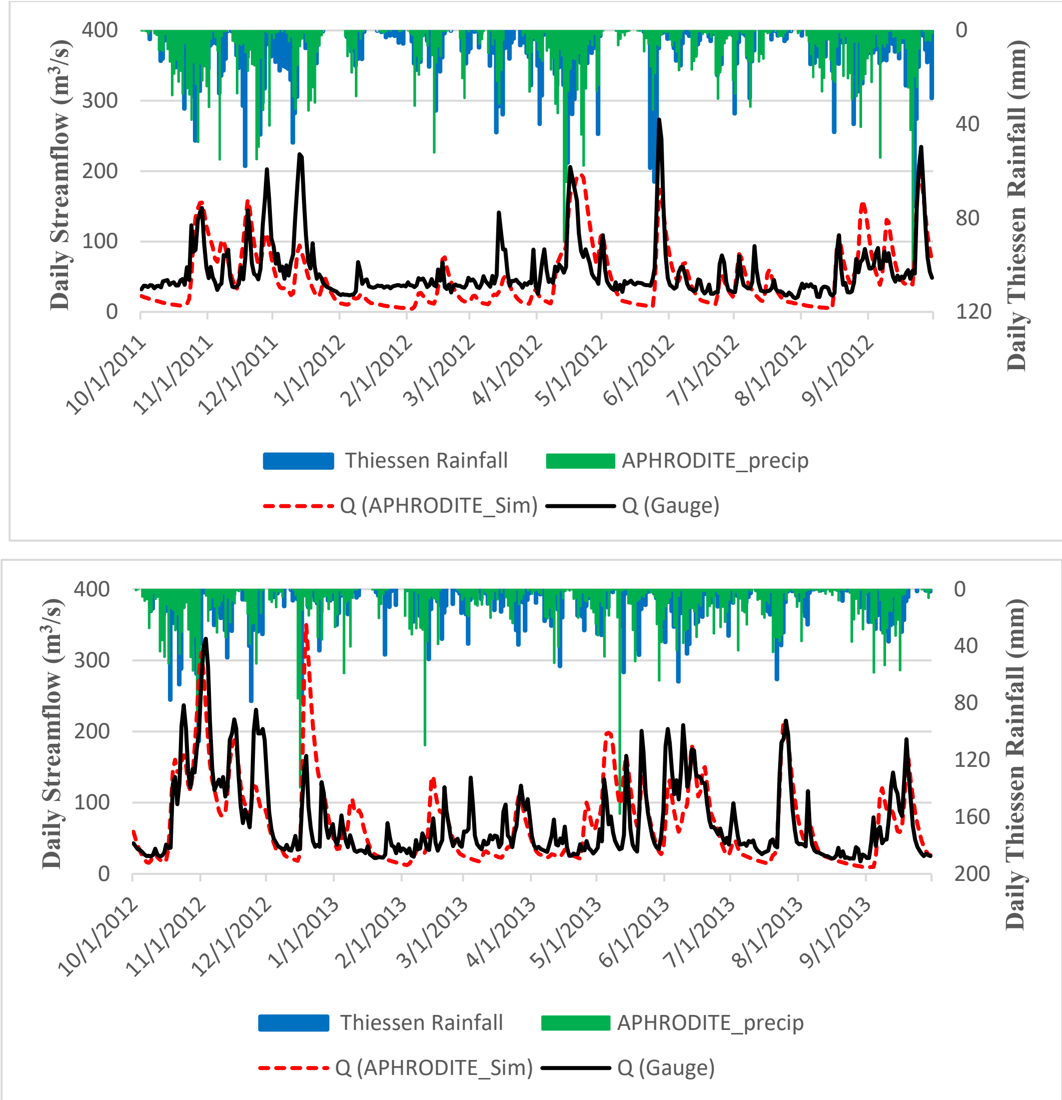

Figure 6-43: Comparison of daily APHRODITE simulated flow against gauge data (2011/12 and 2012/13)

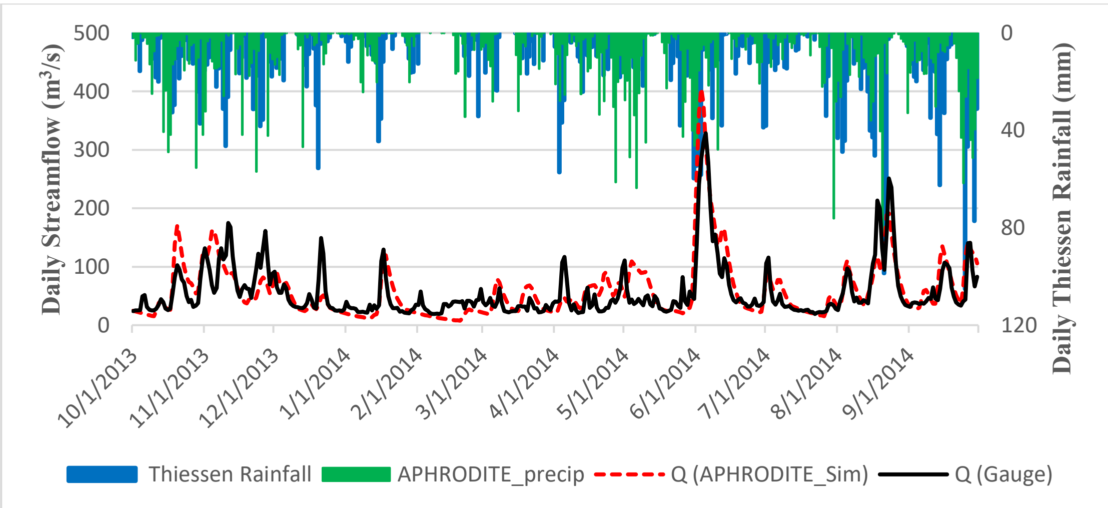

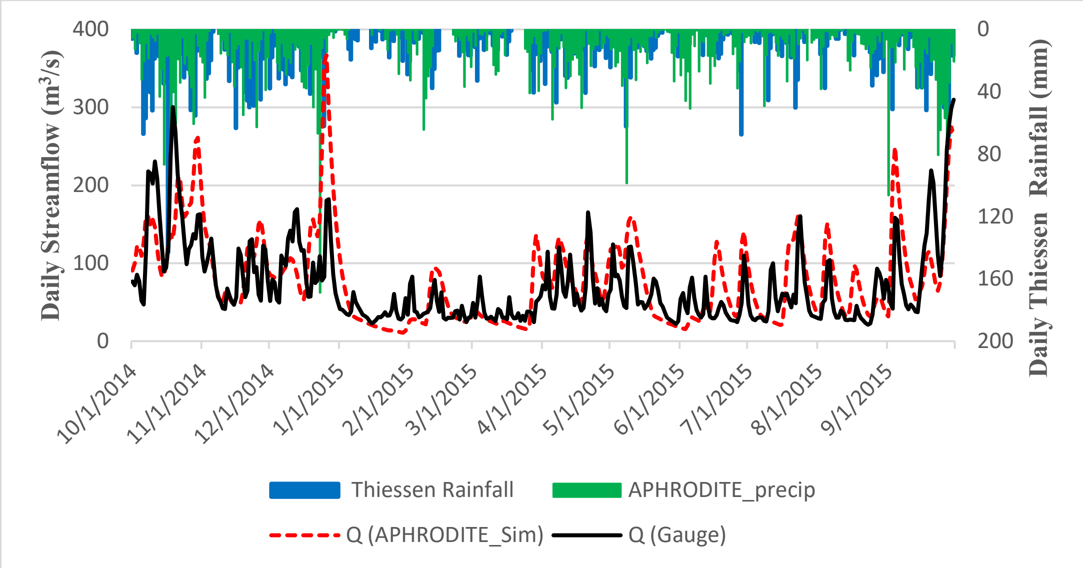

Figure 6-44: Comparison of daily APHRODITE simulated flow against gauge data (2013/14 and 2014/15)

6.6.2 Flow Duration Curve – Calibration Period

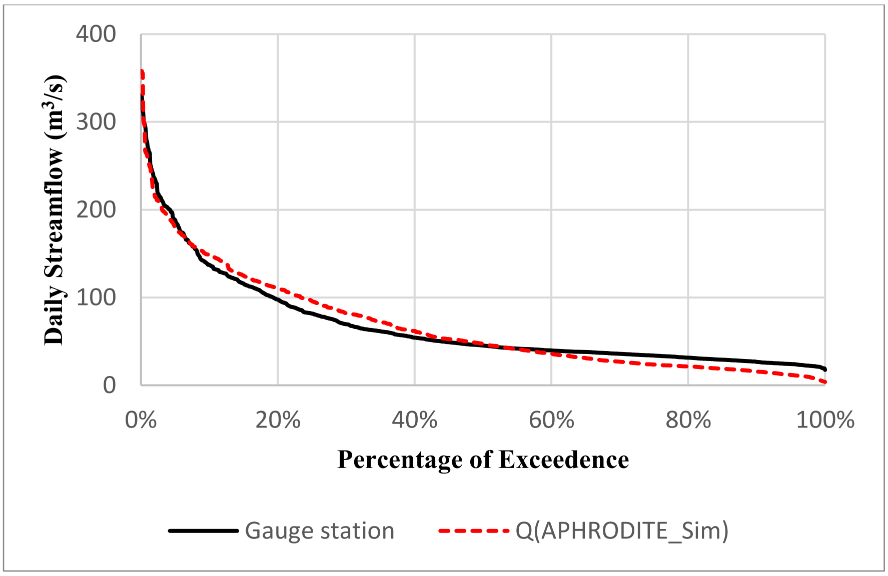

Figure 6-45: Flow duration curve for APHRODITE simulated streamflow against gauge data for validation period – Daily scale

The normal and semi-log flow duration curves were created for the entire validation period (2011/12 -2012/15). The simulated APHRODITE flow is overestimated in the medium region while the low flow is underestimated in the low regions shown in Figure 6-45 and Figure 6-46.

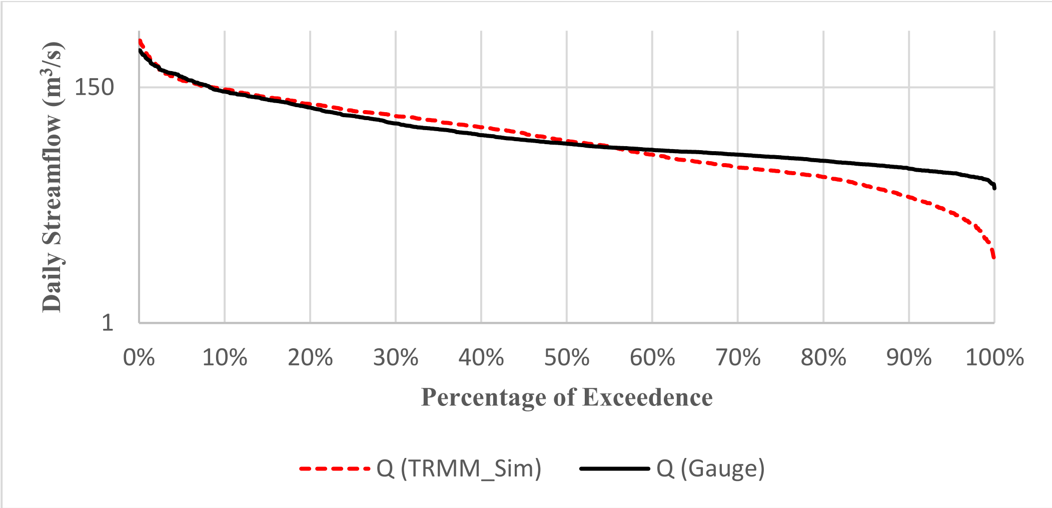

Figure 6-46: Semi log form comparison for simulated APHRODITE data against stream gauge - Validation period

The normal and semi-log scale for validation length (2011/12 -2012/15) for simulated APHRODITE flow and gauge data is shown in Figure 6-47 and Figure 6-48 for the daily scale. The simulated APHRODITE flow shows worst among the other validation part in the high flow regime.

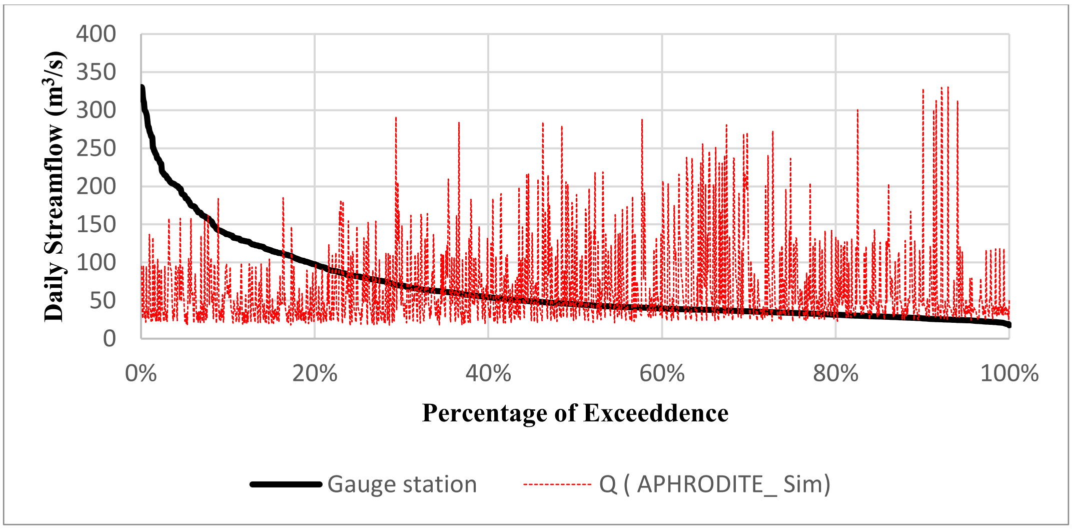

Figure 6-47: Normal FDC comparison for simulated APHRODITE data against stream gauge – Validation period

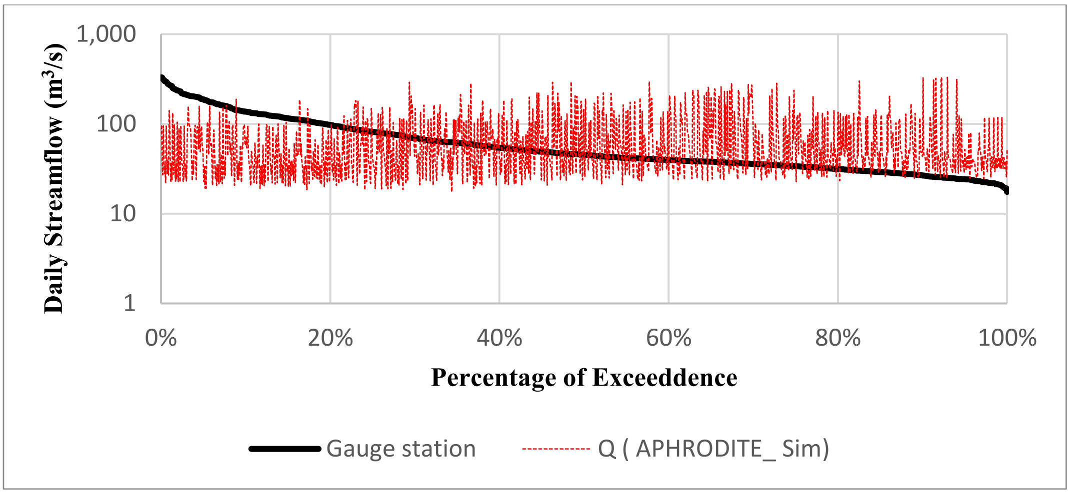

Figure 6-48: Logarithmic plot of flow duration curve for APHRODITE simulated streamflow against gauge data (2011/12 -2012/15)

6.6.3 Annual Water Balance – Validation Period

The results of the annual water balance over the model's calibration period are shown in Table 6-6 and Figure 6-49 each. This calculation is significant for determining the level of accuracy of calculated and observed flows in the year. The annual water balance differences were underestimated in 2012/13, 2013/14, and 2014/15 years while 2011/12 years it overestimates.

Table 6-6: Annual water balance calculation for validation period for APHRODITE data (2011/12 – 2014/15)

Validation						
Water Year	**Sim. SF (mm)**	**Thiessen Avg. RF (mm)**	**Obs. SF (mm)**	**Obs. WB (mm)**	**Sim. WB (mm)**	**Annual WB Diff. (mm)**
2011/12	1,021.06	3,681.25	1,218.47	2,462.78	2,660.20	197.42
2012/13	1,164.49	3,639.47	1,145.50	2,493.97	2,474.98	-18.99
2013/14	1,338.01	4,865.15	1,245.90	3,619.25	3,527.14	-92.11
2014/15	1,374.65	4,012.16	1,246.10	2,766.06	2,637.51	-128.55

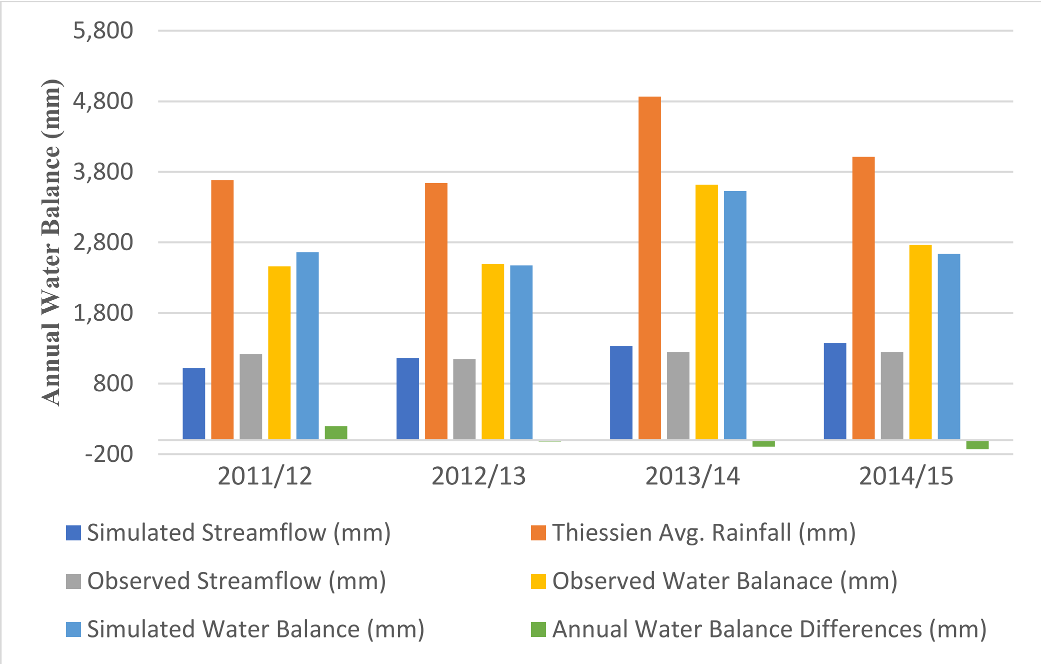

Figure 6-49: Annual water balance graph for calibration period for APHRODITE data (2011/12 – 2014/15)

6.7 Model Visual Comparison of Overall Calibration Result

Figure 6-50 shows the comparison of monthly observed rainfall and two gridded simulation flow against gauge data of streamflow for the calibration period.

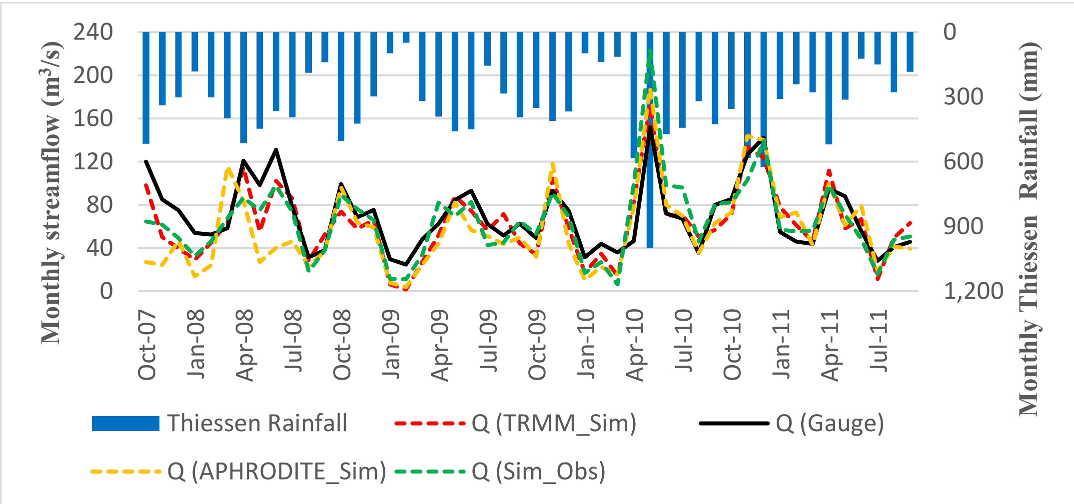

Figure 6-50: Monthly calibration result for 2007/8 – 2010/11

From the normal and semi-log of flow duration curve for the calibration period is shown in Figure 6-51 and Figure 6-52, the observed simulation flow shows close approximate to the gauge station data. While two gridded simulation flows highlight overestimation in the medium region and underestimation in the low flow threshold.

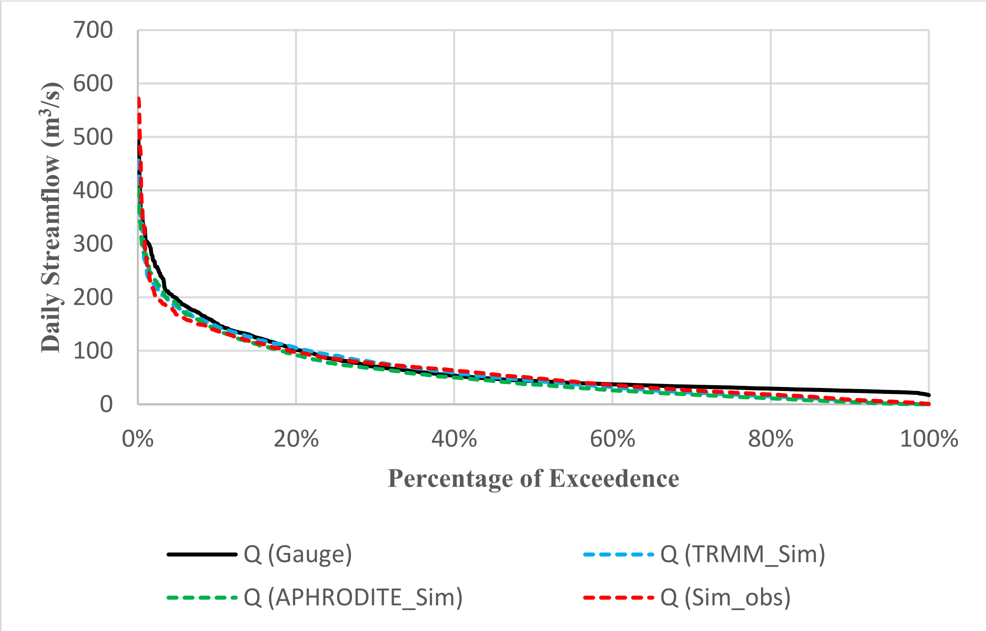

Figure 6-51: Normal plot comparison of gridded precipitation data and observed data against gauge data – Calibration

From the logarithmic plots, it can visualize TRMM simulation flow shows approximate to gauge flow after observed flow in Figure 6-52.

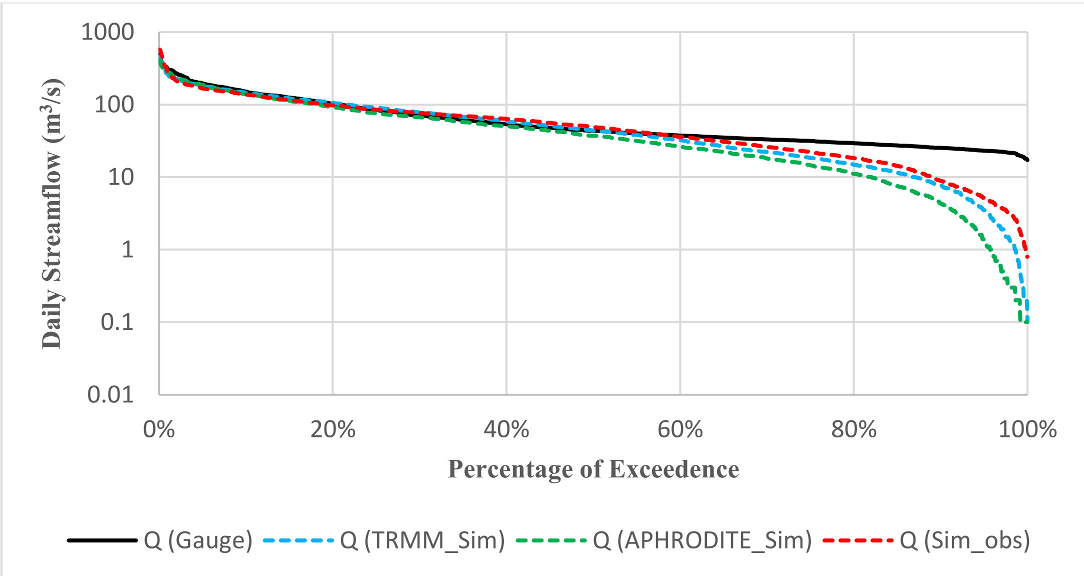

Figure 6-52: logarithmic plot comparison of satellite gridded and observed data against gauge data – Calibration

Figure 6-53 shows simulated observed rainfall pattern followed better with stream gauge in all the regions compared to two gridded data. The simulated TRMM and APHRODITE flow show major underestimation in the intermediate and low regions.

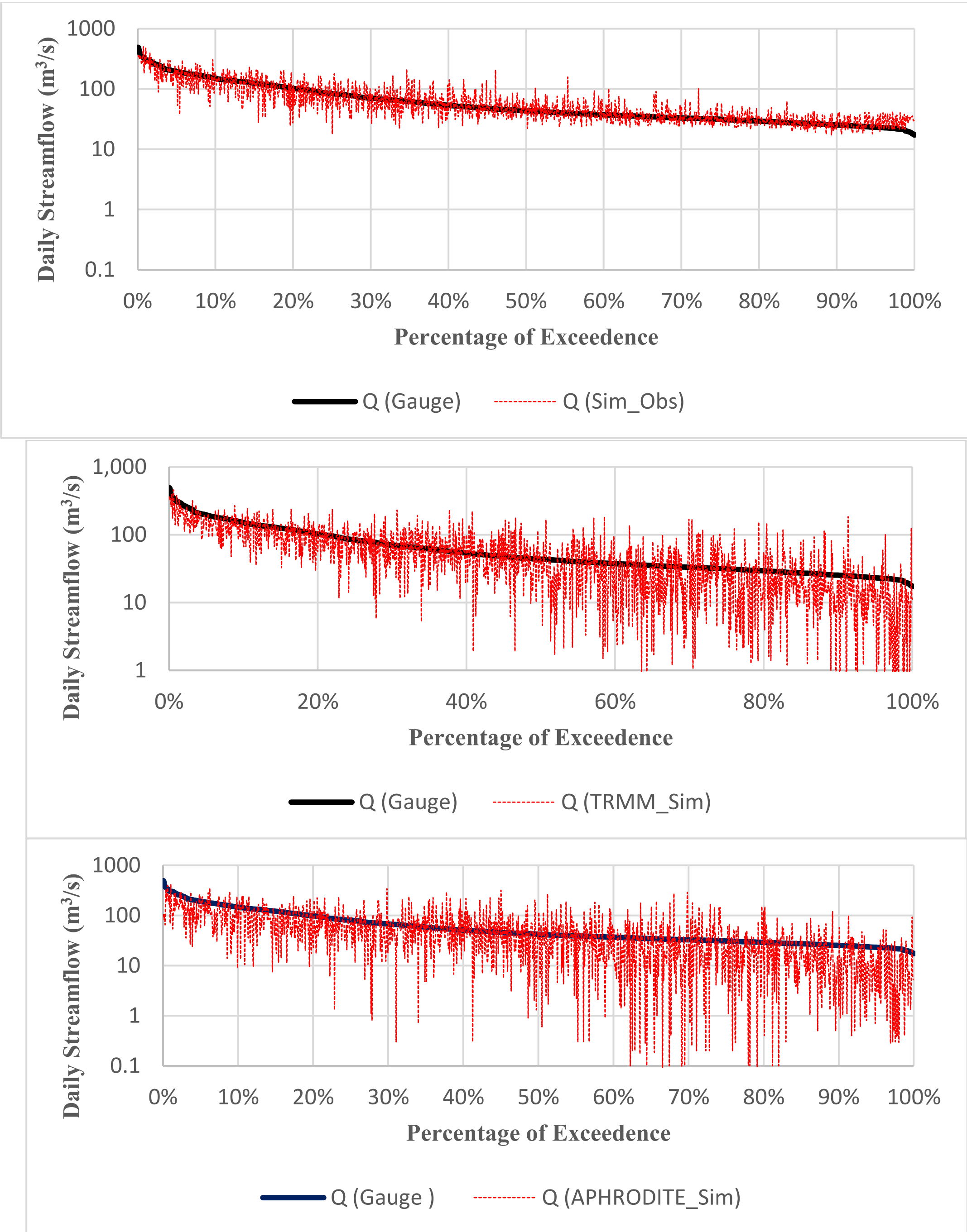

Figure 6-53: Overall comparison of simulated observed rainfall and gridded precipitation flow against stream gauge - Calibration period

Table 6-7 shows simulated observed rainfall and TRMM data perform satisfactorily as per the NSE, RMSE Std Dev., and PBIAS values.

Table 6-7: Calibration result (2007/8-2010/11)

Precipitation Product	Calibration			
	RMSE Std Dev	**NSE**	**PBIAS (%)**	**R^2**
Observed Rainfall	0.50	0.73	-8.39	0.70
TRMM	0.60	0.58	-9.44	0.66
APHRODITE	0.90	0.45	-18.24	0.47

Table 6-8 shows both gridded precipitation data and simulated from observed rainfall shows approximate value stream gauge as per statical value in the daily and monthly scale.

Table 6-8: Summary of statical value comparison for observed and gridded precipitation data (monthly and daily streamflow) – Calibration

	Calibration					
	Daily			Monthly		
	Average (m^3/s)	**Stdv.**	**Max. (m^3/s)**	**Average (m^3/s)**	**Stdv.**	**Max. (m^3/s)**
Gauge Station	69.58	61.99	492.30	69.47	31.53	151.75
Sim. Observed RF	63.74	60.53	572.00	64.87	36.88	222.99
TRMM	63.01	60.50	456.40	62.95	33.99	173.24
APHRODITE	56.88	60.11	402.50	56.82	38.29	187.96

Table 6-9 shows both gridded precipitation data and simulated from observed rainfall shows unsatisfactory value against stream gauge in daily scale while in the monthly, the minimum flow for both gridded precipitation data represents better than simulated from observed rainfall.

Table 6-9: Summary of statical value comparison for observed and gridded precipitation data (monthly and daily streamflow) - Calibration

	Calibration			
	Daily		**Monthly**	
	Min. (m^3/s)	**Correlation**	**Min. (m^3/s)**	**Correlation**
Observed				
Gauge Station	17.20	0.85	69.47	0.82
Observed Simulation	0.80		24.62	
TRMM				
Gauge Station	17.20	0.79	69.47	0.85
TRMM Simulation	0.10		62.97	
APHRODITE				
Gauge Station	17.20	0.60	69.47	0.67
APHRODITE Simulation	0.10		56.82	

Table 6-10 shows percentage error in simulated peak (PEP) and percentage error in volume (PEV) for both gridded precipitation and simulated from the observed rainfall shows low error.

Table 6-10: Comparison of peak discharge and volume against gauge data - Calibration period

	Calibration					
	Peak Discharge (m^3/s)		**PEP**	**Volume (mm)**		**PEV**
	(Gauge)	(Sim)		Q (Gauge)	Q (Sim)	
Observed RF	492.3	572.0	-0.2	13,224.4	12,117.5	0.1
TRMM		456.4	0.1		11,977.7	0.1
APHRODITE		402.5	0.2		10,814.0	0.2

6.8 Model Visual Comparison of Validation Result

The graph shown in Figure 6-54 is the comparison of monthly observed and two gridded simulation flow against gauge data of streamflow for the validation period.

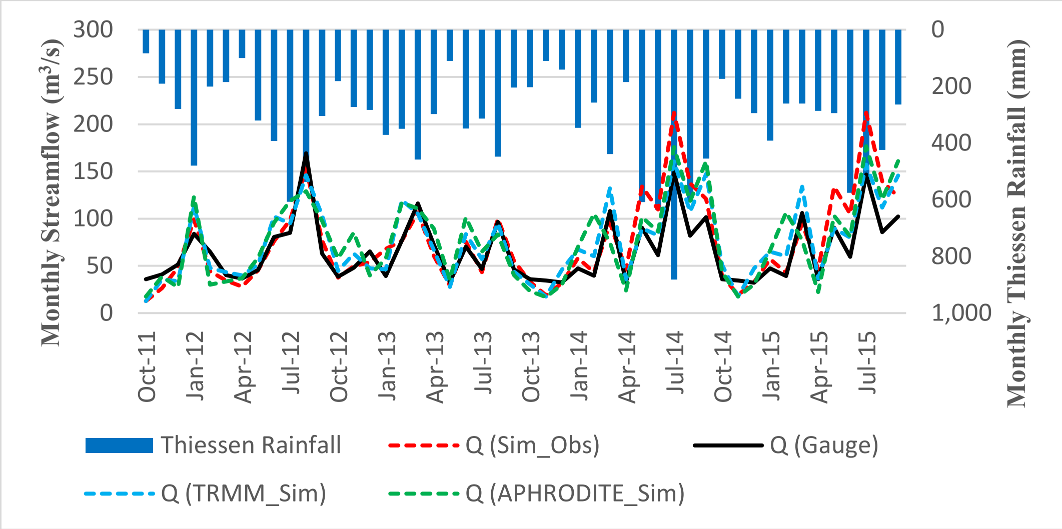

Figure 6-54: Monthly validation result for 2011/12 – 2014

From the normal and semi-log of flow duration curve for the validation period shown in Figure 6-55 and Figure 6-56, the observed and two gridded simulation flow shows close approximate to the gauge station. The observed and two gridded simulation flow highlight underestimations in the low flow region.

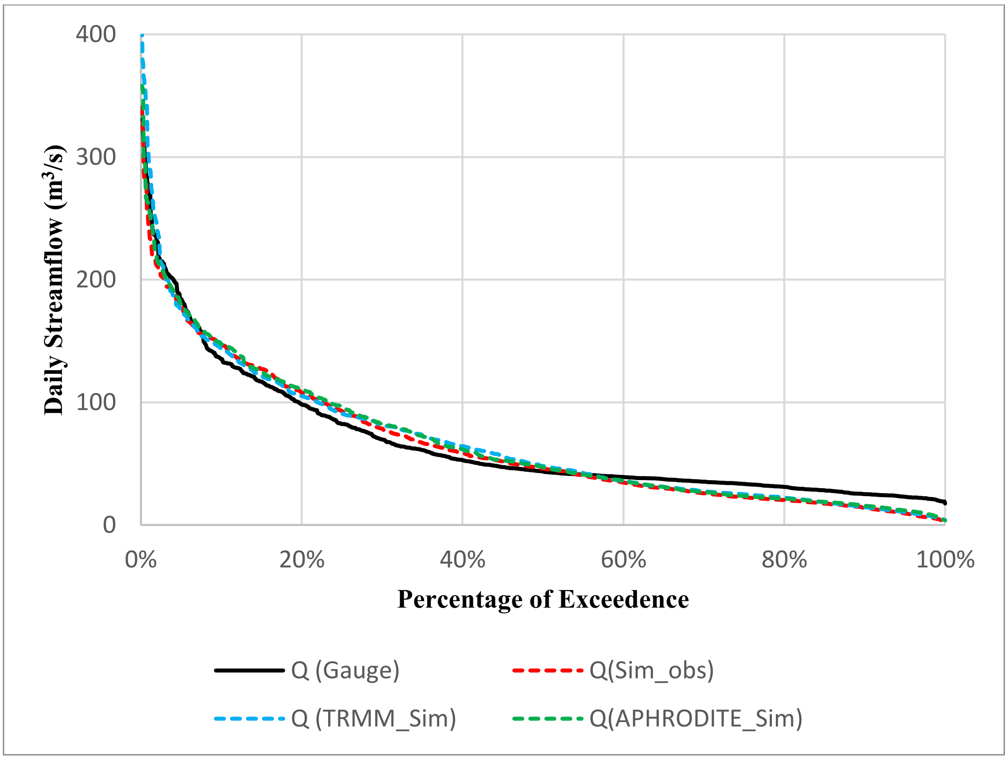

Figure 6-55: Normal plot comparison of gridded precipitation data and observed data against gauge data – validation period

From logarithmic plots on a daily scale, it can visualize simulated TRMM flow shows approximate to gauge flow after simulated observed flow in Figure 6-56**Error! Reference source not found.**.

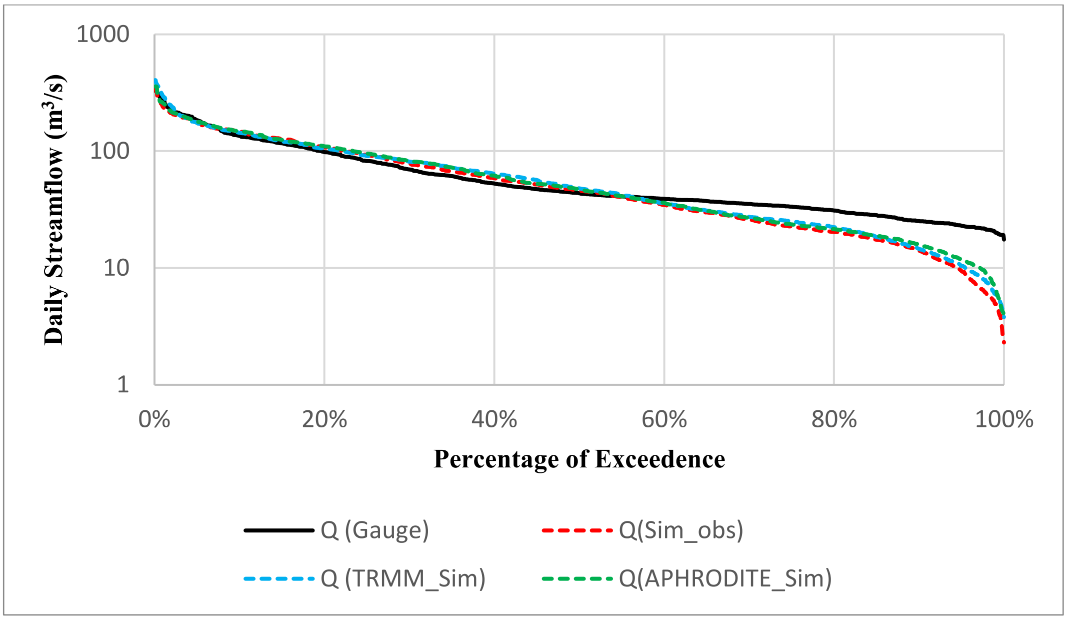

Figure 6-56. Logarithmic plot comparison of gridded precipitation and observed data against gauge data – Validation Period

Figure 6-57 shows a semi-log graph where simulated APHRODITE flow underestimates in high and partly in the intermediate region. And it overestimates in intermediate and low flow regions. The simulated observed rainfall and TRMM flow show overestimate and underestimate in all three regions, but they follow the simulated line with stream gauge.

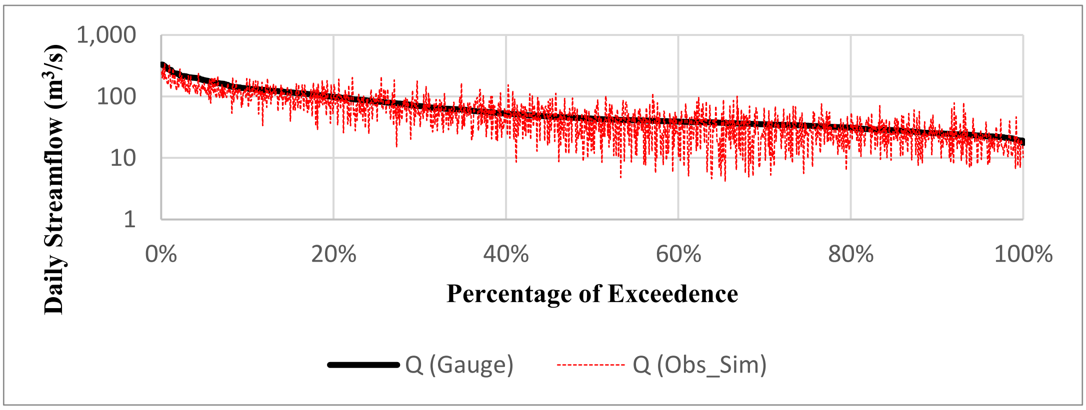

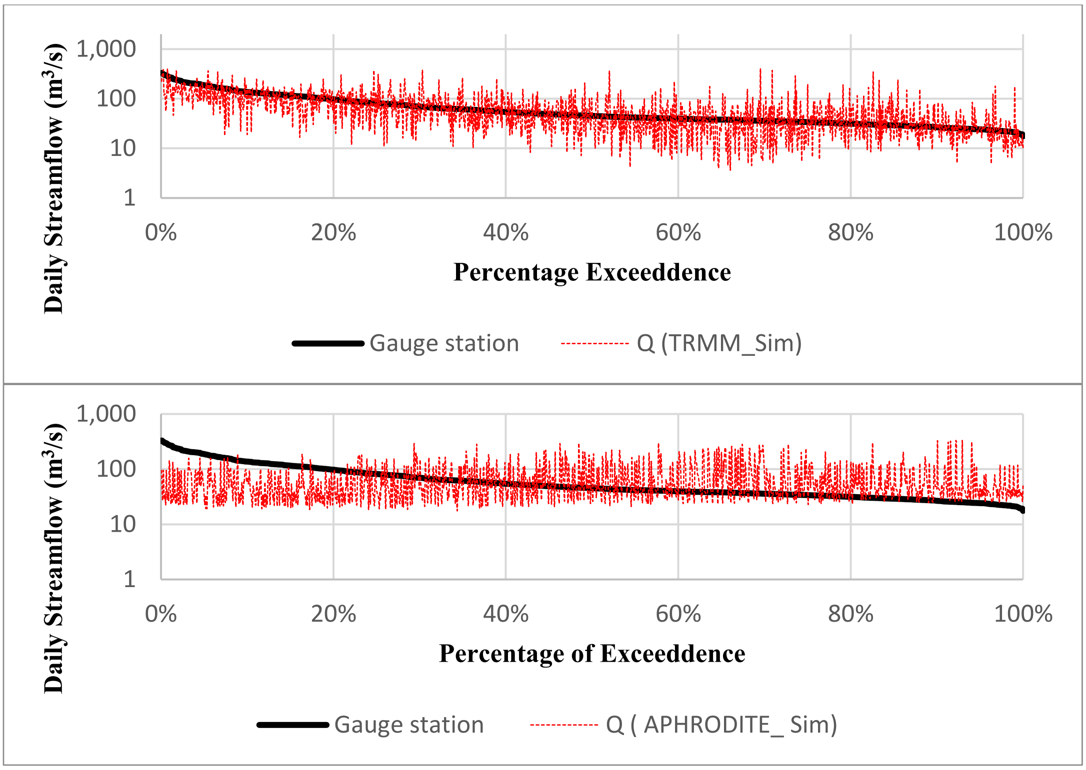

Figure 6-57: Overall comparison of simulated observed rainfall and gridded precipitation flow against stream gauge - validation period

The coefficient of determination was carried and simulated from simulated observed shows better than two gridded data when plotted against stream gauges as shown in Figure 6-58, Figure 6-59, and Figure 6-60.

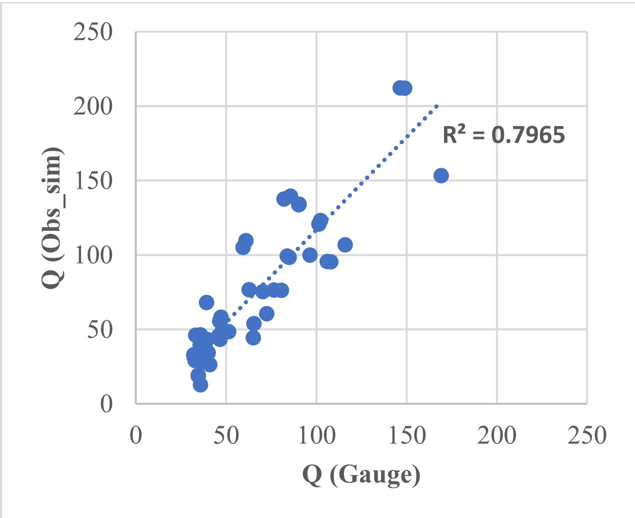

Figure 6-58: Result for validation – Simulation from observed RF

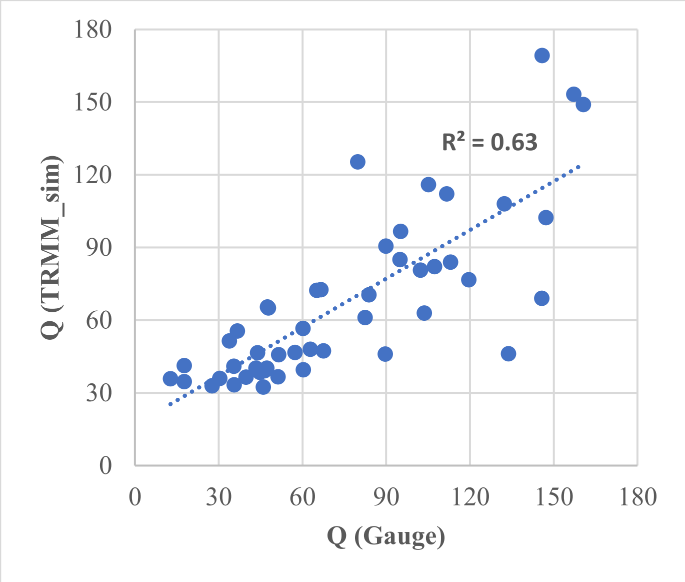

Figure 6-59: Result for validation – TRMM simulation flow

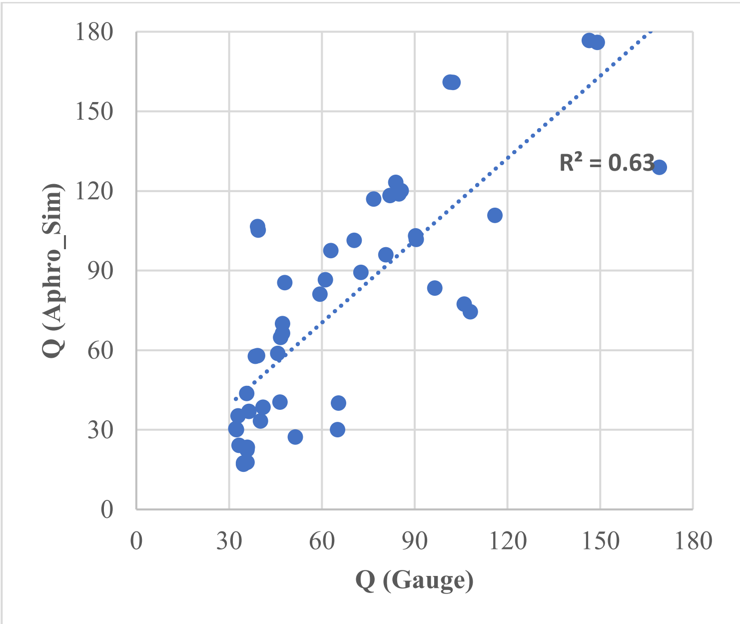

Figure 6-60: Result for validation – APHRODITE simulation flow

Table 6-11 shows simulated from observed rainfall perform satisfactorily while both gridded precipitation data showed unsatisfactory as per the NSE, RMSE Std Dev., and PBIAS values.

Table 6-11: Model Validation Result (2012-2015)

Precipitation Product	Validation			
	RMSE Std Dev	NSE	PBIAS (%)	R^2
Observed Rainfall	0.6	0.66	-2.34	0.80
TRMM	0.8	0.05	-0.22	0.63
APHRODITE	0.9	0.13	0.45	0.63

Table 6-12 shows both gridded precipitation data and simulated from observed rainfall shows approximate value stream gauge as per statical value in the daily and monthly scale.

Table 6-12: Summary of statical value comparison for observed and gridded precipitation data (monthly and daily streamflow) – Validation

	Validation					
	Daily			Monthly		
	Avg. (m^3/s)	Stdv.	Max. (m^3/s)	Avg. (m^3/s)	Stdv.	Max. (m^3/s)
Gauge Station	67.16	53.00	330.40	67.04	33.82	169.22
Observed	67.01	58.99	405.60	74.78	47.26	212.18
TRMM	75.07	60.53	376.30	74.94	40.06	160.64
APHRODITE	66.70	56.71	358.00	76.75	43.70	176.67

Table 6-13 shows both gridded precipitation data and simulated from observed rainfall shows unsatisfactory value against stream gauge in daily scale while in the monthly scale both gridded precipitation data and simulated from observed rainfall shows satisfactory streamflow.

Table 6-13: Comparison of daily and monthly scale for validation

	Validation			
	Daily		Monthly	
	Min. (m^3/s)	Correlation	Min. (m^3/s)	Correlation
Observed RF				
Gauge Station	17.50	0.84	32.19	0.89
Simulation	2.30		12.78	
TRMM				
Gauge Station	17.50		32.19	0.79
Simulation	3.80	0.58	16.98	
APHRODITE				
Gauge Station	17.50	0.60	32.19	0.60
Simulation	3.80		16.98	

Table 6-14 shows percentage error in simulated peak (PEP) and percentage error in volume (PEV) for both gridded precipitation and simulated from the observed rainfall shows low error.

Table 6-14: Comparison of peak discharge and volume against gauge data - Validation period

	Validation					
	Peak Discharge (m^3/s)		PEP	Volume (mm)		PEV
	(Gauge)	(Sim)		(Gauge)	(Sim)	
Observed	330.40	340.50	-0.03	12,618.80	12,259.60	0.03
TRMM		405.60	-0.20		12,729.90	0.00
APHRODITE		358.00	-0.10		12,670.90	0.00

CHAPTER 7

7 DISCUSSION

The HEC-HMS model was selected for the Gin watershed and the input for the model, parameter sensitivity, behavior of the model, performance of the model, and difficulties in processing of model are presented below.

7.1 Data Checking

In the study, the land use map of 1998 was gathered from the Survey Department of Sri Lanka. Though it does not represent land-use of the present year since there may be the development of various infrastructure, urbanization, and decreasing of certain items such as forest, paddy filed, etc. Land use plays a dominant role in the calculation of the percentage of impervious area and storage for the canopy which is one of the components in soil moisture accounting. The percentage of impervious was observed to be one of the sensitive parameters in the model. In the model sensitivity, it was observed with slight change or error leads to challenges for modelling process while canopy storage does not impact directly but land use will have an impact on the overall accuracy of model performance. So, the determination of parameters from land use may not be accurate.

7.2 Model Input

7.2.1 Thiessen average rainfall

Rainfall is a primary key input for the HEC-HMS model. As per WMO (2009), several gauge stations were selected for a reliable representation of rainfall. For interpolation of rainfall for the study area, Thiessen polygon was selected with ArcMap 10.5 version application for modelling, and even most of the authors have used this application for various purposes.

In the Gin watershed, five rain gauge station was used as shown in Figure 3-2 and weighted Thiessen average rainfall is shown in Figure 4-1. The highest average Thiessen weightage is for Tawalama station with 0.24 while Neluwa station show least with 0.17 among five stations. The Gin watershed is in a wet zone where it observed annual average rainfall of 3,668 mm per year. The least annual rainfall was observed in January and maximum rainfall in November as shown in Figure 7-1.

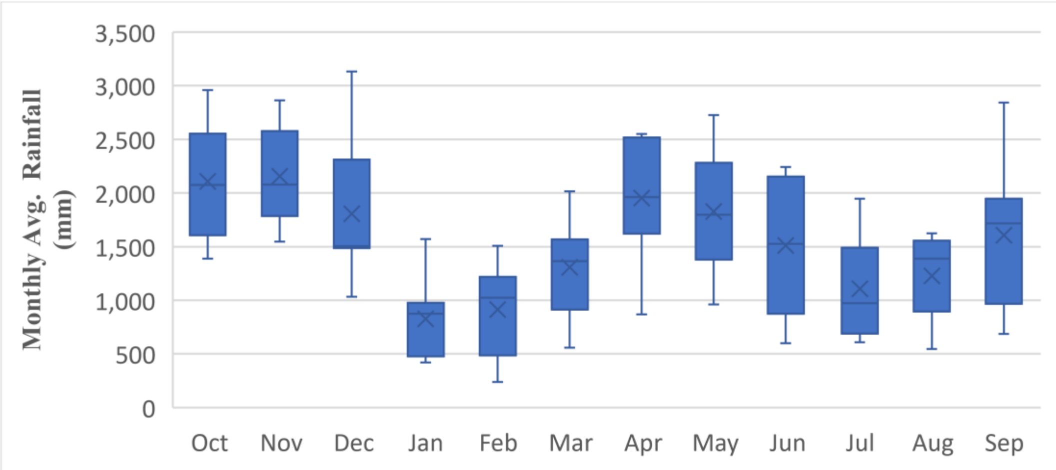

Figure 7-1: Monthly Avg. rainfall - Gin Watershed

7.2.2 Streamflow

The average annual streamflow of the Gin watershed is observed at 2,041 mm/year while the monthly average streamflow of 67 m^3/s. The maximum monthly rainfall was observed in November and less in January as shown in Figure 7-2. A similar high and low flow was observed in calibration and validation outflow in the same month.

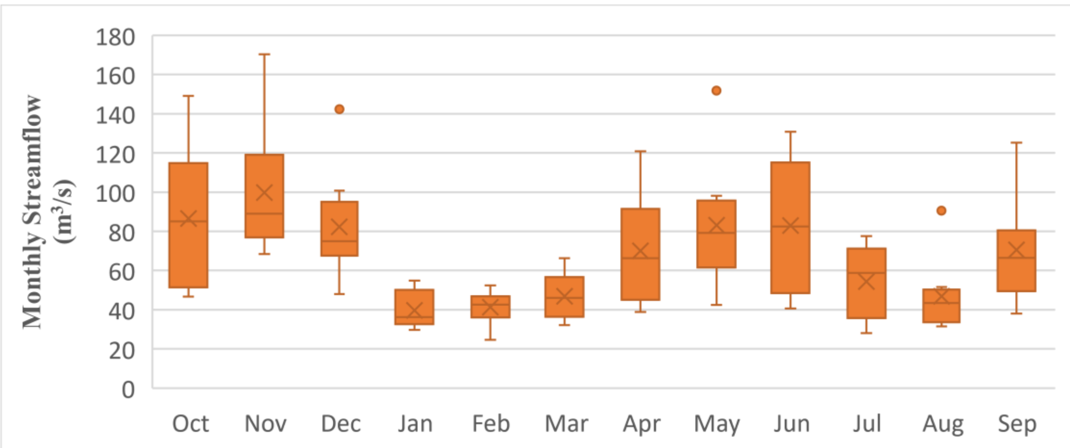

Figure 7-2: Monthly streamflow - Gin Watershed

7.2.3 Evaporation

The maximum average evaporation was observed at 764 mm while the monthly average evaporation with 66.4 mm. It can be visualized from Figure 7-3 with maximum monthly average evaporation in February and least in April month.

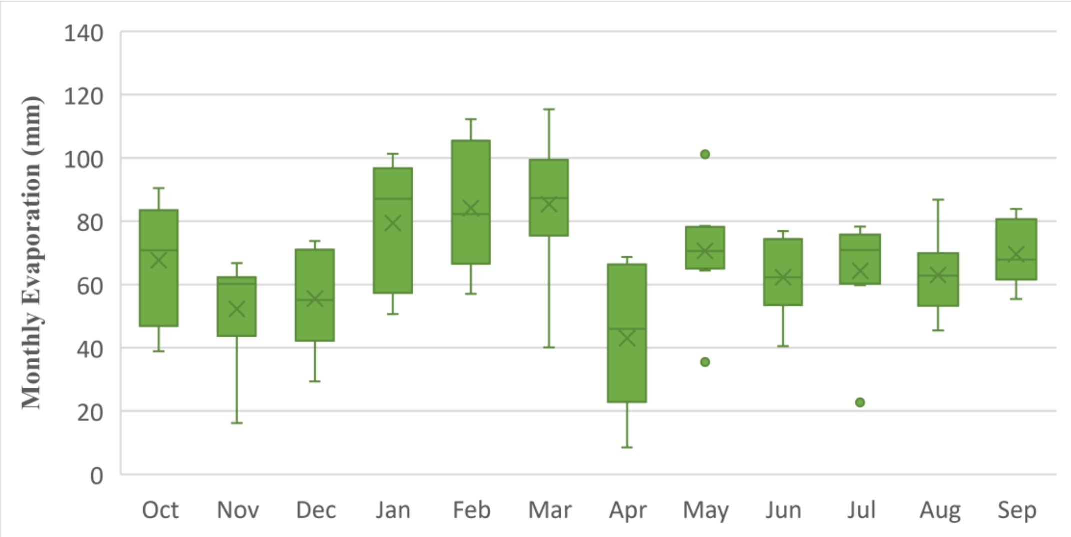

Figure 7-3: Monthly evaporation - Gin Watershed

7.2.4 Gridded precipitation data

Both the gridded precipitation data (TRMM and APHRODITE) show an underestimation of precipitation when compared with gauge rainfall as shown in Figure 4-19. After using linear scaling and cumulative distribution function (CDF) as a bias correction method, the gridded precipitation data improved to a good range as shown in Figure 4-15 and Figure 4-17 respectively for corrected TRMM and APHRODITE. The improved coefficient of determination (R^2) for TRMM and APHRODITE are 0.78 and 0.66 respectively.

7.3 Model Performance

The correlation between observed and two gridded precipitation data is carried out by using the Thiessen average rainfall. Figure 7-4 shows a correlation of calibrated simulated flow, where overestimation of intermediate flow for observed and two gridded precipitation data. The simulated APHRODITE flow overestimates high flow and underestimates low flow in the calibration part. In validation part, it shows a similar overestimation in high flow for simulated of observed rainfall and APHRODITE flow. Both gridded precipitation data show an overestimate for intermediate flow as shown in Figure 7-5.

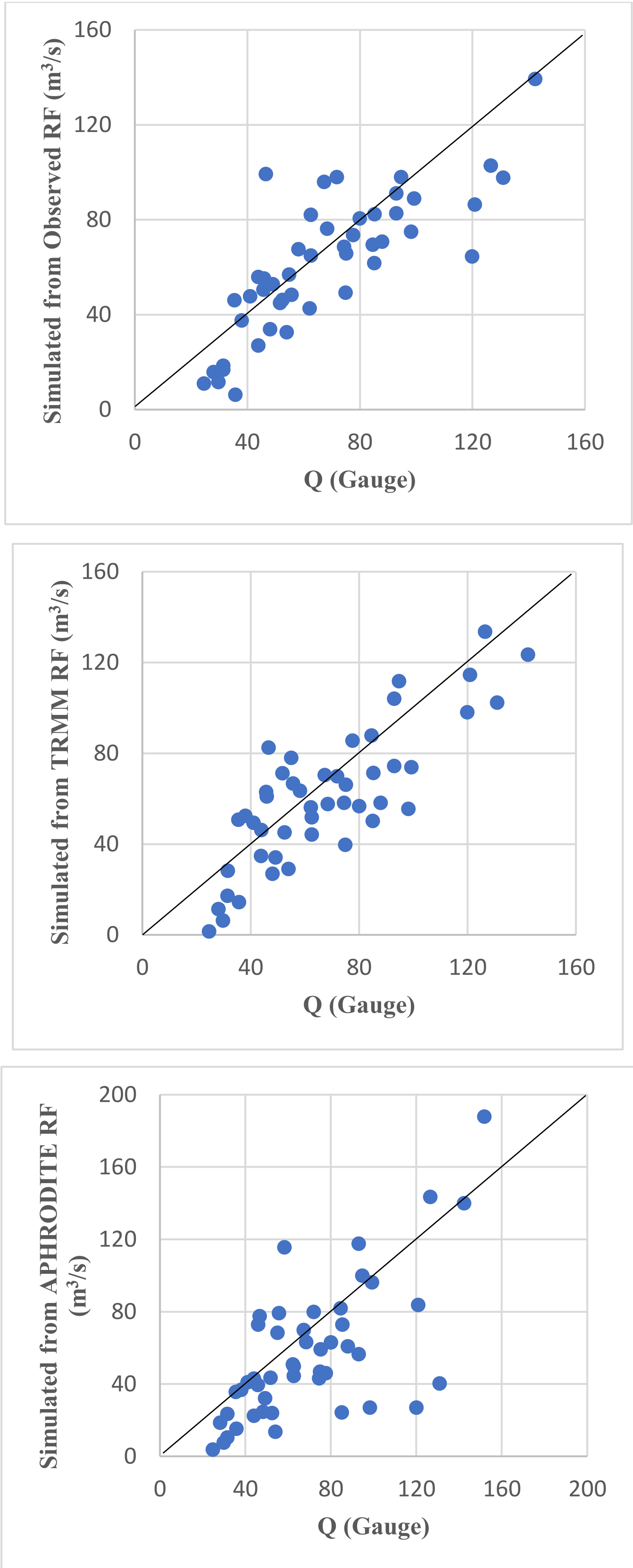

Figure 7-4: Correlation for simulated flow with gauge streamflow – Calibration

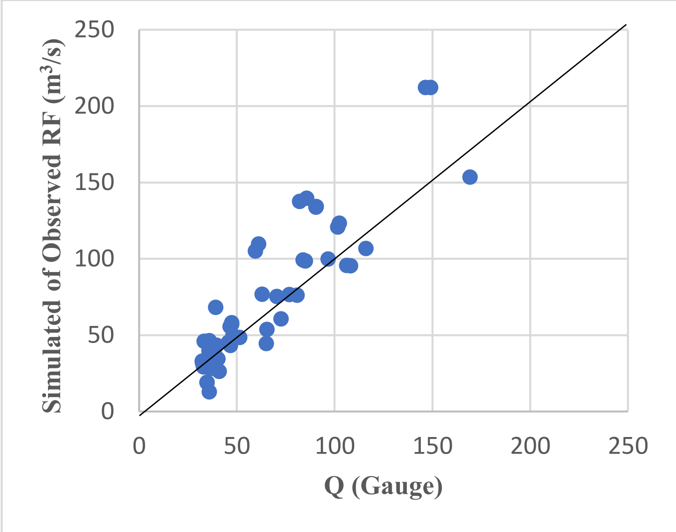

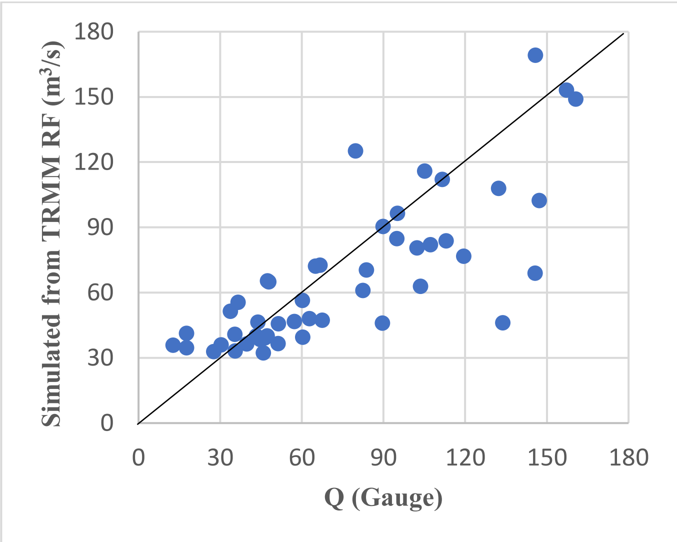

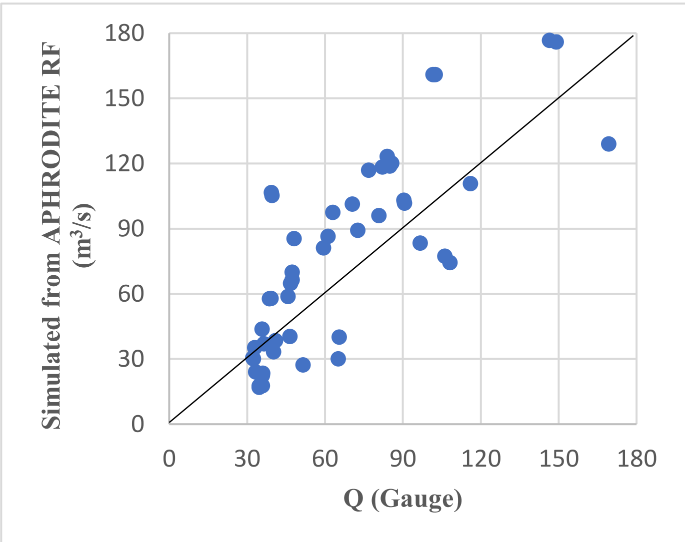

Figure 7-5: Correlation for simulated flow with gauge streamflow - Validation

The overall performance for the model was carried out by Root Mean Square Error (RMSE) as the objective function for this study. Nash–Sutcliffe model efficiency coefficient (NSE), Root Mean Square Error standard deviation (RMSE std. Dev), Coefficient of Determination, Percent Streamflow Volume Error (PVE), the percentage error in peak discharge (PEP), and percent bias (PBIAS) are considered for checking the variation for model calibration and validation result.

In calibration, the simulated from observed rainfall perform well while simulated TRMM flow performs satisfactory and simulated APHRODITE shows unsatisfactory performance as shown in Table 6-7. The observed data performed good in a simulation of streamflow compared to two gridded precipitation data with Nash–Sutcliffe model efficiency coefficient (NSE) value of 0.66, Root Mean Square Error standard deviation (RMSE Std Dev) of 0.66, and percent bias (PBIAS) of -2.34% for validation. It shows simulated from observed rainfall perform well compared to two gridded precipitation data.

The overall percentage error in volume (PEV) and percentage error in simulated peak discharge (PEP) for the developed HEC-HMS model for the Gin watershed ranges from -0.01% to 0.28% and 0.08% to 0.18% respectively with very good model performance. In the calibration part, the percentage error in volume (PEV) for observed volume shows 0.08%, TRMM data of 0.09%, and APHRODITE data of 0.19% as shown in Table 6-10. While percentage error in simulated peak (PEP) for observed shows -0.16%., TRMM data of 0.07% and APHRODITE of 0.18%.

In the validation part, the percentage error in volume (PEV) for observed volume shows 0.03%, TRMM data of -0.01%, and APHRODITE data of 0.00% as shown in Table 6-14. While percentage error in simulated peak (PEP) for observed data shows -0.03%., TRMM data of -0.23%, and APHRODITE of -0.08%.

When the monthly model streamflow is compared with the gauge station, the coefficient of determination (R^2) for observed simulated flow shows 0.80, and 0.63 for both TRMM and APHRODITE simulated flow. The TRMM gridded data captured the rain gauges statistics satisfactory in the study area. However, the fit between APHRODITE and rain gauges records shows poorly. TRMM is a good product when one wants to investigate rainfall patterns. The usage of this gridded precipitation data is, however, restrained through its temporal decision, which is not always adequate to analyze in the case of event-scale.

The above performance of the model and obtained result from calibration and validation shows the model performs satisfactorily for the Gin watershed.

7.4 Sensitivity of Model

A comparable sensitivity assessment of a continuous HEC-HMS model was achieved for the Dale hole basin in Kentucky and Tennessee. The author observed the most infiltration rate, the soil depth, the tension zone depth, and to be the sensitive parameters (Fleming & Neary, 2004). Although, another author performs runoff simulation in Ruiru reservoir catchment by HEC-HMS model. The finding reveals soil storage to be the maximum sensitive parameter, accompany by the groundwater storage coefficient and the soil tension storage capacity (Ismael et al., 2017). And the different authors also performed continuous hydrological modeling in Vamsadhara River Basin (India) by using the soil moisture accounting (SMA) model and discovered soil storage to be the most sensitive parameter (W. R. Singh & Jain, 2015). In the presents study, the most sensitive parameter in soil storage, tension zone storage, and impervious area while the second storage of groundwater (GW2) was found to be the least sensitive parameter.

7.5 Discussion of Model Result

The comparison of simulated results is carried out in the study area to determine the accuracy and suitability of simulated from observed rainfall and two gridded precipitation data.

7.5.1 Statistical Value Comparison

In the calibration part, simulated flow from observed rainfall and two gridded precipitation data show unsatisfactory for minimum flow in daily scale as shown in Table 6-8. The monthly minimum simulated flow shows close to stream gauge compared to simulated flow from observed rainfall (Table 6-8). The average simulated flow from observed rainfall and APHRODITE gridded data show close approximate to stream gauge in daily scale and monthly scale shown in Table 6-8. The correlation for simulated observed flow and two gridded precipitation data against stream gauge show satisfactory to very good performance as shown in Table 6-9.

In the validation, the average daily and monthly simulation flow from simulated observed flow and two gridded precipitation data show close to stream gauge (Table 6-12). And for the maximum average simulation for both daily and monthly two gridded precipitation shows close to stream gauge as shown in Table 6-12. The minimum simulated flow from observed rainfall and two gridded precipitation data show unsatisfactory (Table 6-13). The correlation for simulated observed flow and two gridded precipitation data against stream gauge show satisfactory to very good performance as shown in Table 6-13.

In the absence of the ground-based rainfall and streamflow observations, it can rely on TRMM and APHRODITE based on statical value (mean, standard deviation, and maximum streamflow/rainfall) as shown in Table 4-5 and Table 4-6**Error! Reference source not found.**. The low flow threshold simulation does not perform well for two gridded precipitation data as shown in Table 6-13. The two gridded precipitation data shows very low model efficiencies and correlation among observation and simulation flow. Those variations are due to uncertainties within the streamflow dataset. The multiple gauge stations may improve the model's overall performance.

7.5.2 Annual Water Balance

In calibration, the annual water balance differences for simulated from observed rainfall, TRMM and APHRODITE flow shows a weighted average overestimation of 106 mm, 120 mm, and 234 mm respectively (Table 6-1, Table 6-3, and Table 6-5).

The annual water balance differences for simulated from observed rainfall, TRMM, and APHRODITE flow shows a weighted average overestimation of 35.81 mm, underestimation of -13.68 mm, and -10.56 mm respectively as shown in Table 6-2, Table 6-4, and Table 6-6 for validation part. From the overestimation and underestimation of simulated flow within the acceptable error range, the Gin watershed model has a potential for water resources and flood management (Madhushankha & Wijesekera, 2021).

7.5.3 Flow Duration Curve

Flow Duration Curve (FDC) analysis shows overestimation and underestimation of simulated flow when compared to stream gauge. It can visualize a low flow for observed and two gridded precipitation data was underestimated but the high and intermediate flow was matching to stream gauge in calibration part in the logarithmic plot shown in Figure 6-52. In the validation part, the high flow was matching, and intermediate flow was overestimated in the logarithmic plot as shown in Figure 6-56.

CHAPTER 8

8 CONCLUSIONS

The HEC-HMS conceptual model turned into efficaciously calibrated and proven for the Gin watershed on a continuous time scale. The most sensitive parameters were soil percolation, tension zone storage, and impervious area while second storage of groundwater (GW2) was found to be the least sensitive parameter. The downloaded gridded precipitation data (TRMM and APHRODITE) from an online source consist of uncertainties and biases on the precipitation estimates over the Gin watershed.

The simulations with input from observed rainfall perform the best streamflow estimates compared to the streamflow generated from gridded precipitation data. The lumped model shows a good fit for observed data while TRMM data performed satisfactorily in the calibration part. In the validation part, TRMM performed satisfactorily in the case of coefficient of determination ($R^{2)}$ and percent bias (PBIAS). The TRMM data showed good potential to be used for hydrological on daily and monthly time scales based on statical value (mean, standard deviation, and maximum rainfall/streamflow).

The observed data performed well in a simulation of streamflow compared to two gridded precipitation data with Nash–Sutcliffe model efficiency coefficient (NSE) value of 0.66, Root Mean Square Error standard deviation (RMSE std. Dev) of 0.66, and percent bias (PBIAS) of -2.34% for validation. The percentage error in volume (PEV) for observed, TRMM data, and APHRODITE volume shows 0.03%, -0.01%, and 0.00% respectively for validation. While percentage error in simulated peak (PEP) for observed, TRMM and APHRODITE data shows -0.03%, -0.23%, and -0.08%.

The simulated monthly average flow from observed rainfall shows 74.78 m^3/s, stream gauge of 66.21 m^3/s, simulated TRMM flow of 74.94 m^3/s, and simulated APHRODITE flow of 76.75 m^3/s. The simulated streamflow from the model shows both gridded precipitation data perform unsatisfactorily because it could be because of the uncertainty of the model though gridded precipitation data was corrected by linear scaling and cumulative distribution function and compared against observed rainfall before modelling.

CHAPTER 9

9 RECOMMENDATIONS

1. Developed lumped models can be used for water resource management in similar hydrologic characteristics.
2. It is essential to choose the appropriate method and parameter as per the objective purpose of the study.
3. The gridded precipitation data with good resolution could give a better outcome for future hydrologic and water resources analysis.
4. In the absence of ground-based rainfall and streamflow observations, it can rely on two gridded data (TRMM and APHRODITE data) based on statistical values (maximum, standard deviation, mean, and minimum rainfall/streamflow).
5. The suitable bias correction method plays a key role in the study. The advance fine-tuning for bias correction is essential for a better outcome for research purposes.
6. For better performance of model results, spatial variability of data should be examined besides the Thiessen polygon method.
7. The other loss method like the SCN curve and Green Ampt method can be selected and compared the degree of variation in result.
8. In the SMA algorithm, intense attention should be embedded for determining the initial parameter for a degree of correctness.

BIBLIOGRAPHY

Adib, M. N. M., Rowshon, M. K., Mojid, M. A., & Habibu, I. (2020). Projected Streamflow in the Kurau River Basin of Western Malaysia under Future Climate Scenarios. *Scientific Reports*, *10*(1). https://doi.org/10.1038/S41598-020-65114-W

Ahbari, A., Stour, L., Agoumi, A., & Serhir, N. (2018). Estimation of initial values of the HMS model parameters: Application to the basin of Bin El Ouidane (Azilal, Morocco). *Journal of Materials and Environmental Science*, *9*(1), 305–317. https://doi.org/10.26872/JMES.2018.9.1.34

Alahacoon, N., & Edirisinghe, M. (2021). Spatial variability of rainfall trends in Sri Lanka from 1989 to 2019 as an indication of climate change. *ISPRS International Journal of Geo-Information*, *10*(2). https://doi.org/10.3390/IJGI10020084

Ali, M., Khan, S. J., Aslam, I., & Khan, Z. (2011). Simulation of the impacts of land-use change on surface runoff of Lai Nullah Basin in Islamabad, Pakistan. *Landscape and Urban Planning*, *102*(4), 271–279. https://doi.org/10.1016/J.LANDURBPLAN.2011.05.006

Arnold, J. G., Allen, P. M., Muttiah, R., & Bernhardt, G. (1995). Automated Base Flow Separation and Recession Analysis Techniques. *Groundwater*, *33*(6), 1010–1018. https://doi.org/10.1111/J.1745-6584.1995.TB00046.X

Azmat, M., Choi, M., Kim, T. W., & Liaqat, U. W. (2016). Hydrological modeling to simulate streamflow under changing climate in a scarcely gauged cryosphere catchment. *Environmental Earth Sciences*, *75*(3), 1–16. https://doi.org/10.1007/S12665-015-5059-2

Banerjee, A., Chen, R., Meadows, M. E., Singh, R. B., Mal, S., & Sengupta, D. (2020). An Analysis of Long-Term Rainfall Trends and Variability in the Uttarakhand Himalaya Using Google Earth Engine. *Remote Sensing 2020, Vol. 12, Page 709*, *12*(4), 709. https://doi.org/10.3390/RS12040709

Bao, Z., Liu, J., Zhang, J., Fu, G., Wang, G., Yan, X., Zhang, A., Xu, Q., & Shang, M. (n.d.). Estimation of baseflow parameters of variable infiltration capacity model with soil and topography properties for predictions in ungauged basins. *Hydrology and Earth System Sciences Discussions*, *8*(4), 7017–7053. Retrieved September 19, 2021, from https://www.academia.edu/8402815/Estimation_of_baseflow_parameters_of_variable_infiltration_capacity_model_with_soil_and_topography_properties_for_predictions_in_ungauged_basins

Barnston, & G., A. (1992). Correspondence among the Correlation, RMSE, and Heidke Forecast Verification Measures; Refinement of the Heidke Score. *WtFor*, *7*(4), 699–700. https://doi.org/10.1175/1520-0434(1992)007

Barros, A. P., Joshi, M., Putkonen, J., & Burbank, D. W. (2000). A study of 1999 monsoon rainfall in a mountainous region in central Nepal using TRMM products and rain gauge observations. *Geophysical Research Letters*, *27*(22), 3683–3686. https://doi.org/10.1029/2000GL011827

Barua, S., Muttil, N., Ng, A. W. M., & Perera, B. J. C. (2013). *Rainfall trend and its implications for water resource management within the Yarra River catchment, Australia*. *27*, 1727–1738. https://doi.org/10.1002/hyp.9311

Beck, H. E., Dijk, A. I. J. M. van, Miralles, D. G., Jeu, R. A. M. de, Bruijnzeel, L. A. (Sampurno), McVicar, T. R., & Schellekens, J. (2013). Global patterns in base flow index and recession based on streamflow observations from 3394 catchments. *Water Resources Research*, *49*(12), 7843–7863. https://doi.org/10.1002/2013WR013918

Bennett, T. H., & Peters, J. C. (2004). Continuous Soil Moisture Accounting in the Hydrologic Engineering Center Hydrologic Modeling System (HEC-HMS). *Joint Conference on Water Resource Engineering and Water Resources Planning and Management 2000: Building Partnerships*, *104*, 1–10. https://doi.org/10.1061/40517(2000)149

Bhuiyan, H. A. K. M., McNairn, H., Powers, J., & Merzouki, A. (2017). Application of HEC-HMS in a Cold Region Watershed and Use of RADARSAT-2 Soil Moisture in Initializing the Model. *Hydrology 2017, Vol. 4, Page 9*, *4*(1), 9. https://doi.org/10.3390/HYDROLOGY4010009

Bloomfield, J. P., Allen, D. J., & Griffiths, K. J. (2009). Examining geological controls on the baseflow index (BFI) using regression analysis: An illustration from the Thames Basin, UK. *Journal of Hydrology*, *373*(1–2), 164–176. https://doi.org/10.1016/J.JHYDROL.2009.04.025

Bormann, H., Breuer, L., Giertz, S., Huisman, J. A., & Viney, N. R. (n.d.). Spatially explicit versus lumped models in catchment hydrology – experiences from two case studies. *NATO Science for Peace and Security Series C: Environmental Security*, 3–26. Retrieved November 1, 2021, from https://www.academia.edu/28521884/Spatially_explicit_versus_lumped_models_in_catchment_hydrology_experiences_from_two_case_studies

Boyle, D. P., Gupta, H. V., Sorooshian, S., Koren, V., Zhang, Z., & Smith, M. (2001). Toward improved streamflow forecasts: The value of semi-distributed modeling. *Water Resources Research*, *37*(11), 2749–2759. https://doi.org/10.1029/2000WR000207

Brandes, D., Hoffmann, J. G., & Mangarillo, J. T. (2005). Baseflow recession rates, low flows, and hydrologic features of small watersheds in Pennsylvania, USA. *JAWRA Journal of the American Water Resources Association*, *41*(5), 1177–1186. https://doi.org/10.1111/J.1752-1688.2005.TB03792.X

Caloiero, T. (2015). Analysis of rainfall trend in New Zealand. *Environmental Earth Sciences*, *73*(10), 6297–6310. https://doi.org/10.1007/S12665-014-3852-Y

Cameron, D. S., Beven, K. J., Tawn, J., Blazkova, S., & Naden, P. (1999). Flood frequency estimation by continuous simulation for a gauged upland catchment (with uncertainty). *JHyd*, *219*(3), 169–187. https://doi.org/10.1016/S0022-1694(99)00057-8

Chen, J., Del Genio, A. D., Carlson, B. E., & Bosilovich, M. G. (2008). The spatiotemporal structure of twentieth-century climate variations in observations and reanalyses. Part I: Long-term trend. *Journal of Climate*, *21*(11), 2611–2633. https://doi.org/10.1175/2007JCLI2011.1

Clift, P. D. (Peter D. ., & Plumb, R. A. (2008). *The Asian monsoon : causes, history and effects*. 270.

Costa, W. De. (2008). Climate change in Sri Lanka: myth or reality? Evidence from long-term meteorological data. *Journal of the National Science Foundation of Sri Lanka*, *36*(0), 63–88. https://doi.org/10.4038/JNSFSR.V36I0.8048

Déqué, M. (2007). Frequency of precipitation and temperature extremes over France in an anthropogenic scenario: model results and statistical correction according to observed values. *Global and Planetary Change*, *57*(1–2), 16–26. https://doi.org/10.1016/J.GLOPLACHA.2006.11.030

Dijk, Albert I. J. M. van, Peña-Arancibia, J. L., Wood, E. F., Sheffield, J., & Beck, H. E. (2013). Global analysis of seasonal streamflow predictability using an ensemble prediction system and observations from 6192 small catchments worldwide. *Water Resources Research*, *49*(5), 2729–2746. https://doi.org/10.1002/WRCR.20251

Ebert, E. E., Janowiak, J. E., & Kidd, C. (2007). Comparison of near-real-time precipitation estimates from satellite observations and numerical models. *Bulletin of the American Meteorological Society*, *88*(1), 47–64. https://doi.org/10.1175/BAMS-88-1-47

Feldman, A. (2000a). *Hydrologic modeling system HEC-HMS : technical reference manual*. US Army Corps of Engineers Hydrologic Engineering Center.

Feldman, A. (2000b). Hydrologic Modeling System HEC-HMS. *Hydrologic Modeling System HEC-HMS Technical Reference Manual*, *March*, 148.

Fleming, M., & Neary, V. (2004). Continuous Hydrologic Modeling Study with the Hydrologic Modeling System. *Journal of Hydrologic Engineering*, *9*(3), 175–183. https://doi.org/10.1061/(ASCE)1084-0699(2004)9:3(175)

Gallart, F., Latron, J., Llorens, P., & Beven, K. (2007). Using internal catchment information to reduce the uncertainty of discharge and baseflow predictions. *Advances in Water Resources*, *4*(30), 808–823. https://doi.org/10.1016/J.ADVWATRES.2006.06.005

Gebert, W. A., Radloff, M. J., Considine, E. J., & Kennedy, J. L. (2007). Use of Streamflow Data to Estimate Base Flow/Ground-Water Recharge For Wisconsin1. *JAWRA Journal of the American Water Resources Association*, *43*(1), 220–236. https://doi.org/10.1111/J.1752-1688.2007.00018.X

Gebre, S. L. (2015). *Application of the HEC-HMS Model for Runoff Simulation of Upper Blue Nile River Basin*. https://doi.org/10.4172/2157-7587.1000199

Gebrechorkos, S. H., Hülsmann, S., & Bernhofer, C. (2019). Long-term trends in rainfall and temperature using high-resolution climate datasets in East Africa. *Scientific Reports 2019 9:1*, *9*(1), 1–9. https://doi.org/10.1038/s41598-019-47933-8

Gudmundsson, L., Bremnes, J. B., Haugen, J. E., & Engen-Skaugen, T. (2012). Technical Note: Downscaling RCM precipitation to the station scale using statistical transformations – A comparison of methods. *Hydrology and Earth System Sciences*, *16*(9), 3383–3390. https://doi.org/10.5194/HESS-16-3383-2012

Gupta, H. V., Sorooshian, S., & Yapo, P. O. (1999). Status of Automatic Calibration for Hydrologic Models: Comparison with Multilevel Expert Calibration. *Journal of Hydrologic Engineering*, *4*(2), 135–143. https://doi.org/10.1061/(ASCE)1084-0699(1999)4:2(135)

Haberlandt, U., Klöcking, B., Krysanova, V., & Becker, A. (2001). Regionalization of the base flow index from dynamically simulated flow components - A case study in the Elbe River Basin. *Journal of Hydrology*, *248*(1–4), 35–53. https://doi.org/10.1016/S0022-1694(01)00391-2

Haddad, Z. S., & Rosenfeld, D. (1997). Optimality of empirical Z-R relations. *Quarterly Journal of the Royal Meteorological Society*, *123*(541), 1283–1293. https://doi.org/10.1002/QJ.49712354107

Holberg, J. (2015). *Purdue e-Pubs Downward model development of the soil moisture accounting loss method in HEC-HMS: Revelations concerning the soil profile*. https://docs.lib.purdue.edu/open_access_theses/501

Hong, Y., Gochis, D., Cheng, J.-T., & Hsu, K.-L. (2007). *Evaluation of PERSIAN-CCS Rainfall Measurement Using the NAME Event Rain Gauge Network*. https://doi.org/10.1175/JHM574.1

Horton, P., Schaefli, B., Mezghani, A., Hingray, B., & Musy, A. (2006). Assessment of climate-change impacts on alpine discharge regimes with climate model uncertainty. *Hydrological Processes*, *20*(10), 2091–2109. https://doi.org/10.1002/HYP.6197

Hrachowitz, M., Savenije, H. H. G., Blöschl, G., McDonnell, J. J., Sivapalan, M., Pomeroy, J. W., Arheimer, B., Blume, T., Clark, M. P., Ehret, U., Fenicia, F., Freer, J. E., Gelfan, A., Gupta, H. V., Hughes, D. A., Hut, R. W., Montanari, A., Pande, S., Tetzlaff, D., … Cudennec, C. (2013). A decade of Predictions in Ungauged Basins (PUB)—a review. *Https://Doi.Org/10.1080/02626667.2013.803183*, *58*(6), 1198–1255. https://doi.org/10.1080/02626667.2013.803183

Huffman, G. J., Adler, R. F., Bolvin, D. T., Gu, G., Nelkin, E. J., Bowman, K. P., Hong, Y., Stocker, E. F., & Wolff, D. B. (2007). The TRMM Multisatellite Precipitation Analysis (TMPA): Quasi-global, multiyear, combined-sensor precipitation estimates at fine scales. *Journal of Hydrometeorology*, *8*(1), 38–55. https://doi.org/10.1175/JHM560.1

Hughes, D. A. (2006). *An evaluation of the potential use of satellite rainfall data for input to water resource estimation models in southern Africa*. *308*.

Ines, A. V. M., & Hansen, J. W. (2006). Bias correction of daily GCM rainfall for crop simulation studies. *Agricultural and Forest Meteorology*, *138*(1–4), 44–53. https://doi.org/10.1016/J.AGRFORMET.2006.03.009

Irvem, A., & Ozbuldu, M. (2019a). Evaluation of Satellite and Reanalysis Precipitation Products Using GIS for All Basins in Turkey. *Advances in Meteorology*, *2019*. https://doi.org/10.1155/2019/4820136

Irvem, A., & Ozbuldu, M. (2019b). Evaluation of Satellite and Reanalysis Precipitation Products Using GIS for All Basins in Turkey. *Advances in Meteorology*, *2019*. https://doi.org/10.1155/2019/4820136

Islam, M. N., & Uyeda, H. (2007). Use of TRMM in determining the climatic characteristics of rainfall over Bangladesh. *Remote Sensing of Environment*, *108*(3), 264–276. https://doi.org/10.1016/J.RSE.2006.11.011

Ismael, O., Joseph, S., & Patrick, H. (n.d.). Hec-Hms Model for Runoff Simulation in Ruiru Reservoir Watershed. *American Journal of Engineering Research*. Retrieved December 24, 2021, from www.ajer.org

Jain, S. K. (Sharad K., & Singh, V. P. (Vijay P. . (2003). *Water resources systems planning and management*. 858.

Jale, J. da S., Júnior, S. F. A. X., Xavier, É. F. M., Stošić, T., Stošić, B., & Ferreira, T. A. E. (2019). Application of Markov chain on daily rainfall data in Paraíba-Brazil from 1995-2015. *Acta Scientiarum. Technology*, *41*(1), e37186. https://doi.org/10.4025/actascitechnol.v41i1.37186

Janardhana Raju, N., Shukla, U. K., & Ram, P. (2010). Hydrogeochemistry for the assessment of groundwater quality in Varanasi: a fast-urbanizing center in Uttar Pradesh, India. *Environmental Monitoring and Assessment 2010 173:1*, *173*(1), 279–300. https://doi.org/10.1007/S10661-010-1387-6

Jayadeera, P. M., & Wijesekera, N. T. S. (2019). A Diagnostic Application of HEC–HMS Model to Evaluate the Potential for Water Management in the Ratnapura Watershed of Kalu Ganga Sri Lanka. *Engineer: Journal of the Institution of Engineers, Sri Lanka*, *52*(3), 11. https://doi.org/10.4038/ENGINEER.V52I3.7361

Jiang, Q., Li, W., Wen, J., Fan, Z., Chen, Y., Scaioni, M., & Wang, J. (2019). Evaluation of satellite-based products for extreme rainfall estimations in the eastern coastal areas of China. *China, Journal of Integrative Environmental Sciences*, *16*(1), 191–207. https://doi.org/10.1080/1943815X.2019.1707233

K. Ajami, N., Gupta, H., Wagener, T., & Sorooshian, S. (2004). Calibration of a semi-distributed hydrologic model for streamflow estimation along with a river system. *Journal of Hydrology*, *298*(1–4), 112–135. https://doi.org/10.1016/J.JHYDROL.2004.03.033

Kamau Muthoni, F., Omondi Odongo, V., Ochieng, J., Mugalavai, E. M., Kajumula Mourice, S., Hoesche-Zeledon, I., Mwila, M., Bekunda, M., Hoesche-Zeledon IHoeschle-Zeledon, I., & Mulundu Mwila, cgiarorg. (2019). Long-term spatial-temporal trends and variability of rainfall over Eastern and Southern Africa. *Theoretical and Applied Climatology*, *137*, 1869–1882. https://doi.org/10.1007/s00704-018-2712-1

Karaseva, M. O., Prakash, S., & Gairola, R. M. (2012). Validation of high-resolution TRMM-3B43 precipitation product using rain gauge measurements over Kyrgyzstan. *Theoretical and Applied Climatology*, *108*(1–2), 147–157. https://doi.org/10.1007/S00704-011-0509-6

Katsanos, D., Retalis, A., Tymvios, F., & Michaelides, S. (2016). Analysis of precipitation extremes based on satellite (CHIRPS) and in situ dataset over Cyprus. *Natural Hazards 2016 83:1*, *83*(1), 53–63. https://doi.org/10.1007/S11069-016-2335-8

Krause, P., Boyle, D. P., & Bäse, F. (2005). Comparison of different efficiency criteria for hydrological model assessment. *Advances in Geosciences*, *5*, 89–97. https://doi.org/10.5194/ADGEO-5-89-2005

Krause, Peter. (2002). Quantifying the impact of land- use changes on the water balance of large catchments using the J2000 model. *Physics and Chemistry of the Earth*, *27*(9–10), 663–673. https://doi.org/10.1016/S1474-7065(02)00051-7

Krishnamurti, T. N., Kumar, V., Simon, A., Bhardwaj, A., Ghosh, T., & Ross, R. (2016). A review of multimodel super ensemble forecasting for weather, seasonal climate, and hurricanes. *Reviews of Geophysics*, *54*(2), 336–377. https://doi.org/10.1002/2015RG000513

Kundzewicz, Z. W., Mata, L. J., Arnell, N. W., Döll, P., Jimenez, B., Miller, K., Oki, T., Şen, Z., & Shiklomanov, I. (2008). The implications of projected climate change for freshwater resources and their management. *Hydrological Sciences-Journal-Des Sciences Hydrologiques*, *53*(1), 3–10. https://doi.org/10.1623/hysj.53.1.3

Leander, R., & Buishand, T. A. (2007). Resampling of regional climate model output for the simulation of extreme river flows. *Journal of Hydrology*, *332*(3–4), 487–496. https://doi.org/10.1016/J.JHYDROL.2006.08.006

Levina, Hatmoko, W., Seizarwati, W., & Vernimmen, R. (2016). Comparison of TRMM Satellite Rainfall and APHRODITE for Drought Analysis in the Pemali-comal River Basin. *Procedia Environmental Sciences*, *33*, 187–195. https://doi.org/10.1016/j.proenv.2016.03.069

Liang, X., Lettenmaier, D. P., Wood, E. F., & Burges, S. J. (1994). A simple hydrologically based model of land surface water and energy fluxes for general circulation models. *Journal of Geophysical Research*, *99*(D7). https://doi.org/10.1029/94JD00483

Lobligeois, F., Andréassian, V., Perrin, C., Tabary, P., & Loumagne, C. (2014). When does higher spatial resolution rainfall information improve streamflow simulation? An evaluation using 3620 flood events. *Hydrology and Earth System Sciences*, *18*(2), 575–594. https://doi.org/10.5194/HESS-18-575-2014

Longobardi, A., & Villani, P. (2008). Baseflow index regionalization analysis in a Mediterranean area and data scarcity context: Role of the catchment permeability index. *Journal of Hydrology*, *355*(1–4), 63–75. https://doi.org/10.1016/J.JHYDROL.2008.03.011

Madhushankha, J. M. L., & Wijesekera, N. T. S. (2021). Application of HEC-HMS Model to Estimate Daily Streamflow in Badddegama Watershed of Gin Ganga Basin Sri Lanka. *Engineer: Journal of the Institution of Engineers, Sri Lanka*, *54*(1), 89. https://doi.org/10.4038/ENGINEER.V54I1.7438

Mao, Q., Mcnider, R. T., Mueller, S. F., & Juang, H. M. H. (1999). An optimal model output calibration algorithm is suitable for objective temperature forecasting. *Weather and Forecasting*, *14*(2), 190–202. https://doi.org/10.1175/1520-0434(1999)014<0190:AOMOCA>2.0.CO;2

Mazvimavi, D., Meijerink, A. M. J., Savenije, H. H. G., & Stein, A. (2005). Prediction of flow characteristics using multiple regression and neural networks: A case study in Zimbabwe. *Physics and Chemistry of the Earth*, *30*(11-16 SPEC. ISS.), 639–647. https://doi.org/10.1016/J.PCE.2005.08.003

Meenu, R., Rehana, S., & Mujumdar, P. P. (2013). Assessment of hydrologic impacts of climate change in Tunga–Bhadra river basin, India with HEC-HMS and SDSM. *Hydrological Processes*, *27*(11), 1572–1589. https://doi.org/10.1002/HYP.9220

Miao, D., Young, S. L., & Golden, C. D. (2015). A meta-analysis of pica and micronutrient status. *American Journal of Human Biology*, *27*(1), 84–93. https://doi.org/10.1002/AJHB.22598

Michelson, D. B. (2004). Systematic correction of precipitation gauge observations using analyzed meteorological variables. *Journal of Hydrology*, *290*(3–4), 161–177. https://doi.org/10.1016/J.JHYDROL.2003.10.005

Nair, S., & Srinivasan, G. (2009). Evaluation of Multi-Satellite TRMM Derived Rainfall Estimates over a Western State of India. *Journal of the Meteorological Society of Japan*, *87*(6), 927–939. https://doi.org/10.2151/jmsj.87.927

Nalaka Gunasekara, D., & Lanka, S. (2018). *Application of "abcd" monthly water balance model for Kalu Ganga and Gin Ganga basins and its application potential for water resources investigation*.

Nash, J. E., & Sutcliffe, J. V. (1970). River flow forecasting through conceptual models part I — A discussion of principles. *Journal of Hydrology*, *10*(3), 282–290. https://doi.org/10.1016/0022-1694(70)90255-6

Nastos, P. T., Kapsomenakis, J., & Philandras, K. M. (2016). Evaluation of the TRMM 3B43 gridded precipitation estimates over Greece. *Atmospheric Research*, *169*, 497–514. https://doi.org/10.1016/J.ATMOSRES.2015.08.008

National Atlas. (2007). *The National Atlas of Sri Lanka*.

Naveendrakumar, G., Vithanage, M., Kwon, H. H., Iqbal, M. C. M., Pathmarajah, S., & Obeysekera, J. (2018). Five decadal trends in averages and extremes of rainfall and temperature in Sri Lanka. *Advances in Meteorology*, *2018*. https://doi.org/10.1155/2018/4217917

Nisansala, W. D. S., Abeysingha, N. S., Islam, A., & Bandara, A. M. K. R. (2020). Recent rainfall trend over Sri Lanka (1987–2017). *International Journal of Climatology*, *40*(7), 3417–3435. https://doi.org/10.1002/JOC.6405

Nishat, B., & Rahman, S. M. M. (2009). Water Resources Modeling of the Ganges-Brahmaputra-Meghna River Basins Using Satellite Remote Sensing Data1. *JAWRA Journal of the American Water Resources Association*, *45*(6), 1313–1327. https://doi.org/10.1111/J.1752-1688.2009.00374.X

Panegrossi, G., Casella, D., Dietrich, S., Marra, A. C., Sano, P., Mugnai, A., Baldini, L., Roberto, N., Adirosi, E., Cremonini, R., Bechini, R., Vulpiani, G., Petracca, M., & Porcu, F. (2016). Use of the GPM Constellation for Monitoring Heavy Precipitation Events over the Mediterranean Region. *IEEE Journal of Selected Topics in Applied Earth Observations and Remote Sensing*, *9*(6), 2733–2753. https://doi.org/10.1109/JSTARS.2016.2520660

Panofsky, H., and G. B. (1958). (1958). *Some applications of statistics to meteorology,*.

Piani, C., Haerter, J. O., & Coppola, E. (2010). Statistical bias correction for daily precipitation in regional climate models over Europe. *Theoretical and Applied Climatology*, *99*(1–2), 187–192. https://doi.org/10.1007/S00704-009-0134-9/FIGURES/4

Ponce, V. M. (1989). *Engineering hydrology : principles and practices*. 640.

Porcù, F., Milani, L., & Petracca, M. (2014). On the uncertainties in validating satellite instantaneous rainfall estimates with rain gauge operational network. *Atmospheric Research*, *144*, 73–81. https://doi.org/10.1016/j.atmosres.2013.12.007

Qian, S. S., Cuffney, T. F., Alameddine, I., McMahon, G., & Reckhow, K. H. (2010). On the application of multilevel modeling in environmental and ecological studies. *Ecology*, *91*(2), 355–361. https://doi.org/10.1890/09-1043.1

Ramanarayanan, T. (n.d.). Large Area Hydrologic Modeling and Assessment Part II: Model APPLICATION1. *Jawra Journal of the American Water Resources Association*. Retrieved September 19, 2021, from https://www.academia.edu/22511065/Large_Area_Hydrologic_Modeling_and_Assessment_Part_II_Model_APPLICATION1

Ratnayake, A. S., & Pitawala, A. (2014). Prediction of the ungauged river basin for hydropower potential and flood risk mitigation: a case study at Gin River, Sri Lanka. *Interdisciplinary Environmental Review*, *15*(4), 203. https://doi.org/10.1504/ier.2014.065015

Rawls, W. J., Brakensiek, D. L., & Miller, N. (1983). Greenampt Infiltration Parameters from Soils Data. *Journal of Hydraulic Engineering*, *109*(1), 62–70. https://doi.org/10.1061/(ASCE)0733-9429(1983)109:1(62)

Reed, S., Koren, V., Smith, M., Zhang, Z., Moreda, F., & Seo, D. J. (2004). Overall distributed model intercomparison project results. *Journal of Hydrology*, *298*(1–4), 27–60. https://doi.org/10.1016/J.JHYDROL.2004.03.031

Refsgaard, J. C., & Knudsen, J. (1996). Operational Validation and Intercomparison of Different Types of Hydrological Models. *Water Resources Research*, *32*(7), 2189–2202. https://doi.org/10.1029/96WR00896

Salvadore, E., Bronders, J., & Batelaan, O. (2015). Hydrological modelling of urbanized catchments: A review and future directions. *Journal of Hydrology*, *529*(P1), 62–81. https://doi.org/10.1016/J.JHYDROL.2015.06.028

Samady, K. (2017). *Continuous hydrologic modeling for analyzing the continuous hydrologic modeling for analyzing the effects of drought on the lower Colorado river in effects of drought on the lower Colorado river in Texas part of the civil and environmental engineering com*. https://doi.org/10.37099/mtu.dc.etdr/460

Sampath, D. S., Weerakoon, S. B., & Herath, S. (2015). HEC-HMS model for runoff simulation in a tropical catchment with intra-basin diversions – case study of the Deduru Oya river basin, Sri Lanka. *Engineer: Journal of the Institution of Engineers, Sri Lanka*, *48*(1), 1. https://doi.org/10.4038/ENGINEER.V48I1.6843

Santos, V. C. dos, Blanco, C., & Oliveira Júnior, J. F. de. (2019). Distribution of rainfall probability in the Tapajos River Basin, Amazonia, Brazil. *Revista Ambiente & Água*, *14*(3), 1. https://doi.org/10.4136/AMBI-AGUA.2284

Sayama, T., Tachikawa, Y., & Takara, K. (2011). *Spatial lumping of a distributed rainfall-sediment-runoff model and its effective lumping scale*. https://doi.org/10.1002/hyp.8300

Scharffenberg, W. A. (2016). *Hydrologic Modelling System HEC-HMS User's Manual," 2016.*

Schmidli, J. ¨ U., Frei, C., & Vidale, P. L. (2006). Downscaling from GCM precipitation: a benchmark for dynamical and statistical downscaling methods. *INTERNATIONAL JOURNAL OF CLIMATOLOGY Int. J. Climatol*, *26*, 679–689. https://doi.org/10.1002/joc.1287

Seibert, J. (2005). *HBV light version 2 User's Manual*.

Shah, S. M. S., O'Connell, P. E., & Hosking, J. R. M. (1996). Modelling the effects of spatial variability in rainfall on catchment response. 2. Experiments with distributed and lumped models. *Journal of Hydrology*, *175*(1–4), 89–111. https://doi.org/10.1016/S0022-1694(96)80007-2

Shrestha, S., Shrestha, M., & Babel, M. S. (2016). Modelling the potential impacts of climate change on hydrology and water resources in the Indrawati River Basin, Nepal. *Environmental Earth Sciences*, *75*(4), 1–13. https://doi.org/10.1007/s12665-015-5150-8

Singh, L., & Saravanan, S. (2020). Evaluation of various spatial rainfall datasets for streamflow simulation using SWAT model of Wunna basin, India. *Https://Doi.Org/10.1080/15715124.2020.1776305*. https://doi.org/10.1080/15715124.2020.1776305

Singh, W. R., & Jain, M. K. (2015). Continuous Hydrological Modeling using Soil Moisture Accounting Algorithm in Vamsadhara River Basin, India. *Journal of Water Resource and Hydraulic*, *4*(4), 398–408. https://doi.org/10.5963/JWRHE0404011

Siriwardana, S. T., & Wijesekera, N. T. S. (2020). Review of Yield Comparison Options for Planning Irrigation Reservoirs in Ungauged Watersheds. *Engineer: Journal of the Institution of Engineers, Sri Lanka*, *53*(1), 77. https://doi.org/10.4038/ENGINEER.V53I1.7401

Sivapalan, M. (2003). Prediction in ungauged basins: a grand challenge for theoretical hydrology. *Hydrological Processes*, *17*(15), 3163–3170. https://doi.org/10.1002/HYP.5155

Smakhtin, V. U. (2001). Low flow hydrology: a review. *Journal of Hydrology*, *240*(3–4), 147–186. https://doi.org/10.1016/S0022-1694(00)00340-1

Smakhtin, V. Y., Hughes, D. A., & Creuse-naudin, E. (1997). Régionalisation des caractéristiques des débits journaliers dans une région du Cap Oriental (Afrique du Sud). *Hydrological Sciences Journal*, *42*(6), 919–936. https://doi.org/10.1080/02626669709492088

Smith, M. B., Koren, V., Zhang, Z., Zhang, Y., & Reed, S. M. (2012). *Results of the DMIP 2 Oklahoma experiments*. https://doi.org/10.1016/j.jhydrol.2011.08.056

Soares, A. S. D., da Paz, A. R., & Piccilli, D. G. A. (2016). Avaliação das estimativas de chuva do satélite TRMM no Estado da Paraíba. *Revista Brasileira de Recursos Hidricos*, *21*(2), 288–299. https://doi.org/10.21168/RBRH.V21N2.P288-299

Sorooshian, S., Aghakouchak, A., Arkin, P., Eylander, J., Foufoula-Georgiou, E., Harmon, R., Hendrickx, J. M. H., Imam, B., Kuligowski, R., Skahill, B., & Skofronick-Jackson, G. (2011). Advancing the remote sensing of precipitation. *Bulletin of the American Meteorological Society*, *92*(10), 1271–1272. https://doi.org/10.1175/BAMS-D-11-00116.1

Su, C.-H., Peterson, T. J., Costelloe, J. F., & Western, A. W. (2016). A synthetic study to evaluate the utility of hydrological signatures for calibrating a base flow separation filter. *Water Resources Research*, *52*(8), 6526–6540. https://doi.org/10.1002/2015WR018177

Suryantoro, A., Pusat, P., Sains Atmosfer, P., & Iklim, D. (2010). Siklon tropis di selatan dan barat daya indonesia dari pemantauan satelit trmm dan kemungkinan kaitannya dengan gelombang tinggi dan puting beliung. *Majalah Sains Dan Teknologi Dirgantara*, *3*(1). http://jurnal.lapan.go.id/index.php/majalah_sains_tekgan/article/view/8

Tallaksen, L. M. (1995). A review of baseflow recession analysis. *Journal of Hydrology*, *165*(1–4), 349–370. https://doi.org/10.1016/0022-1694(94)02540-R

Tan, M. L., & Duan, Z. (2017). Assessment of GPM and TRMM Precipitation Products over Singapore. *Remote Sensing 2017, Vol. 9, Page 720*, *9*(7), 720. https://doi.org/10.3390/RS9070720

Tapiador, F. J., Turk, F. J., Petersen, W., Hou, A. Y., García-Ortega, E., Machado, L. A. T., Angelis, C. F., Salio, P., Kidd, C., Huffman, G. J., & de Castro, M. (2012). Global precipitation measurement: Methods, datasets and applications. *Atmospheric Research*, *104–105*, 70–97. https://doi.org/10.1016/j.atmosres.2011.10.021

Tramblay, Y., Bouvier, C., Martin, C., Didon-Lescot, J. F., Todorovik, D., & Domergue, J. M. (2010). Assessment of initial soil moisture conditions for event-based rainfall–runoff modelling. *Journal of Hydrology*, *387*(3–4), 176–187. https://doi.org/10.1016/J.JHYDROL.2010.04.006

Uhlenbrook, S., Seibert, J., Leibundgut, C., & Rodhe, A. (2009). Prediction uncertainty of conceptual rainfall-runoff models caused by problems in identifying model parameters and structure. *Https://Doi.Org/10.1080/02626669909492273*, *44*(5), 779–797. https://doi.org/10.1080/02626669909492273

Van Dijk, A. I.J.M. (2010). Climate and terrain factors explaining streamflow response and recession in Australian catchments. *Hydrology and Earth System Sciences*, *14*(1), 159–169. https://doi.org/10.5194/HESS-14-159-2010

Vansteenkiste, T., Tavakoli, M., Van Steenbergen, N., De Smedt, F., Batelaan, O., Pereira, F., & Willems, P. (2014). Intercomparison of five lumped and distributed models for catchment runoff and extreme flow simulation. *Journal of Hydrology*, *511*, 335–349. https://doi.org/10.1016/J.JHYDROL.2014.01.050

Vogel, R. M., & Fennessey, N. M. (1994). Flow-Duration Curves. I: New Interpretation and Confidence Intervals. *Journal of Water Resources Planning and Management*, *120*(4), 485–504. https://doi.org/10.1061/(ASCE)0733-9496(1994)120:4(485)

Wagener, T., Franks, S. W., International Association of Hydrological Sciences., & International Association of Hydrological Sciences. Scientific Assembly (7th : 2005 : Foz do Iguaçu, B. (2005). *Regional hydrological impacts of climatic change*. https://books.google.com/books/about/Regional_Hydrological_Impacts_of_Climati.html?hl=fr&id=klV7jReHIPcC

Willmott, C. J., & Matsuura, K. (2005). Advantages of the mean absolute error (MAE) over the root mean square error (RMSE) in assessing average model performance. *Climate Research*, *30*(1), 79–82. https://doi.org/10.3354/CR030079

Wittenberg, H., & Sivapalan, M. (1999). Watershed groundwater balance estimation using streamflow recession analysis and baseflow separation. *Journal of Hydrology*, *219*(1–2), 20–33. https://doi.org/10.1016/S0022-1694(99)00040-2

W. M. O. (1995). *World Meteorological Organization - Annual Report 1994*. WMO.

Wood, A. W., Leung, L. R., Sridhar, V., & Lettenmaier, D. P. (2004). Hydrologic Implications of Dynamical and Statistical Approaches to Downscaling Climate Model Outputs. *Climatic Change 2004 62:1*, *62*(1), 189–216. https://doi.org/10.1023/B:CLIM.0000013685.99609.9E

Xu, C. Y., & Singh, V. P. (1998). A Review on Monthly Water Balance Models for Water Resources Investigations. *Water Resources Management 1998 12:1*, *12*(1), 20–50. https://doi.org/10.1023/A:1007916816469

Xue, X., Hong, Y., Limaye, A. S., Gourley, J. J., Huffman, G. J., Khan, S. I., Dorji, C., & Chen, S. (2013). Statistical and hydrological evaluation of TRMM-based Multi-satellite Precipitation Analysis over the Wangchu Basin of Bhutan: Are the latest satellite precipitation products 3B42V7 ready for use in ungauged basins? *Journal of Hydrology*, *499*, 91–99. https://doi.org/10.1016/J.JHYDROL.2013.06.042

Yang, X., & Michel, C. (2000). Flood forecasting with a watershed model: a new method of parameter updating. *Ilydrological Sciences-Journal-Des Sciences Hydrologiques*, *45*(4), 537.

Yatagai, A. (n.d.). *Development of a daily grid precipitation data in the East Mediterranean and its application for the ICCAP studies*.

Yatagai, A., Arakawa, O., Kamiguchi, K., Kawamoto, H., Nodzu, M. I., & Hamada, A. (2009). A 44-year daily gridded precipitation dataset for Asia based on a dense network of rain gauges. *Scientific Online Letters on the Atmosphere*, *5*(1), 137–140. https://doi.org/10.2151/SOLA.2009-035

Yatagai, A., Kamiguchi, K., Arakawa, O., Hamada, A., Yasutomi, N., & Kitoh, A. (2012). APHRODITE: Constructing a Long-Term Daily Gridded Precipitation Dataset for Asia Based on a Dense Network of Rain Gauges. *Bulletin of the American Meteorological Society*, *93*(9), 1401–1415. https://doi.org/10.1175/BAMS-D-11-00122.1

Yatagai, A., Krishnamurti, T. N., Kumar, V., Mishra, A. K., & Simon, A. (2014). Use of APHRODITE rain gauge-based precipitation and TRMM 3B43 products for improving asian monsoon seasonal precipitation forecasts by the superensemble method. *Journal of Climate*, *27*(3), 1062–1069. https://doi.org/10.1175/JCLI-D-13-00332.1

Yong, B., Ren, L.-L., Hong, Y., Wang, J.-H., Gourley, J. J., Jiang, S.-H., Chen, X., & Wang, W. (2010). Hydrologic evaluation of Multisatellite Precipitation Analysis standard precipitation products in basins beyond its inclined latitude band: A case study in Laohahe basin, China. *Water Resources Research*, *46*(7), 7542. https://doi.org/10.1029/2009WR008965

Yu, P. S., & Yang, T. C. (2000). Fuzzy multi-objective function for rainfall-runoff model calibration. *Journal of Hydrology*, *238*(1–2), 1–14. https://doi.org/10.1016/S0022-1694(00)00317-6

Zhang, Y., Vaze, J., Chiew, F. H. S., Teng, J., & Li, M. (2014). Predicting hydrological signatures in ungauged catchments using spatial interpolation, index model, and rainfall-runoff modelling. *Journal of Hydrology*, *517*, 936–948. https://doi.org/10.1016/J.JHYDROL.2014.06.032

ANNEXURE 1

DATA CHECKING FOR THE REMAINING WATER YEAR

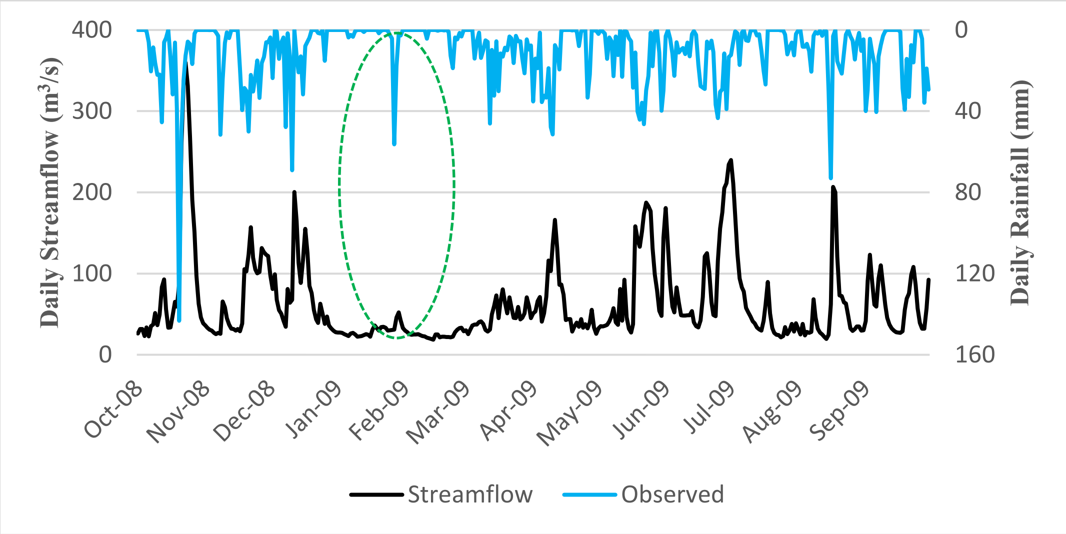

Comparison of streamflow and rainfall for 2008/9 water year

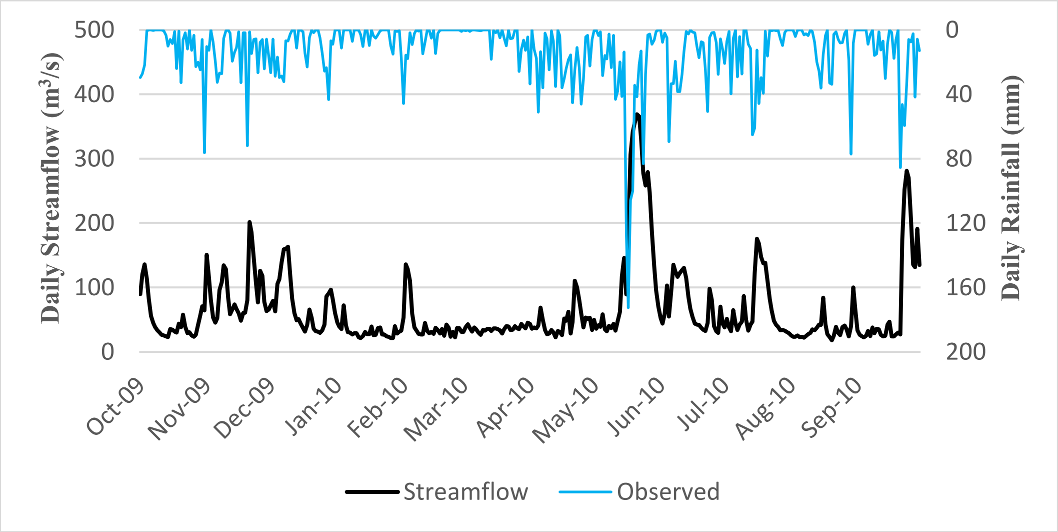

Comparison of streamflow and rainfall for 2009/10 water year

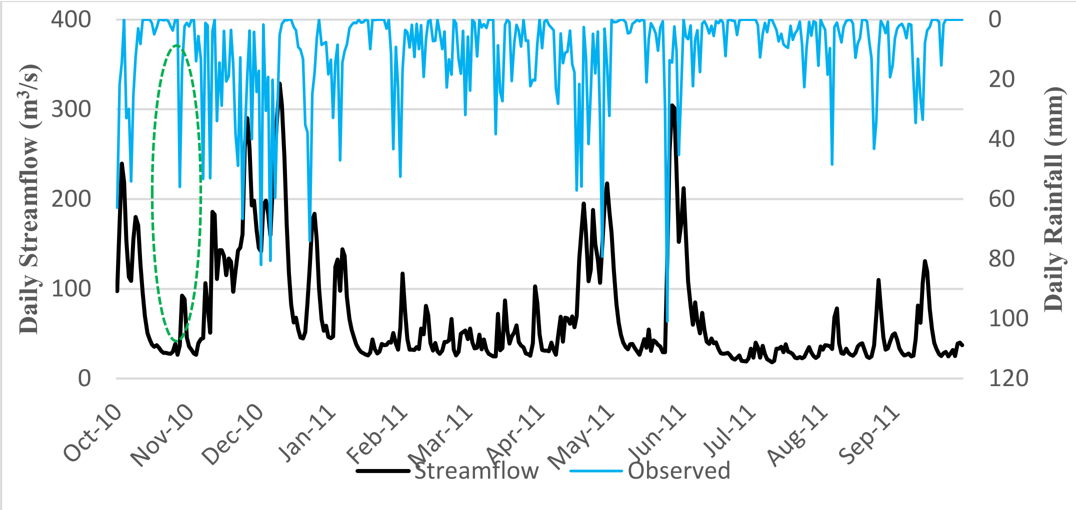

Comparison of streamflow and rainfall for 2010/11 water year

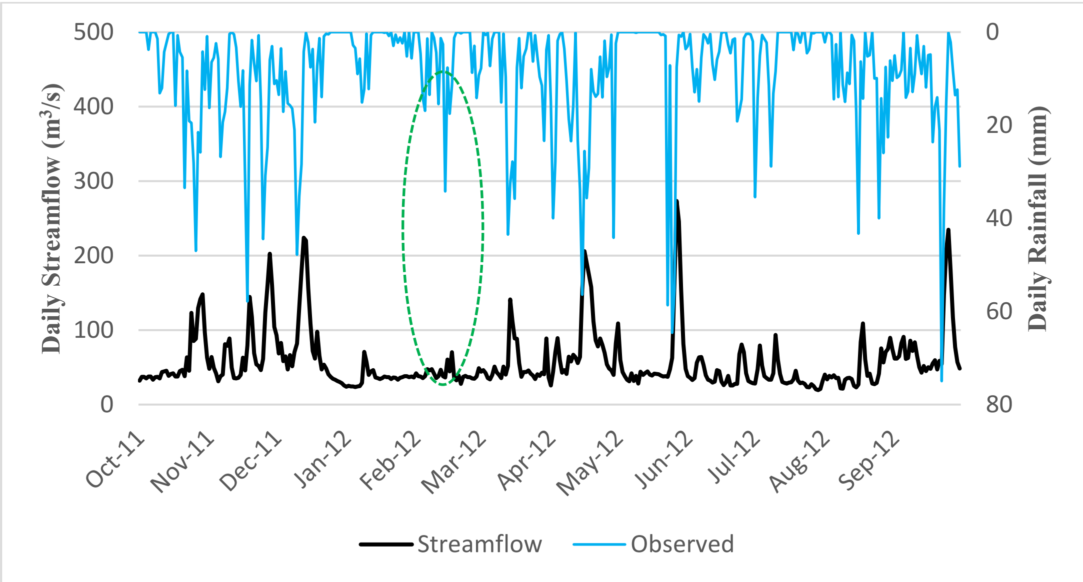

Comparison of streamflow and rainfall for 2011/12 water year

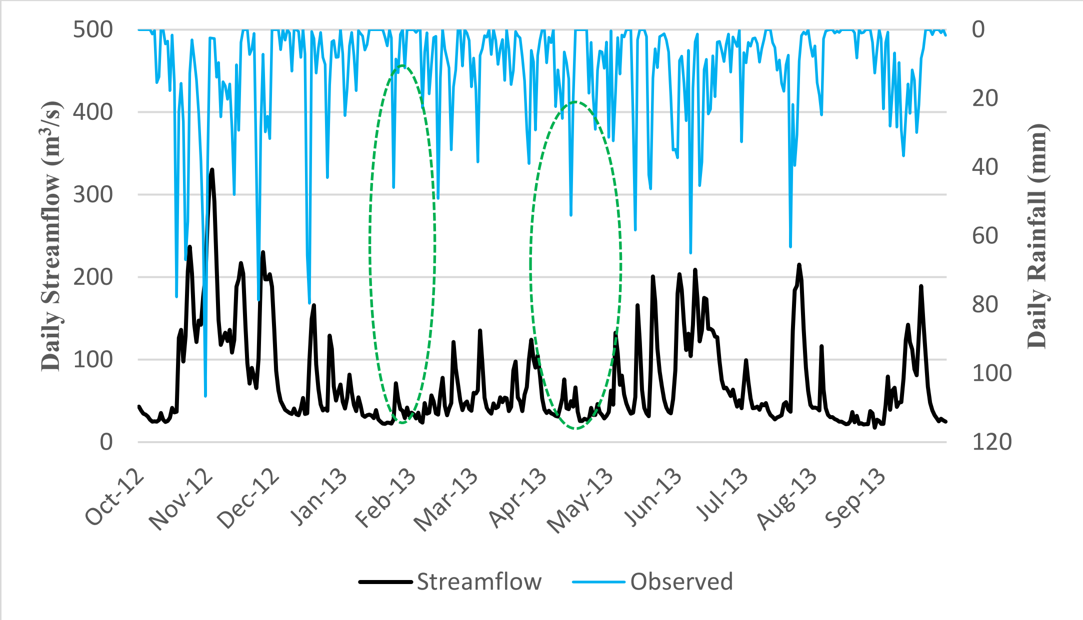

Comparison of streamflow and rainfall for 2012/13 water year

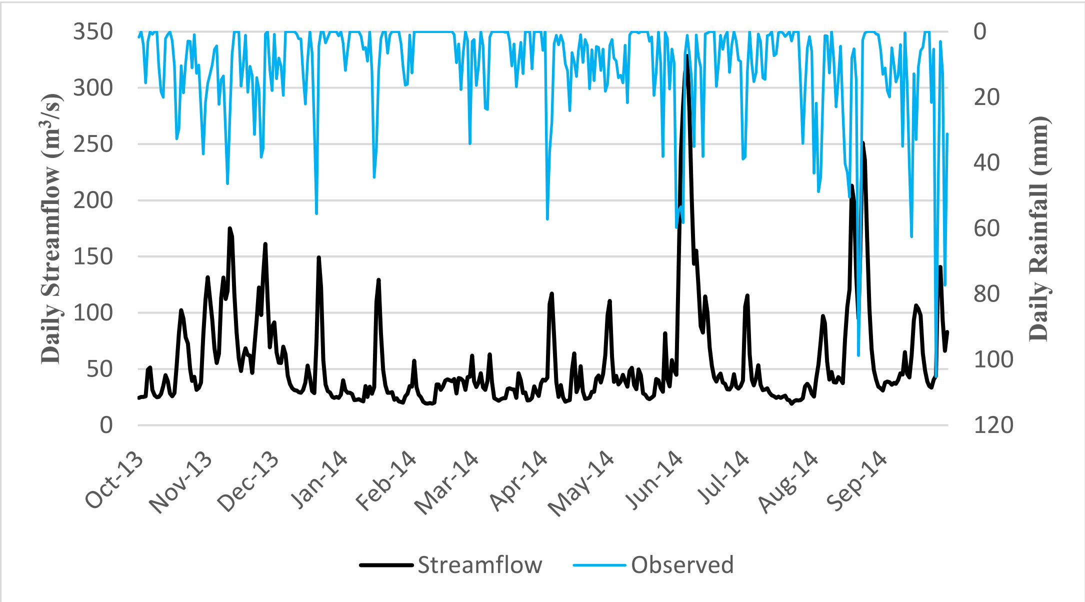

Comparison of streamflow and rainfall for 2013/14 water year

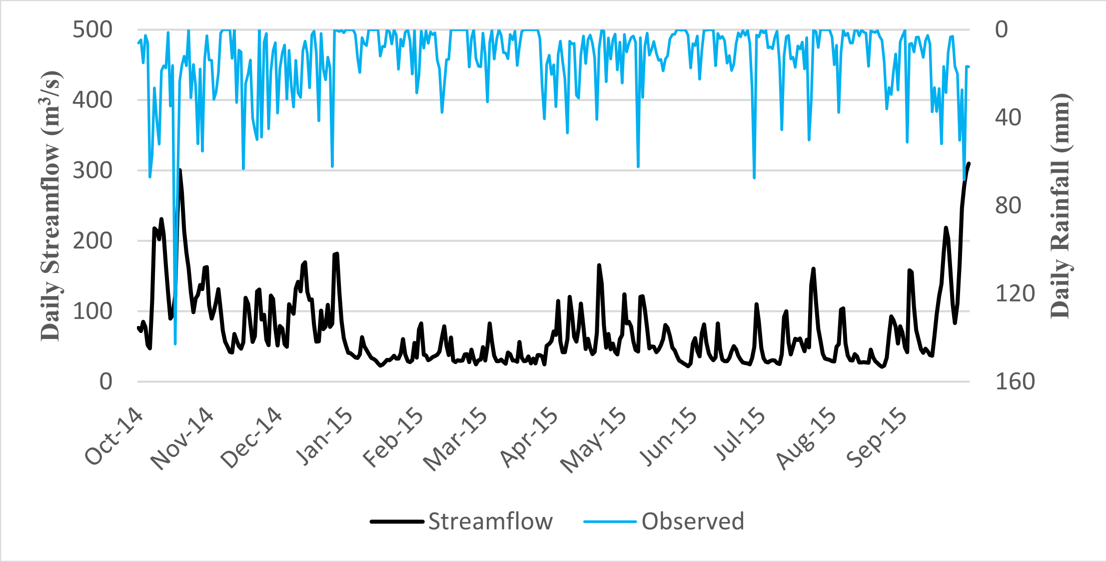

Comparison of streamflow and rainfall for 2014/15 water year

ANNEXURE 2

THE REMAINING COMPARISON OF THE STATION RAINFALL WITH STREAMFLOW

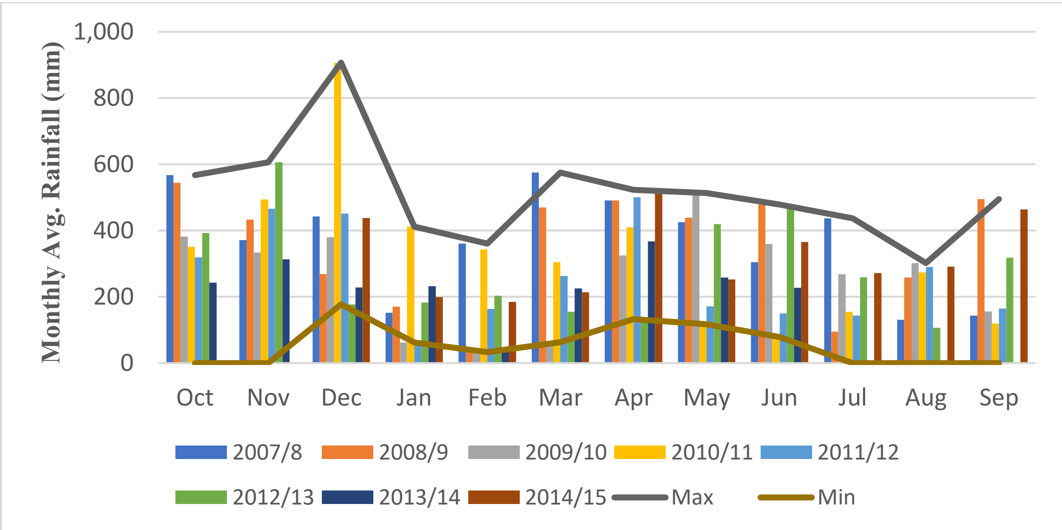

Rainfall distribution – Deniyaya station

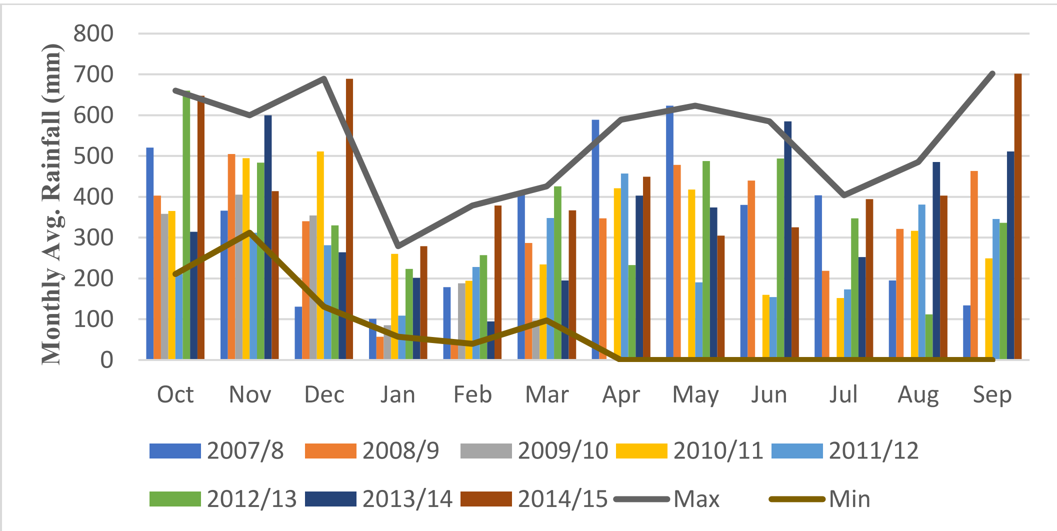

Rainfall distribution – Neluwa station

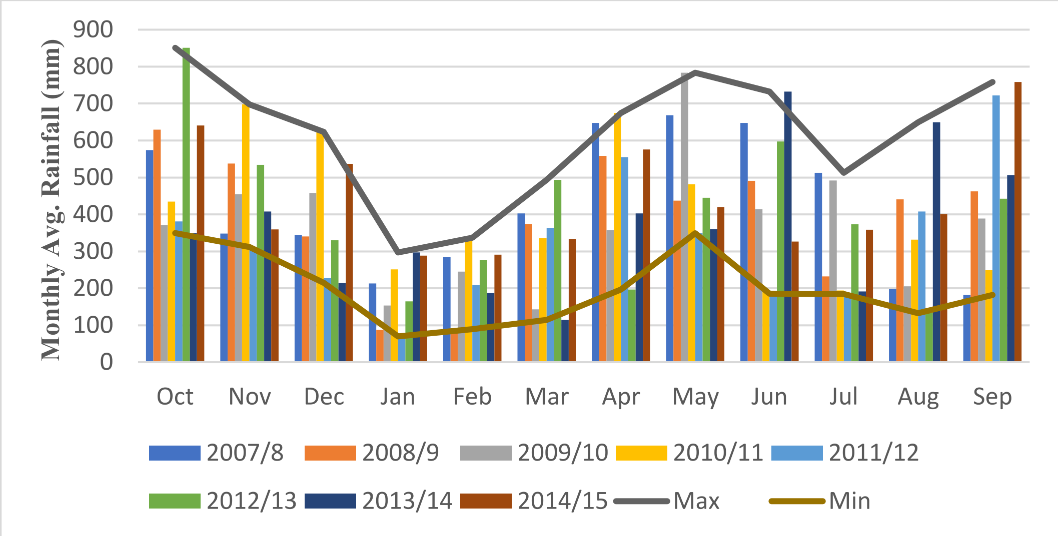

Rainfall distribution – Tawalama station

ANNEXURE 3

THE REMAINING CORRELATION BETWEEN DAILY OBSERVED WITH STATION DATA

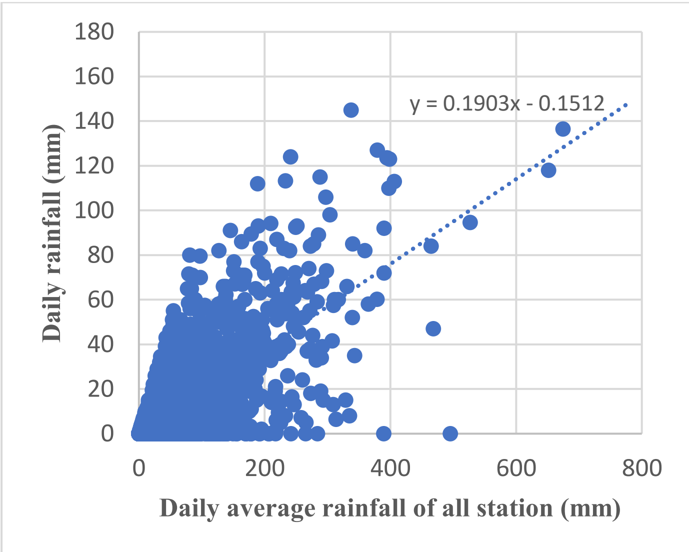

Correlation between daily observed of Deniyaya rainfall with all the average rainfall-Gin Ganga

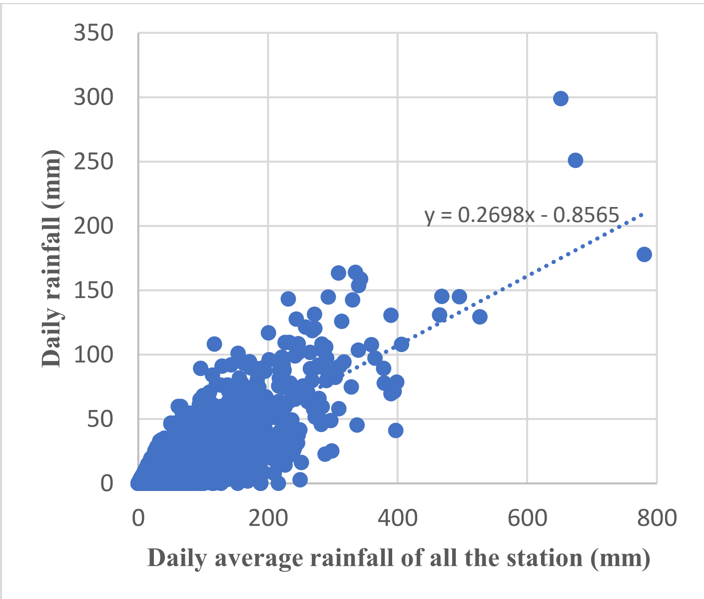

Correlation between daily observed of Tawalama rainfall with all the average rainfall-Gin Ganga

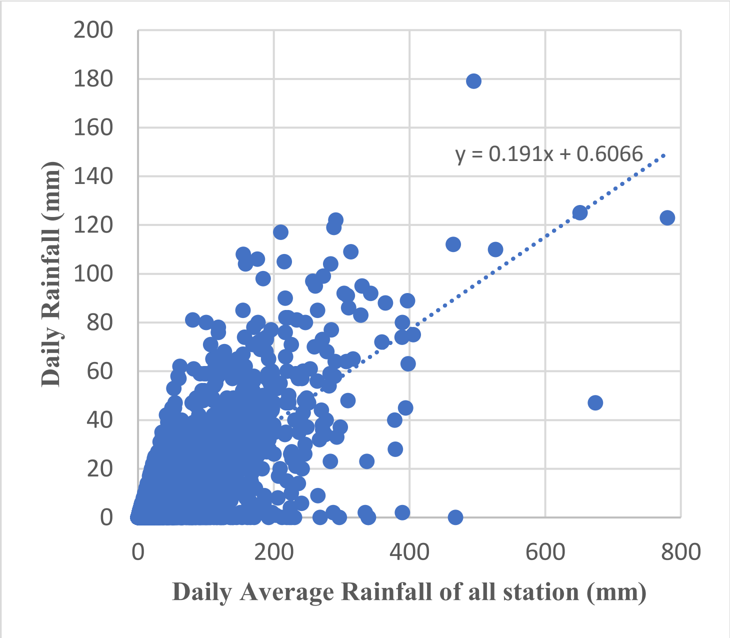

Correlation between daily observed of Neluwa rainfall with all the average rainfall-Gin Ganga

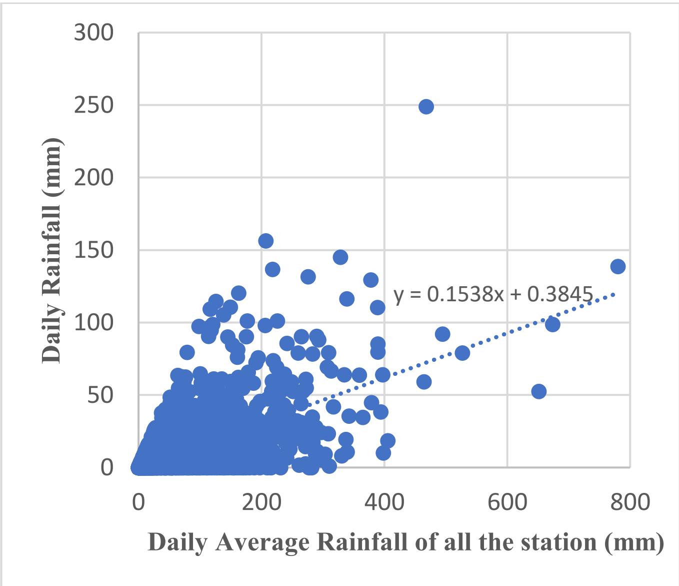

Correlation between daily observed of Baddegama rainfall with all the average rainfall-Gin Ganga

ANNEXURE 4

THE REMAINING DOUBLE MASS CURVE

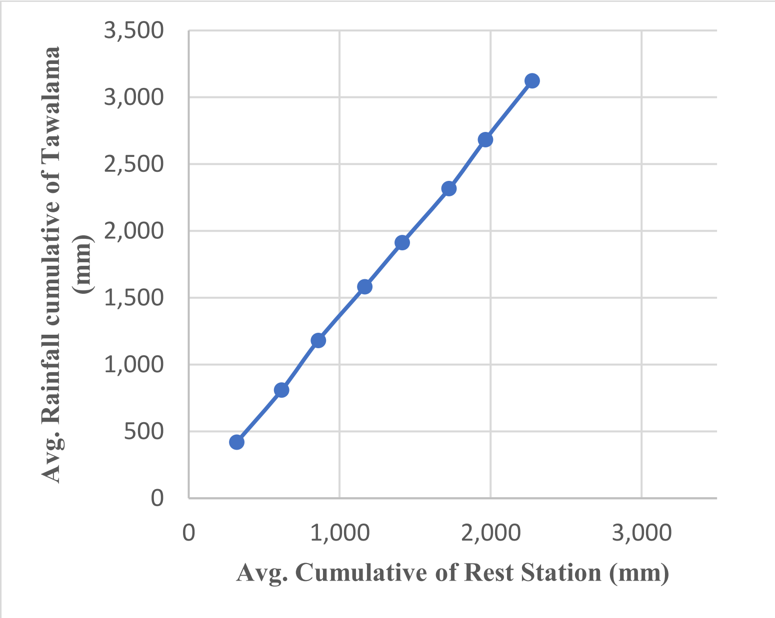

The double mass curve for the Tawalama station

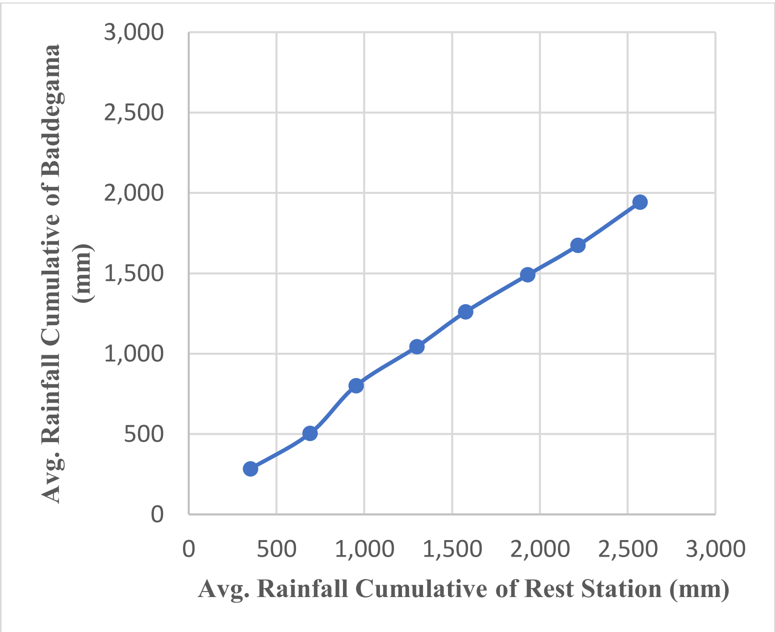

The double mass curve for the Baddegma station

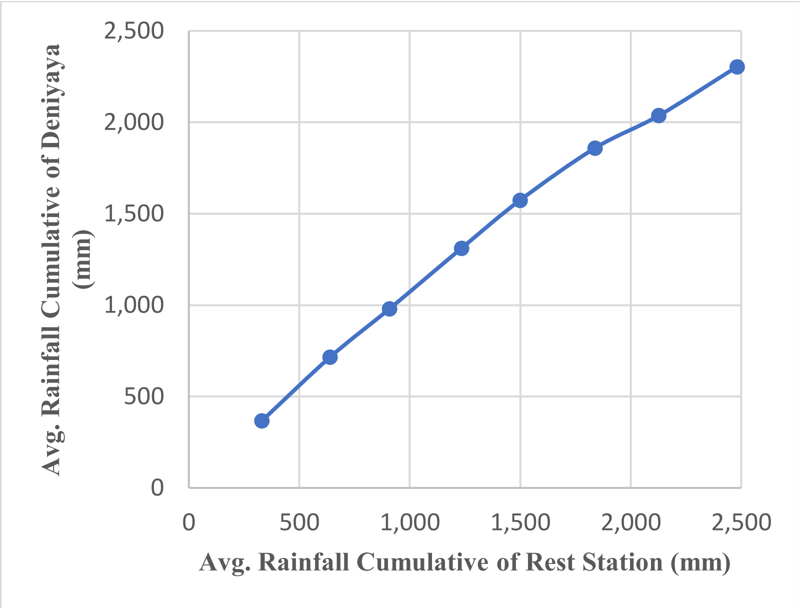

The double mass curve for Deniyaya station

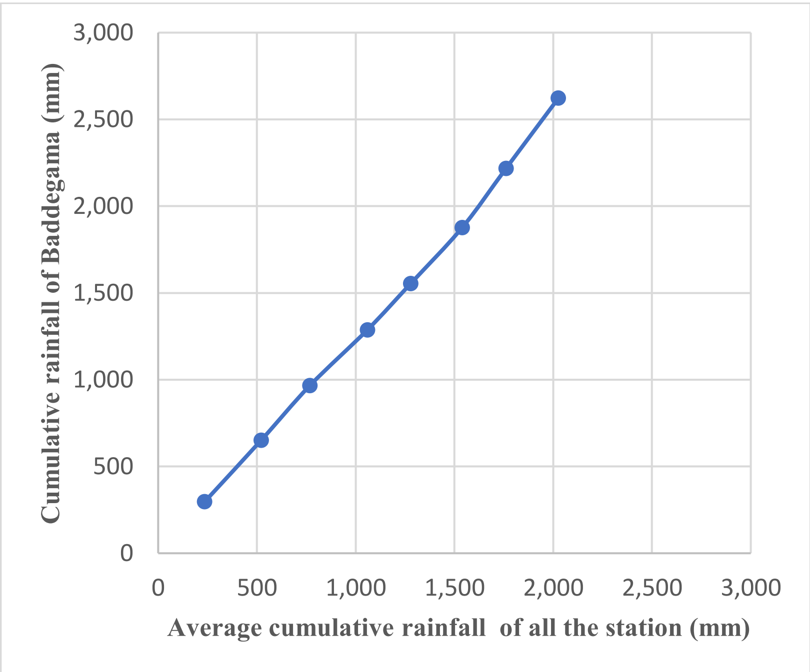

The double mass curve for Niluwa station